Summer 8-2020

Validation of Nanosecond Pulse Cancellation Using a Quadrupole Exposure System

Hollie A. Ryan
Old Dominion University, hryan4@alumni.jh.edu

VALIDATION OF NANOSECOND PULSE CANCELLATION USING A QUADRUPOLE EXPOSURE SYSTEM

by

Hollie Ann Ryan
M.S. May 2013, Johns Hopkins University
M.A. November 2004, Royal Military College of Canada
B.Soc.Sci. May 1998, University of Ottawa

A Dissertation Submitted to the Faculty of
Old Dominion University in Partial Fulfillment of the
Requirements for the Degree of

DOCTOR OF PHILOSOPHY

BIOMEDICAL ENGINEERING

OLD DOMINION UNIVERSITY

August 2020

Approved by:

Shu Xiao (Director)

Christian Zemlin (Member)

Chunqi Jiang (Member)

Patrick Sachs (Member)

ABSTRACT

VALIDATION OF NANOSECOND PULSE CANCELLATION USING A QUADRUPOLE EXPOSURE SYSTEM

Hollie A. Ryan
Old Dominion University, 2020
Director: Dr. Shu Xiao

Nanosecond pulsed electric fields (nsPEFs) offer a plethora of opportunities for developing integrative technologies as complements or alternatives to traditional medicine. Studies on the biological effects of nsPEFs *in vitro* and *in vivo* have revealed unique characteristics that suggest the potential for minimized risk of complications in patients, such as the ability of unipolar nsEPs to create permanent or transient pores in cell membranes that trigger localized lethal or non-lethal outcomes without consequential heating. A more recent finding was that such responses could be diminished by applying a bipolar pulse instead, a phenomenon dubbed *bipolar cancellation*, paving the way for greater flexibility in nsPEF application design. Transitioning nsPEFs into practical use, however, has been hampered by both device design optimization and the intricacies of mammalian biology. Generating electric fields capable of beneficially manipulating human physiology requires high-voltage electrical pulses of nanosecond duration (nsEPs) with high repetition rates, but pulse generator and electrode design in addition to the complex electrical properties of biological fluids and tissues dictate the strength range and distribution of the resulting electric field. Faced with both promising and challenging aspects to producing a biomedically viable option for inducing a desired nsPEF response that is both focused and minimally invasive, the question becomes: *how can the distinct features of unipolar and bipolar nsPEF bioeffects be exploited in a complex electrode exposure system to spatially modulate cell permeabilization?*

This dissertation presents a systematic study of an efficient coplanar quadrupole electrode nsPEF delivery system that exploits unique differences between unipolar and bipolar nsPEF effects to validate its ability to control cell responses to nsPEFs in space. Four specific aims were established to answer the research question, with specific attention to the roles played by pulse polarity, grounding configuration and electric field magnitude in influencing nsPEF stimulation of electropermeabilization in space. Using a prototype wire electrode applicator charged by a custom-built multimodal pulse generator, the aims were to spatially quantify

electropermeabilization due (1) unipolar and (2) bipolar nsPEF exposure, to (3) apply synchronized pulses with a view to canceling bipolar cancellation (CANCAN) through superposition that could shift the effective nsPEF response, and to (4) evaluate the ability of the quadrupole system to facilitate remote nsPEF electropermeabilization. Numerical simulations were employed to approximate the nsPEF distribution for a two-dimensional (2-D) area resulting from unipolar, bipolar or CANCAN exposure in a varied-pulse quadrupole electrode configuration. For all experiments, the independent variables were fixed for pulse width (600 ns), pulse number (50) and repetition rate (10 Hz). Electropermeabilization served as the biological endpoint, with green fluorescence due to cell uptake of the nuclear dye YO-PRO-1® (YP1) tracer molecule serving the response variable. An agarose-based 3-D tissue model was used to acquire, quantify and compare fluorescence intensity data *in vitro*, which was measured by stereomicroscopy to enable macro versus micro level 2-D visualization.

Results of this investigation showed that increasing the magnitude of the applied voltage shifts unipolar responses from localization at the anodal to cathodal electrode, and that adding a second proximal ground electrode increases the response area. Bipolar nsPEF responses were generally less intense than unipolar, but these depended on both the inter-electrode location measured and amplitude of the second phase. CANCAN preliminary indicated some ability to decrease strong uptake at electrodes, but evaluation across experimental and published data indicate that greater differences between unipolar and bipolar responses are needed to improve possibilities for distal stimulation. Overall, this work demonstrated the potential for more complex pulser-electrode configurations to successfully modulate nsPEF electropermeabilization in space by controlling unipolar and bipolar pulse delivery and contributed to a deeper understanding of bipolar cancellation. By providing a set of metrics for test and evaluation, the data provided herein may serve to inform model development to support prediction of nsPEF outcomes and help to more acutely define spatial-intensity relationships between nsPEFs and cell permeabilization as well as delineate requirements for future non-invasive nsPEF therapies.

Dedication

To my father and step-father. I wish I could have done more, sooner…

ACKNOWLEDGEMENTS

I would first like to acknowledge my advisor, Dr. Shu Xiao, for guiding me to the successful completion of my dissertation. He took me on as his student despite our different areas of specialization and pushed me to work outside of my comfort zone. I am grateful for both the technical knowledge and personal growth I have gained as a result. To the members of my committee: Dr. Christian Zemlin, Dr. Chunqi Jiang, Dr. Patrick Sachs, and especially Dr. Jiang, thank you so much for sticking with me.

There were other colleagues and mentors outside the "inner circle" to whom I owe much. First are Dr. Andre Pakhomov and Dr. Olga Pakhomova, who introduced me to the exciting field of bioelectrics and lent various forms of intellectual and resource support throughout. I also want to thank Dr. Stephen Beebe and Dr. Loree Heller for their guidance and support during my early research stage.

To the unsung heroes of my doctoral journey, my fellow graduate students, post-doctoral researchers, external faculty and staff members, I would like to express my genuine love and appreciation. Johanna Neuber, Ross Petrella, Dr. Anthony Asmar, Dr. Maisoun Bani Hani, Dr. Elena (Gianulis) Bruno, Dr. Iurii Semenov, Dr. Kiril Hristov, Dr. Barbara Hargrave, Betsy Gregory, Barbara Carroll and many others always willing to lend an ear, moral support or academic input – I doubt I could have done this without you. I am grateful further to Dr. Caleb Roth for his mentorship during my internship in San Antonio and beyond. Finally, my many thanks to Navy Captain Dr. Allen Garner, whose enthusiasm and advice from Purdue University and during visits to the DMV helped me to navigate some of the unseen hurdles.

I recognize and express sincere gratitude for funding and resource support provided by the Air Force Research Laboratory and Oak Ridge Institute for Science and Education (ORISE), as well as by Mr. Frank Reidy, the National Military Family Association and their sponsors.

I am humbled by the love and support of my family despite so much hardship. I expect to hear a collective "FINALLY!" across the miles from them upon learning I'm now 'done' with school. Finally, I am eternally grateful for my loving and hard-working husband, David, without whom taking this risky detour from an established career would not have been possible. I can't forget, too, our Vizsla, Laszlo, who kept me going with his infectious goofy smile, 'lean-in' hugs and boundless energy that forced me out on many walks and away from the computer.

ABBREVIATIONS

A–	anodal
BP	bipolar
C+	cathodal
Ca^{2+}	calcium ion
CST	Computer Simulation Technology
DC	direct current
DPBS	Dulbecco‘s Phosphate Buffered Saline Solution
FIT	finite integration technique
FITC	fluorescein isothiocyanate
FWHM	full width at half-maximum
FBS	foetal bovine serum
d_g	electrode gap distance [mm]
E	electric field strength [kV/cm]
E_c	critical electric field strength [kV/cm]
E_{max}	maximum electric field strength [kV/cm]
I	electric current [A]
N	pulse number
Na^+	sodium ion
nsEP	nanosecond electric pulse
nsPEF	nanosecond pulsed electric field
PI	propidium iodide
PS	phosphatidylserine
RC	resistance-capacitance
RT	room temperature
SD	standard deviation
SEM	standard error of the mean
τ_{FWHM}	time at full width half-maximum
U	voltage [V]
UP	unipolar
YP1	YO-PRO®-1

TABLE OF CONTENTS

Page

LIST OF TABLES

Table Page

LIST OF FIGURES

Figure Page

CHAPTER 1

INTRODUCTION

Whether it is pain, anxiety, depression or a major disease, there is no “magic bullet” for treating these or other pervasive medical conditions without concomitant negative health or financial consequences. Demands for medical treatment technologies with higher specificity, lower mortality and lower costs thus persist, but what if it was possible to control the body’s natural responses to stress to promote healing without the risk of drug dependency or to destroy disease without damaging healthy tissue? This dissertation focuses on the exploitation of characteristic properties of nanosecond pulsed electric fields (nsPEFs) to assess how the permeabilization of mammalian cells can be modulated using a versatile quadrupole electrode system. This first chapter provides context by introducing the history and technology behind nsPEF research and details the motivations for the current work. It concludes by laying out the research strategy pursued, including an overview of how bipolar cancellation may be applied as a unique nsPEF phenomenon to improve the control of biological responses to a quadrupole electrode exposure to support a potential biomedical application. It sets up an approach for next step in nsPEF study that supports the long-term development of a bioelectric technology that can deliver more efficient, safer and less invasive forms of treatment than conventional medicine.

1.1 Electrical Properties of Cells and their Behavior in an Electric Field

Long considered a potentially safe and viable alternative or complement to traditional medicine [7], electromagnetic (EM) energy has the potential to meet many of the current challenges in medicine. By exploiting the EM energy inherent in biological systems, for several decades, therapeutic doses of direct electrical current (DC) have been shown to augment healing of chronic wounds in human subjects and induced wounds in animal models. In early studies of cell cultures using microsecond (μs) and millisecond (ms) long pulses, electric fields were shown to influence the migratory, proliferative, and functional capacity of cells involved in the healing process.

In biomedical research, much of the work is focused on alleviating illness or enhancing physical function. The human body relies on the integrated activity of multiple life processes to

execute organization, responsiveness, movement, respiration, metabolism, reproduction, growth, homeostasis, cognitive abilities, digestion, and excretion in fine-tuned balance for the well-being of the individual and to maintain life. Despite these various functions, the basic element common to all is the mammalian cell. Each tissue, muscle, nerve and skin cell is similarly composed in that it contains most of the same organelles and has essentially the same construction: a nucleus surrounded by cytoplasm contained by a plasma membrane. The ability each cell has to respond in different ways to various stimuli allows for the particular functioning of a biological system. How a cell can respond to these exogenous physiological stimuli is a matter of the various signaling networks and pathways that provide cells the means to respond precisely and effectively.

Part of what defines these signal transduction mechanisms is based on what are inherently electrical features of cells. As electrical energy requires a medium in which to travel, the physical properties of the various cellular components influence how energy is transmitted. Biological cells are made up of charge carriers in the form of ions and charged molecules whose motion and ability to exchange energy with their environments are responsible for driving cellular processes. Modern understanding of how these components interact with each other permits the formulation of modules that act as discrete functional systems. For instance, the extracellular medium, cytoplasm and organelle interiors serve as conductive electrolytes, whereas the plasma and organelle membranes act as insulators. A biological cell can thus be modeled as an electrical circuit, where the capacity of various cellular compartments to either separate charges or prevent their flow are defined as capacitors or resistors, respectively (Fig. 1-1).

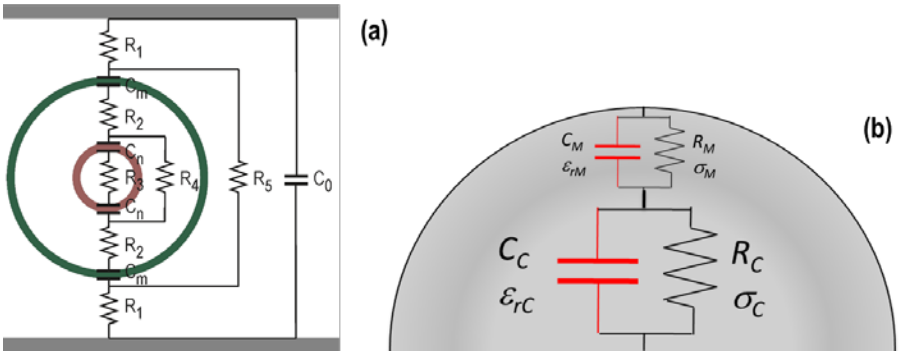

Fig. 1-1 Electric circuit model of the cell. Such models differ in complexity and may (a) include or (b) exclude the nucleus, for example.

The lipid molecules that are arranged to form the plasma membrane act as a dielectric layer, the interior of which is the conductive cytoplasmic medium. Cell membranes are not perfect insulators, however, due to the presence of protein channels and pumps that actively transport ions against their concentration gradient with the help of ATP. This activity functions to maintain higher intracellular concentrations of Na^+, Ca^{2+} and Cl^- relative to extracellular concentrations, with the reverse being true for K^+. Membranes at equilibrium also comprise many open K^+ channels that allow intracellular potassium ions to passively diffuse through the membrane into the extracellular space, which results in the accumulation of positive charge on the outside of the cell and of negative charges on the inside, close to the membrane. This difference in charge creates a potential difference across the membrane of between 50 and 70 mV. Since the maintenance of these concentration and electrical gradients is necessary for biological health, disruption from any source can impact essential biological process in ways that may be either harmful or helpful.

One way to interfere with this homeostasis is through the application of an exogenous electric field. Electric fields have demonstrated a range of effects on cells and tissues [8-16] and can affect cell division, polarization and migration, in particular at low intensities (tens of mV/cm to a few V/cm) [17]. Incorporating experimental findings, electrical model simulations show that exposing a cell to a sufficiently high pulsed electric field (above a few hundred V/cm to one kV/cm) generated from a ~1 microsecond (μs) to ~20 millisecond (ms) pulse charges the plasma membrane by accumulating charges and altering the resting potential difference across it [18-21]. This activity creates pores in the lipid bilayer in a process known as “electroporation” [22, 23] leading to increased permeability of the cell membrane and allowing molecules as large as DNA to pass through. With pore transience or permanence depending on the magnitude of the field, this effect has respective biomedical applications in gene transfection and drug delivery or tissue ablation [24]. Because these traditional pulses primarily operate at the plasma membrane and the application is longer than the membrane charging time constant, they can produce unwanted heating and painful consequences such as nerve stimulation and muscle contraction, as well as other undesirable effects in non-target tissue areas. With longer pulse durations, it takes longer for charges to accumulate along the membrane than it does to charge the plasma membrane itself [25].

With pulses in the nanosecond range, as the membrane is charged within a time frame that is shorter than the pulse duration, intracellular components are effectively shielded from the exogenous electric field, much like how a Faraday cage operates. For a sub-microsecond (μs) pulse, the timescale during which the corresponding electric field is applied is shorter than the charging time of the plasma membrane such that, at higher potential, charges are unable to amply accumulate at the plasma membrane, allowing the field to be experienced inside the cell. Notwithstanding the above, generating electric fields capable of sub-cellular manipulation, especially that may be medically beneficial, requires high-voltage electric pulses. Advances in pulsed power technology over the last two decades have made that possible.

1.2 Biological Effects of nsPEFs

Electric pulses with nanosecond durations (nsEPs) producing kV/cm magnitude electric fields have been available since the mid-1990s. Nanosecond pulsed electric fields (nsPEFs) are characterized as high voltage (>1 kV/cm), ultra-short (sub-μs) electrical pulses capable of inducing cellular responses distinguished from those typical of longer pulses. Research over the past few decades on the effects of nsPEFs has demonstrated minimal to no risk of side effects [26], offering opportunities for the development of alternative biomedical therapies with greater flexibility and clinical potential. While the plasma membrane is particularly more responsive to longer pulses than with short ones [27], nsPEFs can stimulate various types of biological responses in a highly cell-specific manner, namely the creation of dense, homogenous ‘nanopores’ in the plasma membrane [28], much smaller than those of conventional electroporation with diameters less than 1 nm.

NsPEF induced membrane permeabilization (“electropermeabilization”) effects are usually measured indirectly based on the degree to which a cell or cells allow the passage of fluorescent molecules across the plasma membrane. Early published research on the effects of nsPEFs on various cell types reported biological responses without permeabilization based on the absence of cellular uptake of such plasma membrane integrity markers as Trypan blue and propidium iodide [29-31]. Observations from experiments since have supported the notion that nsPEFs can disrupt the cell membrane in various ways [18, 32], among which is the externalization of phosphatidylserine (PS), a common indicator of apoptosis [33] in addition to cell swelling [2, 22] and small molecule uptake [33-35]. Computational models that show

nsPEFs form nanometer scale pores in the plasma membrane [36-38] corroborated claims of the latter's disruption from nsPEFs, suggesting that the fluorescent molecules traditionally used to detect membrane permeability (*e.g.* PI, ~1.5 nm in diameter) were too large to pass through these nanopores, especially those formed by nsPEFs of lower relative field strength or pulse number [28] Despite these findings, the debate regarding the size, duration and transmembrane passage properties of nanopores persists.

The implication that nanopore size may restrict certain biological marker molecules from passing through the cell plasma membrane was confirmed by the subsequent demonstration of nsPEF electropermeabilization by detection of early uptake by smaller fluorescent markers YO-PRO®-1 (with a Van der Waals diameter ~1 nm) and thallium (~0.39 nm) plus thallium-sensitive fluorophore, followed by PI detection [39, 40] leading to the conclusion that nsPEF-induced nanopores are smaller than 1.0-1.5 nm. However, the sensitivity of membrane-impermeant fluorescent dyes is limited by the number and size of pores generated. For weaker nsPEF exposures, this means there must be enough fluorescence emission due to pore formation to distinguish it from background, along with available and effective imaging systems.

In the last decade, in addition to nanopore formation, researchers have reported changes in cell volume, notably swelling, following nsPEF exposure [41, 42]. Increases in cell volume are most likely due to water uptake initiated by an nsPEF-induced osmotic imbalance across cell plasma membrane [41, 43, 44]. Smith *et al*. (2008) [45] demonstrated that nsPEF pore creation dominates pore expansion, meaning that the flux of smaller species like calcium and monovalent ions that cause osmotic imbalance exceeds the transport of even the smallest dye molecules through nanopores created by nsPEF exposure. In work performed leading into this dissertation [2] and briefly described in Chapter 2, it was observed that a 20 kV/cm exposure that just a single 600 ns pulse could induce cell swelling. These findings suggest a role for cell swelling in serving as a highly or even more sensitive indicator, beyond the common fluorescent indicators of membrane integrity, of nsPEF-induced electropermeabilization.

Another hallmark of nsPEF effects is that exposure may also disrupt intracellular structures such as organelle membranes and modulate cell signaling functions, which may or may not exhibit observable effects at the outer plasma membrane. With sufficiently high field strength, nsPEFs can penetrate the plasma membrane to reach the cell interior and create a potential difference across organelle membranes substantial enough to permeabilize them [33,

36-38, 45-48], opening up possibilities for nsPEF in targeting and manipulating intracellular compartments and components without destroying the cell. This concept offers the potential for intracellular applications including nsPEF control of apoptosis [18, 30, 31], malignant tumor reduction or elimination [19, 49], neuromuscular response stimulation [30, 50, 51], and platelet activation and growth factor release to promote wound healing [52]. Intracellular studies of nsPEFs that may trigger, for example, metabolic responses or changes in gene expression, are still nascent, and such effects are, in any case, beyond the scope of this investigation.

1.3 Factors Affecting the Electropermeabilization Response to nsPEFs

The type of physiological response biological cells give to nsPEF exposure varies based on multiple possible pulse parameters and exposure conditions, namely pulse shape, duration, rise time, number, frequency and repetition rate, as well as electric field strength, medium conductivity, target density and electrode arrangement. Along with these pulse parameters, nsPEF efficiency depends on cell type, cell concentration and even the ambient temperature [53]. According to Zimmermann *et al*. (1974) [54], cell size also affects electropermeabilization since the transmembrane potential is proportional to the cell radius. Lower intensity electric fields are thus required to achieve membrane permeabilization in larger cells. In order for nsPEF exposure protocols to be optimized, it is thus crucial that experimental studies provide data on the above variables. Information gleaned from these can then allow researchers to predict the biological effects linked to nsPEF exposure and design appropriate pulsing protocols with less guesswork and time invested.

1.4 Impediments to Clinical Translation of nsPEFs Technology

Despite the potential nsPEF has for multiple applications, the lack of flexibility inherent in current nsPEF delivery confounds ideal matching between biologically effective nsPEFs and complex target treatment areas. Tackling this problem requires overcoming multiple challenges. First, to optimize research outcomes, pulse generators must have the capacity to generate high-voltage pulses with waveform quality suited to the desired biomedical application (*e.g.* on-microscope versus *in vivo* versus clinical). Pulse generators are still largely custom-built and exclusively unipolar (UP) or bipolar (BP), and although simple conversion of the former to the latter is achievable, fidelity of wave shape and symmetry is often lost and subsequent phases tend

to suffer from longer fall times [55, 56]. Second, effective nsPEF system biological interface design requires accounting for topological, dielectric and size differences. Electrode geometries commonly used to generate nsPEFs – typically parallel plate or needle-like configurations – introduce spatial constraints or are inherently invasive, and electric field values beyond regions that are strictly of uniform field are often assumed or ignored in analyses [27]. The third challenge is closing the enduring knowledge and/or consensus gap regarding physical and biophysical mechanisms of nsPEF action. While researchers generally accept the equivalent circuit model of the cell [57] and the role of biomolecules such as Ca^{2+} in many observed effects, the multitude of parameter combinations confound holistic comprehension of direct links between nsPEF and biological responses. Requirements therefore often exceed the capacity of most available custom-built systems to adapt. Better tools and techniques are needed to improve the ability to spatially predict biological responses and to control nsPEF generation.

1.5 Bipolar Cancellation

Perhaps one of the most relevant discoveries in nsPEF research over the past decade has been that of “bipolar cancellation” (BPC), a term used to describe a phenomenon whereby biological responses to UP nsEPs – namely viability, membrane permeabilization and intracellular calcium release – are reduced or obliterated when a second phase of opposite polarity is applied (Fig. 1-2) [58]. What makes BPC remarkable is the fact that bipolar nsEPs were shown to be much less efficient than unipolar nsEPs despite twice the duration and assumed energy [59]. While the mechanisms of bipolar cancellation remain unknown, early research findings warrant the exploration of how BPC can be applied to modulate nsPEF bioeffects. While there is some evidence to conclude that BPC is not strictly limited to nanosecond pulses [60], given the specificity of nsPEF bioeffects, BPC in this context provides an opportunity to overcome the hurdle of nsPEF precision by presenting the possibility of tailoring electric pulses to modulate specific biological responses. This topic is elaborated on in Chapter 2.

1.6 CANCAN

As ions and charged molecules are influenced by the electric field when a biological cell is placed inside it. The presence of multiple electrodes, each contributing to the existing electric field in a system, means a method can be devised to control the biological response. It is

expected that varying the voltage difference between two or more electrodes can alter the effective field and thus enable control of the spatial biological response. As biological responses to UP nsPEFs are known to be typically stronger than responses to BP nsPEFs, with the right exposure system, bipolar cancellation may be exploited using a specific pulsing technique to deliberately weaken biological responses at electrodes, where the field is typically highest, and strengthen them at a point away from the electrodes, increasing flexibility and improving focus (Fig. 1-2). The effectiveness of the method depends on the shape and orientation of the conducting surfaces, which dictate how charges are distributed.

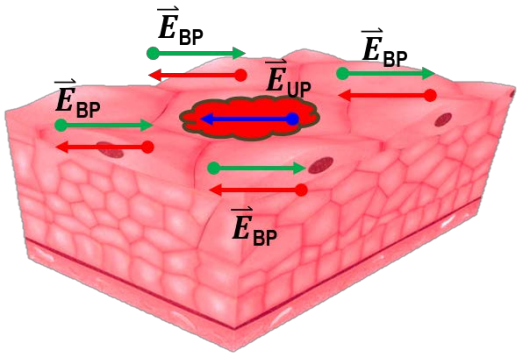

Fig. 1-2 Biomedical application for bipolar cancellation. If electrodes are properly configured, the strongest nsPEF from a unipolar pulse will be delivered to a target tissue area while non-target tissues will be exposed to weaker bipolar nsPEFs.

Pakhomov *et al*. [61] suggested that it might be possible to synchronize the delivery of multiple independent nsEPs in a two-fold process that relies on the proper combination of electrode configuration and bipolar pulse synchronization to produce a biologically effective UP nsPEF at a distal target. A near-term goal of this work was to demonstrate remote electrostimulation through the application of properly shaped nsEPs in an electrode configuration that would shape the resulting electric field to a target tissue area. It was expected, for example, that if two independent pulses of equal amplitude, but opposite polarity were delivered simultaneously to electrodes in a linear configuration, a region of "0" field would result. By the same vector calculation approach, given a bipolar nsEP with number of phases φ in the same configuration, if a matching separate pulse with φ*-1* was initiated at the second phase, the opposing vector electric fields would cancel each other, leaving only the electric field resulting

from the unipolar pulse ($\varphi = 1$). The effect of bipolar cancellation would essentially be cancelled by the subsequent pulse. This cancellation of cancellation is referred to as CANCAN [6].

Limited knowledge of bipolar cancellation and its study in primarily uniform electric fields constitute two major gaps in effectively applying variable polarity nsEPs in a manner that is both focused and minimally invasive. Several variations of research-grade solid-state and non-solid state [62] DC-powered nanosecond pulse generators capable of producing unipolar and/or bipolar rectangular waveforms are in operation for research purposes, but electrode interfaces used to study nsPEF both *in vitro* and *in vivo* are either invasive or impractical for medical use. One approach to closing this gap was to marry controlled nanosecond pulse generation with an appropriate method of delivery, which in this case was a moderately complex electrode geometry. This would enable spatial alteration of both the vector and strength of the PEF and allow for cell responses to be potentially modulated by field strength and/or pulse phase polarity. Ultimately, by synchronizing the delivery of anti-polar pulses, typically high nsPEF cell responses proximal to electrodes could be eliminated or reduced while being enhanced distally. This work revealed factors influencing remote nsPEF stimulation achievement, permitting better approaches to realizing versatile, non-invasive, precision-based biotechnology to be defined.

1.7 Research Strategy

The purpose of this research was to test and evaluate the ability of a coplanar quadrupole electrode system to spatially modulate cell membrane permeabilization non-invasively through the selective individual and synchronized surface application of unipolar and bipolar nanosecond pulses. This was accomplished using electric field modeling and simulation, select *in vitro* experiments, and image analysis in two dimensions (2-D) to assess responses for spatial, waveform and dose-response resolution. Exposures were performed on cells suspended in a 3-D agarose gel to mimic a simple tissue environment. Given its relatively small molecular size and sensitivity to early membrane permeabilization events [35], cellular uptake of a known concentration of a membrane-impermeable fluorescent nuclear dye was employed to visualize electropermeabilization. Fluorescence was imaged by stereomicroscope and then analyzed using image processing software.

The long-term goal is to optimize multimodal pulse delivery and enable remote CANCAN through the application of synchronized polyphasic ultra-wide band or radiofrequency

pulses. Accomplishing this goal will reduce the risk of unwanted high-field effects and eliminate the possibility of contamination (of patient and/or equipment). Although such an optimized design promises standoff exposure, the initial use here of an electrode-based system permitted the limits of bipolar cancellation and the feasibility of a BPC application to be tested and evaluated on a small, adaptable scale.

Formulated on the finding that a strong linear correlation exists between nsPEF strength ("dose") and electropermeabilization ("response") under ideal conditions, the governing hypothesis is that if the two are linearly correlated, the spatial cell response can be predicted if the local electric field is known. By extension, given a known electrode geometry and biological system characteristics plus a flexible nsEP generator, an electric field can be generated at a region in space to produce a desired biological effect. A growing body of work is emerging in the study of bipolar nsEPs, largely in uniform fields and in single cells, and is illustrated in more detail in Chapter 2. These various approaches to studying the effects of bipolar nsPEFs have revealed some interesting features of BPC, but many questions remain. The principle research question here is, *how can the distinct features of unipolar and bipolar nsPEF bioeffects be exploited in a complex electrode exposure system to spatially modulate electropermeabilization?* Specifically, *how do pulse polarity, grounding configuration and electric field magnitude influence nsPEF stimulation in space?*

Using coplanar quadrupole wire electrodes charged by a multimodal pulse generator, four specific aims were established to answer these questions. Using the 2-D electric field magnitude in a 3-D tissue model as the explanatory variable, these aims are: 1) to spatially quantify electropermeabilization by unipolar nsPEF exposure; 2) to spatially quantify electropermeabilization by bipolar nsPEF exposure; 3) to validate CANCAN as a technique for implementing spatial modulation of nsPEF electropermeabilization; and 4) to evaluate the remote nsPEF biomodulation capability of the coplanar quadrupole electrode system. Based on a set of conditions and assumptions defining the scope of the thesis, special attention has been paid to electrode geometry, the identification of specific exposure parameters necessary to induce electropermeabilization, the differentiation of unipolar and bipolar nsPEF spatial responses, and the spatial nature of the pulses generating the electric field. Incorporating the above, this dissertation builds upon nsPEF and bipolar cancellation research to date by focusing on the

various objectives established for each specific aim plus additional delimitations and justifications.

1.8 Significance

Significant and beneficial contributions to biomedical science and engineering, both primary and secondary, were produced in achieving the above aims. The major innovation of this effort was in moving beyond the standard dipole electrode system to a quadrupole electrode system, expanding the study of nsPEF bioeffects from one dimension (1-D) to 2-D. The combination of a novel modular nanosecond pulse generator and basic quadrupole electrode design used in this study multiplied the flexibility of current nsEP delivery and nsPEF generation, which has typically been limited by pulsers having the capacity to only produce a single waveform by simple electrode geometry. The system allowed for increased parameter control and variable active and ground positioning to create and alter a 2-D electric field gradient profile, and to support the creation of biologically effective nsPEFs of various shapes in numerous inter-electrode regions.

This work included a detailed analysis of the non-uniform 2-D electric field distribution created by sophisticated pulse types. Computational modeling of the quadrupole electrode system and numerical analysis of the non-uniform electric field in 3-D provided more insight into spatio-temporal electric field dynamics than has been reported in previous studies, if conducted at all. Specifically, time domain approximation of the electric field allowed for the dynamic evolution of the localized pulse waveform to be observed and the electric field vector to be identified and integrated into comparative analyses of *in vitro* responses.

The characterization of these exposure-response relationships represents the third main contribution of this dissertation. The comparative analysis of electropermeabilization responses to unipolar and bipolar pulse waveforms contributes to existing quantification of this relationship through access to the corresponding field vector data that permits better understanding of the nature of the membrane response. A broader spectrum of continuous, distributional unipolar and bipolar nsPEF intensity profiles is provided in tandem with biological effects against a greater range of data with which to better assess BPC and nsPEF-response relationships in the same sample, such as macro-biological investigation of dielectric polarization. Visualization of gradient responses also provides a more precise estimate of transitional states, namely the critical

threshold for cell electropermeabilization, than other studies using discrete nsPEF data allow.

Finally, preliminary assessment of the CANCAN technique using this multimodal exposure system demonstrated that some superposition of synchronized nsPEFs occurs in the fringe field of blunt-end electrodes. This challenges the paradigm that effective electrode-based treatments are limited to regions proximal to electrodes. Preliminary findings presented here thus create possibilities for the selective and controlled application of unipolar and bipolar pulses and further expands opportunities for remote nsPEF biomodulation technology.

In addition to the above, common features of multimodal pulse system operation are illustrated and important variables for designing experimental protocols using surface contact electrodes and a 3-D tissue model are highlighted. This dissertation contributes a holistic analytical approach that gives both bipolar cancellation mechanistic insight as well as a quantitative foundation to advance the state of medical nsPEF technology, supporting additional engineering research and design using bipolar pulses so that nsPEF-based treatment regimens can be optimized.

1.8.1 Scope and Delimitations

- NsPEF electropermeabilization was spatially examined in cells cultured in a semi-solid gel suspension after application of both unipolar and bipolar nsEPs to facilitate broad understanding of the biophysical effect that nsPEF magnitude, along with pulse polarity and electrode grounding, have in 2-D.
- Electric field strength is specified here as the explanatory variable rather than the broader term “dependent variable” because the same set of conditions that induce the membrane response can also be described in terms of the applied voltage (or pulse amplitude) and electrode geometry. It is also explanatory because limited understanding of the biological mechanisms means that the degree to which secondary or tertiary level interactions may influence nsPEF electropermeabilization is unknown.
- The biological endpoint was electropermeabilization, with the response variable defined as intensity of green fluorescence due to cell uptake of a nuclear dye tracer molecule. Cell membrane responses to nsPEF are known to correspond linearly with the electric field generated in/at the biological target under an ideal set of nsEP conditions [3]. The temporal dynamics of membrane permeabilization in general belongs in the realm of

biophysics, but since it was intended that this study leverage electropermeabilization to visualize and indirectly verify the electric field distribution, a single timepoint was used to measure the endpoint for all conditions tested. The investigation of other biological endpoints was outside the scope of this study.

- As electropermeabilization was predominately selected to aid visualization of a biological response that has been shown to correlate strongly with the electric field magnitude, the possible existence of bystander, abscopal or sub-cellular effects was acknowledged but beyond the scope of this study.
- It is acknowledged that both reversible and irreversible electropermeabilization could have occurred at various points along the nsPEF gradient formed in the quadrupole field, based in part on published research regarding membrane resealing after nsPEF exposure [63]. Confirming these dynamics across the area under study, however, was deemed unnecessary, given the relatively short (<30 min) period within which data was collected post-exposure.
- To maintain gel integrity and because differences in temperature have been shown to affect cell responses to nsPEF exposure, experiments were conducted at room temperature (25°C $\pm$ 2°C).
- To allow meaningful analysis of results for a given electric field value at a point in space, it was necessary to discretize fluorescence values across a gradient of ~5-10% of the in-sample range due in part to the inherent variance arising from inhomogeneity of cell distribution in the gel. Multiple exposures were performed in the same culture dish both to reduce inter-sample variation and to conserve resources. Notably, the exposures selected for this work relied on a gradient that would bracket the threshold expected for electropermeabilization.
- The models used to simulate nsEP delivery in order to numerically approximate the complex electric field were not optimized. The use of electrodes with curved surfaces and various combinations of high-voltage and ground electrode activation not only created a time-variant, inhomogeneous electric field, but also presented some challenges in assuring accurate measurements at edges and material interfaces. The goal in simulation was to obtain reasonably accurate field values that could be roughly verified based on well-known electropermeabilization response data and an available analytical solution for

the simple case of the electrostatic model. Despite this lack of optimization, the care taken to verify that Fourier transformed frequency spectra from experimental pulses matched software-determined excitation signal spectra, and to ensure dielectric material properties, mesh generation and input parameters obtained were sourced from published peer-reviewed research and in-house experimentation, provided confidence that values were well within expected ranges.

- The strategy of quantitatively assessing electropermeabilization in 2-D substantially expanded the data available for collection and thus the possibilities for exposure-response analysis beyond what was feasible for this dissertation. Numerous avenues for design modification and research interrogation therefore had to be restricted, beginning with electrode shape. Various designs were initially modeled with different diameters to determine which might produce the optimum focused electric field. While a rounded applicator would have minimized fringe effects, a pre-made custom blunt-end wire quadrupole electrode design was selected due to the challenges of locally manufacturing a potentially more effective set of electrodes and of determining the proper perpendicular alignment.
- The higher-dimensional complexity associated with this research also necessitated narrow delimitation of exposure parameters. The independent variables were thus limited to a pulse duration, pulse number and repetition rate of 600 ns, 50 and 10 Hz, respectively, for all experiments. It was already well known that applying multiple pulses does not simply lead to additive effects, so the pulse number *N* of 50 pulses was selected to avoid: 1) electrical breakdown at the load, which occurred during experimental optimization at N = 100; 2) consequential heating, and 3) excessive time between sample exposures. The choice of 10 Hz was also selected to minimize exposure time and to be consistent and enable later comparison with the results of the linear quadrupole electrode study. Pulse duration is defined as the time between the waveform's rising and falling edges representing the full width at half the maximum amplitude of the pulse (τ_{FWHM}). A 600 ns trapezoidal pulse was selected to ensure that membrane effects could be expected at relatively low pulse numbers for a wide range of voltages. Previously published studies had shown that the 300 and 600 ns pulses above 5 kV/cm typically cause

electropermeabilization in the same 3-D cultured CHO-K1 cell system used in the current work, which could be easily visualized and quantified using stereomicroscopy [4, 5].

- A limited number of experiments were performed to pilot test the CANCAN technique due to both time constraints and to the current electrical configuration of the pulser.
- Given the array of exposure conditions and surface area requiring analysis, biological results are largely reported on only three experiments for each condition. While this sample size may have been too small to ensure high enough statistical power to draw significant inferences about the validity of hypotheses, it was nonetheless informative in cases where sample standard deviation was low and was sufficient to provide evidence of the reproducibility of the main results.

1.8.2 Dissertation Outline

Chapter 2 reviews major findings to date on common observations regarding BPC, postulated mechanisms and limited techniques employed to explore these and other nsPEF studies, as well as challenges to developing useful applications based on BPC. It provides the theoretical foundation of this investigation and concludes by introducing a potential biomedical application using CANCAN based on two quadrupole electrode configurations, the latter of which is the focus of this dissertation.

Chapter 3 describes the exposure and 3-D cell suspension system components and details of the experimental methods employed, including the commonly applied protocols for image and fluorescence data collection, processing and analysis.

Chapter 4 describes the analytical and numerical framework for the *in silico* determination of the 2-D electric field, including parameters for and results of modeling and simulations used to approximate the inter-electrode electric field distribution and correlate with electropermeabilization responses.

Chapters 5 and 6 present the specific approaches, results and discussion regarding in vitro unipolar and bipolar exposure experiments, respectively. Chapter 7 incorporates a pilot study performed involving the application of the CANCAN technique, then provides a qualitative and quantitative assessment of the remote stimulation potential of this technique in the context of findings from Chapters 5 and 6 as well as from published research.

Chapter 8 summarizes the dissertation, highlighting factors contributing to experimental outcomes, and concludes with recommendations for future research and an overall interpretation of the findings.

1.9 Conclusion

This dissertation presents a systematic study of a basic four-electrode array for greater nanosecond pulse delivery options and flexibility in electric field generation. Using verification, validation and evaluation processes that include system characterization, modeling and simulation, *in vitro* experimentation and multi-dimensional data analysis, it will show that nsPEF technologies may be made more biologically effective by improving the control of nsPEFs. Comparative studies performed under this project will allow pulse and synchronization parameters to be determined that will elicit desired special cellular responses.

CHAPTER 2

THEORY AND LITERATURE SURVEY

2.1 Introduction

This chapter is included to provide contextual information on topics relevant to the work outlined by citing major conclusions, findings, and methodological issues related to the gaps in knowledge identified in Chapter 1. The chapter thus begins with a background section that includes quadrupole electric field foundations, namely multipole expansion and superposition, followed by an overview of how certain biomarkers used to measure cell membrane permeabilization are relevant to the field of nsPEF research. It then provides a summary of major research findings on bipolar cancellation in non-excitable cells to date that laid the groundwork crucial to performing the 2-D analysis for this work, specifically the roles of asymmetry, inter-pulse delay, and phase order on biological responses.

The next section comprises the theoretical framework for the dissertation, starting with an examination of competing theories on the electric double layer. Proposed mechanisms responsible for bipolar cancellation emerging from nsPEF research are explored next. A simple model of unipolar versus bipolar nsPEF electropermeabilization that informed the work is described and provides justification for an analytical approach to the overall research problem.

The third and final section critically reviews the current empirical literature and technology pertaining to nsPEF and bipolar cancellation research to expose the paucity of quantitative and interdisciplinary analysis in certain areas, which underpinned the major motivation for this investigation. These mainly regard the exposure system employed, electrode design, exposure method, and visualization and quantitative analytical approaches. The latter portion introduces the design for applied BPC, which is the major comparative source for evaluating remote stimulation by CANCAN. The chapter concludes by exploring how the identified gaps are addressed in the current work, underscoring the overall significance to expanding understanding and application of bipolar cancellation to the field of nanosecond pulsed electric fields in medicine and biomedical research.

2.2 Historical Context and Technical Concepts

In order to understand the phenomenon of BPC and identify optimal strategies for manipulating nsPEFs and their biological responses in 2-D, knowledge of the general technical concepts, variables, terms and issues that defined this research, and the experimental methods and analytical techniques used to conduct the related research, are required. This section contextualizes the current study by identifying and defining key tenets of electric field theory from the perspective of both the laws of physics and electricity. Specifically, a general introduction to the point charge model with respect to the linear quadrupole and the role of superposition in creating the non-uniform electric field distribution is presented. This is followed by an explanation of how fluorescent biomarkers, in particular YO-PRO-1®, are used to visualize and quantify cellular responses to nsPEFs. The section concludes with a comprehensive overview of the main findings and conclusions of research on bipolar cancellation.

2.2.1 Quadrupole electric field foundations

2.2.1.1 Multipole expansion and the quadrupole electric field

In order to understand how an electric field can be manipulated, it is necessary to first consider how the electric field relates to the distribution of charges in space. The measure of a system's overall electric polarity – a major theme of this dissertation – is defined by its dipole moment, which is a measure of the separation of positive and negative electrical charges (in Coulomb-meter or Debye units). An electric dipole, which describes a system of two opposite charges that, theoretically, are infinitely close together, can be defined by the first-order term of the multipole expansion. In principle, a multipole expansion provides an exact description of the potential and generally converges when the sources (*e.g.* charges) are located close to the origin and the point at which the potential is observed (at a distance, r) is far from the origin; or the reverse. This expansion can be made in the Cartesian coordinates x, y, and z by applying a Taylor series, numerous examples of which exist in the literature but are not elaborated on here.

In the simple point charge model system of a monopole, for a single charge in a vacuum, where r represents the distance to a test charge q' at some point distal from the point charge source, the electric field strength decreases as $1/r^2$ at large distances. The simplest case of an electric multipole [64] is described as a dipole, where two point charges have charge magnitudes of $\pm q$, with each positive and negative charge separated by a distance d. Compared to the

monopole electric field, the dipole field decreases as $1/r^3$. For this case, the electric dipole moment has a magnitude

$$\hat{p} = q\hat{d},$$

where $\hat{d}$ is the displacement vector, unless $s = d/2$ is used to denote the distance from each charge to the center of the dipole. The direction of both $\hat{p}$ and $\hat{d}$ is from the negative charge to the positive one.

In the same manner that dipoles arise from point charges, quadrupoles arise from dipoles. An electric quadrupole represents a second-order multipole and consists of a charge distribution of two identical electric dipoles whose dipole moments are of equal magnitude, but opposite in direction, and which are separated from each other by a small distance *s*. Fig. 2-1 illustrates two quadrupoles formed from two different dipole orientations: a) anti-parallel arrangement and b) linear. The relationship between the electric field, the charges and their location are described in the general case by a set of five independent values that together constitute the quadrupole moment of the system. In either case, the absolute value of the quadrupole moment is equal to 2*e*la, where *e* is the charge, *l* is the dimension of the dipoles, and *a* is the distance between their centers. Given two opposing dipoles at a finite separation *s* and taking the limit of $s \longrightarrow 0$, the dipole moments *p* grow to infinity in such a way as to keep *ps* constant. At great distances from the axial center of the planar quadrupole, the electric field intensity decays as $1/r^4$.

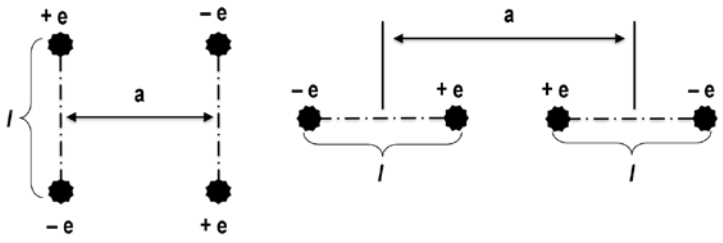

Fig. 2-1 Two dipole orientations forming quadrupoles with potential bipolar cancellation applications: a) anti-parallel (left); and b) linear (right) [2].

2.2.1.2 Superposition

The means to transform two biologically inefficient bipolar nsEPs into a biologically efficient unipolar nsEP stimulus is foremost owing to a property of electric waves and fields known as superposition. In a multiple electrode system, the principle of superposition can be used to determine the electric field at any point. The widely conserved *superposition principle* states that, for all linear systems, the net response caused by two or more stimuli is the sum of the responses that would have been caused by each stimulus individually [65]. In other words:

If stimulus $A \rightarrow$ response X, and; if stimulus $B \rightarrow Y$,
then stimulus $(A + B) \rightarrow$ response $(X + Y)$.

As the superposition principle applies to any linear system, the stimuli and responses may be numbers, vectors, vector fields, time-varying signals, or any other object that satisfies certain axioms. As a time-varying signal, electric pulse waveforms are thus included under these linear systems. They can also be functions, algebraic equations, linear differential equations, or systems of equations of those forms. A linear function is one that satisfies both the additivity and homogeneity properties that comprise the superposition principle, and are respectively defined as

$$F(x_1) + F(x_2) = F(x_1 + x_2), \text{ and}$$
$$F(ax) = aF(x)$$

for a scalar a.

A fundamental component of electromagnetism describes a physical interaction whereby a charge q placed somewhere in space produces an electric field around it in all directions in space. In a uniform field, as is the case between two parallel-plate electrodes, this field has a magnitude $\vec{E} = \vec{F}/q_0$, where $\vec{F}$ is the force exerted by the charge q on a secondary charge, q_0, independent of the presence of other charges in that medium. This field can be calculated with the help of Coulomb's law, which states that the strength of the electric field at position r due to a point charge Q, is given by

$$E = k\frac{Q}{r^2},$$

where *k* is a constant of proportionality determined experimentally to be 9×10^9 Nm^2/C^2. To calculate the electric field for a test charge, P, at the center of an ideal quadrupole, the net electric field *E* is then the vector sum of the related components [66]:

$$E = \overrightarrow{E_1} + \overrightarrow{E_2} + \overrightarrow{E_3} + \cdots \overrightarrow{E_n}.$$

Known as the *superposition theorem* when referring to electrical circuits, the voltage (or current) through an element in a linear circuit is the algebraic sum of the voltages (or currents) through that element due to each independent source acting alone [67, 68]. The superposition principle therefore allows for the combination of two or more electric pulses, as well as electric fields that are created when those pulses are used to charge electrodes. Consider the planar electric quadrupole in Fig. 2-2, described by the arrangement of four charged discs of opposite polarity on the corners of a notional square. The electric fields created by independently charged electrodes do not interact with each other but produce a net field that is just the vector superposition of the fields due to the individual charges emanating in all directions from each point along the entire surface of the electrodes. As such, although yielding a total dipole of zero, the fields created by the dipoles do not fully cancel out, except under the specific condition where the electrodes are in static equilibrium and charged to the same magnitude field, and even then the only location where the field is zero is at a single point, which is at the axial center in the plane. The total charge is canceled, but each point in space otherwise sees a different asymmetrical distribution of charges around it.

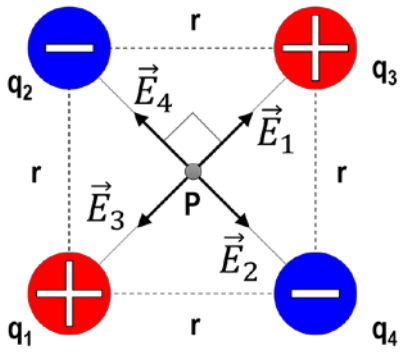

Fig. 2-2 Calculation of the electric field for a test charge, P, at the center of an ideal quadrupole, where the absolute values of the charges q_1, q_2, q_3 and q_4 on each electrode are the same.

2.2.2 Methods used to measure the electric field

The common sensor used to measure electric fields indirectly is an inductively coupled sensor known as a B-dot probe. It uses a single small receiving loop (antenna), the basic theory for which is described by Whiteside and King [69]. The probe functions by picking up part of the magnetic field generated by the pulse as it passes the sensor. The major drawback of this or any magnetic field probe is that the current distribution is induced by both electric and magnetic time varying field components. When placed away from the current flow, the coils are sensitive to the oriented magnetic fields, but the response depends strongly on the orientation of the coil axis, precise area and distance to the current axis. The B-dot probe is thus highly limited due to its sensitivity to the magnetic fields created by other spatial current distributions.

Another widely used electric field sensor is a field coupled sensor known as a D-dot probe, which is also used to measure pulsed electric fields. Favored for its non-intrusive installation, simplicity of construction, and potentially wide bandwidth, D-dot probes are used in combination with passive integrators / low pass filters, providing a broad band capability, but limited sensitivity. The probe has two elements that are sensitive to the same field but measure it in opposite directions. Their main disadvantage as a diagnostic tool in a non-invasive PEF application, however, stems from the fact that they cannot be placed near metallic components.

Where requirements dictate the need to measure an electric field in a very small or compromised space, an electro-optic sensor poses fewer challenges than B-dot and D-dot probes. Electro-optic effects are optical phenomena resulting from the application of a DC pulsed electric field. Electro-optic measurement techniques rely on how a given material rotates the

polarization of light passing through it, a property called birefringence for a molecularly ordered (optically anisotropic) material. Conventional techniques for measuring high voltages, which obtain electric field values indirectly, require that a small amount of the power from the system be consumed during acquisition. With an electro-optic sensor, measurement can instead be acquired from the change in material properties from the surrounding electric or magnetic field. The advantages of this type are its small size, high sensitivity, electrical isolation and immunity from interference due to electromagnetic radiation.

For biomedical PEF device applications, any of the above sensors may suffice given the right combination of size, material properties and configuration. However, in nsPEF research, there remains no reliable way to directly measure the electric field. Typically, inter-electrode spacing is too small to accommodate available probes, or the field is distorted by placement of the sensor itself or its proximity to conductive materials. This might be, for example, those that form part of the pulse generator, or platforms commonly used in experimental settings such as translational stages or microscope components. For these reasons, computational methods such as those employed for this work and described in Chapter 4, must be relied on.

2.2.3 Measuring cell electropermeabilization using YO-PRO-1® fluorescence

YO-PRO-1® (YP1) is a nuclear marker that binds to the DNA of cells whose membranes are compromised either transiently or permanently [70]. At a relatively large size of 630 Da, the dye is thus prevented from penetrating the plasma membrane of living cells. Exogeneous stresses, such as those caused by PEF application, or endogenous processes such as apoptosis threaten membrane integrity, permitting YP1 entry. The mechanism responsible for inducing permeabilization, which is common to multiple stress sources, involves the release of ATP and UTP molecules into the extracellular space, leading to the activation of P2X7 receptors [71]. This leads to the opening of cation channels, which then allows YP1 and other large molecules to enter the cell [71-73]. As cell death induction via P2X7 is complex and relies upon multiple factors, including the nature and duration of the stimulus and cell type investigated, positive YP1 fluorescence may or may not be an early indicator of P2X7 receptor activation and apoptosis [74]. This study focused on the use of YP1 fluorescence due to cell uptake as a method to quantify nsPEF electropermeabilization in 3-D cultured cells and changes due to the electric field gradient for comparison under different exposure conditions described in the next chapter.

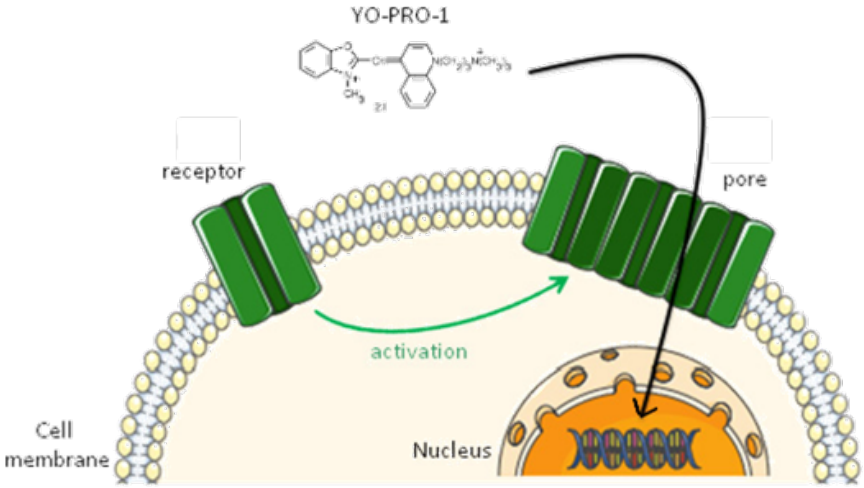

Fig. 2-3 Theoretical mechanism of Yo-Pro-1® molecule uptake [1].

Possessing a strong fluorescent signal, YP1 is used primarily to stain cells *in vitro* and in fewer instances *ex vivo* or *in vivo* [75-77]. However, YP1 can penetrate apoptotic cells in whole mounted live tissue specimens and was previously used successfully to assess the viability of pancreatic islets isolated post-mortem [78]. Expression of YP1 fluorescence has also been used to assess early apoptosis in swine and mouse liver tissues whose cell membranes were compromised by radiofrequency ablation [79]. Other studies have also used YP1 in hepatocyte spheroids grown in culture [80, 81], while a recent nsPEF study used it in 3-D culture of Chinese hamster ovary cells [82, 83]. Based on these findings, it was postulated that YP1 could be used successfully in 3-D cultures of mammalian cells after exposure to quadrupole nsPEFs to allow rapid assessment of electropermeabilization. For this study, cultures were prepared based on the protocol used in the same laboratory by multiple researchers [4, 5]. As a linear relationship has been demonstrated to exist between fluorescence intensity (based on optimized dye concentration) and nsPEF intensity (based on the pulse number and electric field combination) [60, 84-86], the hypothesis established was that YP1 would exhibit fluorescence proportional to the nsPEF magnitude, enabling mapping and spatial quantification of the electric field.

2.2.4 Features of bipolar cancellation (BPC) in non-excitable cells

While it is often necessary to cite studies older than five years to provide a thorough history of related research, as the discovery of BPC was made in less than a decade before the

work of this dissertation began, there is limited published research from which extensive conclusions may be drawn. The object is to acquaint the reader with existing studies relative to the gap in the knowledge and highlight relevant authors, and to describe such things as what approaches were used in terms of the methodology, instrumentation and statistical analyses. In experimental and modeling studies, the addition of a second, anti-polar phase to a monophasic nsEP has been shown to cancel the effects of the first phase for diverse endpoints, exposure conditions, pulse numbers, and electric field strengths [87]. As biological responses to unipolar nsPEFs were observed to be either absent or reduced when a second phase of opposite polarity was applied [58], bipolar cancellation (BPC) is generally defined as the attenuation or absence of a biological response normally resulting from a monophasic nsEP by application of an nsEP of opposite polarity. Given the limitations of current nsPEF technology, the ability to selectively apply bipolar or unipolar nsEPs to spatially stimulate or inhibit certain biological responses expands options for nsPEF generation. Despite relatively few empirical studies specifically directed at BPC to date, several conclusions have been drawn to support its application, many of which have been validated in at least one other study or model.

2.2.4.1 BPC efficacy given bipolar pulses of symmetric amplitude versus width

Early observations of the BPC phenomenon revealed that survival and intracellular calcium activation responses to symmetric-amplitude bipolar 60 ns and 300 ns phase width PEFs were significantly reduced compared to those from unipolar nsPEFs of the same amplitude [58]. In another study, which used multiple endpoint markers comprising Calcium Green 1, FM1-43, Propidium Iodide (PI) and FITC-Annexin V, responses to exposure from a symmetric 300 ns BP nsEP were attenuated compared to those for the UP nsEP, which had twice the phase width and thus overall energy, an effect which tended to abate at higher relative electric fields [59]. However, multiple studies with BP nsEP phase widths ranging from 60 ns to 900 ns, each individual phase being equivalent to the UP nsEP duration, showed that cell responses were not 100% cancelled by the bipolar pulse, despite delivering two-fold energy [2, 58, 83, 88].

2.2.4.2 The effect of introducing an inter-phasic delay on BPC

To tease out a temporal mechanism behind the effects of reversing the pulse polarity and corresponding field, multiple investigators introduced an inter-phasic delay between symmetric

bipolar pulse phases. They found that, for pulse widths ranging from 300 ns to 100 µs, the inter-phasic interval modifies BPC in a manner that is both time-dependent and saturable. For example, published work performed in support of this investigation showed that a 600 ns interval between a ↑600↓600 BP nsEP produced swelling and blebbing observed 20 s after pulse delivery, which was comparable to that observed for the UP, whereas relatively few blebs were observed with a 200 ns delay at 40 s post-exposure to the nsPEF [2]. In other studies, a step-wise increase in the time interval between the phases of a ↑300↓300 BP nsEP annulled BPC of nsPEF intracellular calcium activation and YP1 uptake to levels equivalent to a ↑300 UP nsPEF exposure, with effects gradually tapering out with increasing time delay between phases [58, 83]. In comparison, the efficiency of previously characterized BPC of YP1 uptake induced by symmetrical and asymmetrical BP nsPEF exposures (300–900 ns) was undone when the anti-polar second phase was delayed by 10 ms, resulting in highly effective membrane perturbation [89].

2.2.4.3 The import of pulse sequence on BPC for asymmetric waveforms

Results of studies on asymmetric BP nsEPs are perhaps the most revealing. Research first performed comparing the biological effect of BP nsEPs having phase width (duration) asymmetry showed that not only did a BP ↑300↓900 nsEP produce a strong response equivalent to that from a UP 600 nsEP (the absolute difference between first and second phase widths), but a diminished response equivalent to that from a UP 300 nsEP resulted when the sequence was reversed [88]. In contrast, results of biological exposures to BP nsEPs having asymmetric phase amplitudes (voltages) indicate that, overall, BPC occurs when the second, anti-polar phase is as small as 23% of the first, with peak cancellation occurring for an anti-polar phase of ~50%. Too strong a second phase reduces cancellation, and may have its own effect unless cancelled by an even smaller third phase [90]. Pakhomov *et al*. showed, for example, using 10 pulses of an 830 ns pulse at 5 Hz, that applying the positive (“anodal”, A-) phase at 400 V followed by an 800 V negative (“cathodal”, C+) phase was more effective than when the voltages were applied in the reverse order. This finding may only apply to rectangular-type waveforms, however, as under comparable pulse conditions Gaussian-type appear to produce even greater cancellation when the subsequent phase is more than 50% of the first [87]. Whether this might be due to the presence of a possible third anodal phase remains a valid research question worthy of investigation.

2.3 Theoretical Framework

The conceptual design of the quadrupole electrode system was achieved prior to this work and so is not the focus of this dissertation. As such, this section describes the theoretical framework that the research emerges from or is influenced by, providing the necessary structure within which the modular nanosecond pulse quadrupole system is evaluated. It includes an assessment of proposed mechanisms of bipolar cancellation, consideration of the electric double layer at both electrode-electrolyte and cell membrane–cytosol interfaces, and the basic model used to distinguish between unipolar and bipolar PEF induced electropermeabilization.

2.3.1 Mechanisms of BPC

The recent discovery of bipolar cancellation provides an opportunity to overcome the hurdle of nsPEF precision. The peculiarity of BPC is highlighted by the fact that bipolar nsEPs are much less efficient than unipolar nsEPs, even when they have twice the duration and assumed energy. Although considered unique to nsPEF, exceptions have been noted. For example, in the study by Sweeney *et al*. [60], it was found that short bipolar treatments induced significantly less permeabilization than did long, unipolar PEF treatments tens of microseconds in duration. The opposite phenomenon has been demonstrated in excitable cells and at longer durations. For example, biphasic bipolar pulses are known to improve defibrillation efficacy in canines compared to monophasic unipolar pulses [91, 92]. The former has also shown to be more efficient than the latter at stimulating fibroblast growth under low electric field (<5 kV/cm) and shorter millisecond (<5 ms) durations [93].

In addition to the parameters determined to correlate with bipolar cancellation, findings from the same studies support the conclusion that bipolar cancellation does *not* depend on pulse amplitude [88], repetition rate [87], frequency spectrum [87, 89] or the maximum electric field generated [94]. The phenomenon has otherwise not been predicted by models of conventional electroporation, and contrasts the effects of bipolar micro- and millisecond duration pulses, which typically are equally or more pronounced than unipolar pulses of the same total duration [2, 65, 83, 90, 95-97]. Since its initial discovery and demonstration in multiple cell types using various endpoints, several theories have been presented to describe possible mechanisms of bipolar cancellation, many of which are logical extensions of existing theories on how nanosecond pulses interact with cells *in vitro*.

A few theories have nonetheless been proposed to explain bipolar cancellation, including three that emerged from the seminal paper from Pakhomov *et al*. [58]. The first is based on the concept of assisted membrane discharge, which shortens the time when the membrane potential is above the critical voltage required for nsPEF electropermeabilization. The second views electropermeabilization as a two-step chemical process of charge transfer involving alternating reduction and oxidation events, which are then reverted with electric field reversal. The third considers a primary role for the electrophoretic transport of charged species (Ca^{2+} in particular), so that electric field reversal would decrease the net effect by driving these species out of the cell.

These mechanistic theories to explain bipolar cancellation are, however, nascent and yet to be empirically validated. Evidence is lacking for (e.g. ROS-modulated) charge transfer, and research by Gianulis *et al*. conflicts with the electrophoretic transport (at least in terms of Ca^{2+}) and assisted membrane discharge theories [83, 90]. The authors concluded that data points to electric field reversal as the more plausible explanation for bipolar cancellation, but this reasoning is circular. It is likely that the intent behind this statement, however, aligns with an idea advanced by Valdez *et al*. [88] through a theoretical model that relies on the membrane charging threshold for YP1 uptake and charging and discharging at the anode and cathode. The model describes cancellation as the counteraction of the initial phase (“front” pulse) charging effects on the cell membrane by the charging reversal of the second phase of a bipolar (“back”) pulse; the degree to which these overlapping changes to the membrane potential are driven by BP nsEP exposures and their symmetry. Findings from this model are, of course, limited to cells in a monolayer culture.

While proposed mechanisms of BPC have yet to be fully validated, there is sufficient evidence to support the exploration of how BPC can be applied to modulate nsPEF-induced biological responses. For current BPC theories to be advanced, they must be validated in more complex biological systems, with appropriate hypotheses that consider and incorporate perspectives from other fields of science, engineering and medicine.

2.3.2 *In silico* methods applied to probe mechanisms of BPC

Controlling for multiple variables is a persistent challenge in biomedical experimentation, which is why computational modeling has contributed greatly to medical research. Extensive

work focused on electroporation dynamics provides one quantitative foundation for elucidating BPC mechanisms. Incorporating experimental data produced by Gianulis *et al*. [90], Gowrishankar *et al*. [97] developed a computational model that showed how an extension of the standard electroporation model can account for the relative reduction in signal for a tracer molecule (e.g. YP1) by adding an anti-polar phase to a unipolar pulse, as well as for the recovery of the response from a unipolar signal (i.e. reduction in BPC efficacy) if the time delay between the first and second phase is increased. The model introduces an additional biophysical mechanism and hypothesizes that occluding molecules from outside the membrane enter or relocate within a pore, such that molecules near the membrane can enter pores to block transport of tracer molecules while still allowing small ions (charge number ±1) that govern electrical behavior to pass.

Other computational modeling by Merla *et al*. [98] focused on the frequency spectra of induced electropermeabilization by rectangular symmetric-amplitude BP nsEPs agreed with experimental evaluations of electropermeabilization-induced Ca^{2+} in CHO cells using 7.5 kV/cm electric field, 300 nsEPs. Their results showed that BPC is directly related and proportional to the low-frequency spectral component in the induced transmembrane potential reflecting the charging and discharging of cell membranes, consistent with the hypothesis that BPC is a consequence of the effects of mobile charge migration, which is driven by the low-frequency content of the applied pulse. As noted by Merla *et al*., in addition to the contributions of input pulse amplitude and phase, “experiment and theory regarding the role of mobile charge in the external medium must be extensively corroborated, and also will improve the robustness and reliability of predictions of bipolar pulse cancellation under all conditions” [98].

2.3.3 Electric double layer

In the discussion of nsPEF bioeffects, so far there has either been little mention of the nature of the electrode/electrolyte interface, or boundary effects are ignored in order to simplify analysis of cell membrane responses to an applied nsPEF. Obviously, any interface placed in an electrolyte solution will disrupt it since the interactions between a solid and electrolyte are considerably different to those in solution given inherent differences in their physical properties. Electrodes under potentiostatic control are subject to the additional influence of the charge held at the electrode. These contrasting factors result in strong interactions between ions and

molecules in solution and an electrode surface, giving rise to a region known as the electrical double layer.

Although multiple theoretical models have been advanced that may be represented by the illustration in Fig. 2-4, an electric double layer generally has three components:

1. Surface charge. Charged ions (typically negative) adsorbed on the electrode surface. First proposed by Hermann von Helmholtz in 1853 [99].
2. Stern layer. Counterions (ions whose charges are opposite to the surface charge), attracted to the electrode surface and held closely to it by the electrostatic force. Suggested by Otto Stern in 1924 [100]. Stern's theory states that because ions have finite size, they cannot approach the surface closer than a few nm.
3. Diffuse layer. A film of the solvent adjacent to the electrode containing free ions where the counterions are higher in concentration. The ions in this layer are affected by the electrostatic force of the charged electrode. The Gouy-Chapman diffuse double layer theory first introduced in 1910 includes a cloud of oppositely charged ions in the solution whose concentration decreases with distance from the surface. Stern's theory modified this, adding the Helmholz layer.

The purely diffusive double layer is thus formed to neutralize the charged surface, which causes an electrokinetic potential known as the surface potential, between the surface and any point in the mass of the suspending liquid. The magnitude of voltage difference relates to the surface charge and double layer thickness and is on the order of millivolts. The potential curve is useful because it signifies the strength of the electrical force between particles and the distance at which it becomes relevant. As ionic distance increases away from an electrode surface, electrical potential drops off approximately linearly and more steeply across the Helmholtz Plane than the Stern layer. This decrease becomes exponential across the diffuse layer, where the potential (zeta potential, z) depends on the electrophoretic mobility of the particle, dictated by the dielectric constant and viscosity of the liquid. It then approaches zero at the imaginary boundary between the Stern and diffuse double layers, called the slip plane. The ion concentration in the solution dictates the relationship between the zeta and surface potentials.

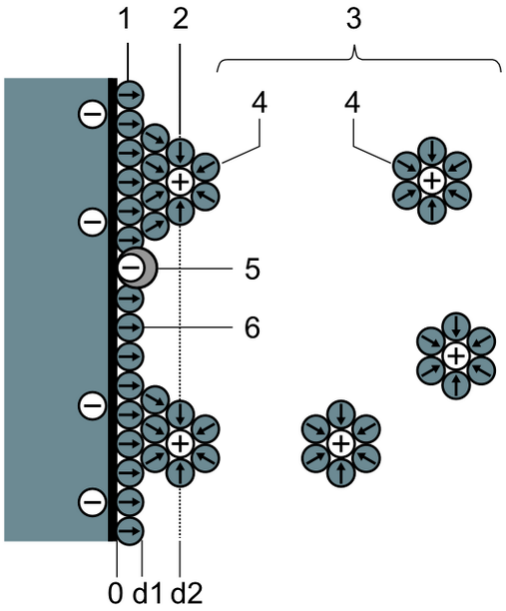

Fig. 2-4 Schematic representation of a double layer on an electrode (BMD model). 1. Inner Helmholtz plane (IHP); 2. Outer Helmholtz plane (OHP); 3. diffuse layer; 4. solvated ions (cations); 5. specifically adsorbed ions (redox ion); 6. molecules of the electrolyte solvent. (Source: "Electric double-layer (BMD model)" by Tosaka is licensed under CC BY 3.0.)

2.3.3.1 The bioelectric double layer

For biological applications, it is well known that the continuous movement of charged ions across a plasma membrane leads to net charges around the cell and hence, interaction of cells with an external electric field is expected. As introduced in Chapter 1, the electrochemical gradient determines the direction an ion moves across a cell membrane. In the mitochondria, proton gradients are used to generate a chemiosmotic potential, also known as a proton motive force, and this potential energy is used in oxidative phosophorylation to synthesize ATP. Second, a differential concentration of ions across the membrane adds a chemical component to the electrical gradient. These factors combined determine the direction of an ion's movement across a membrane that is thermodynamically favorable. The difference in the electrochemical potential on either side of the membrane provides the driving force that moves ions across the membrane. Since cellular membranes and cytoplasm possess diverse dielectric properties, each cell type exhibits specific characteristics, a property that makes a useful tool for identifying, manipulating or separating cells. It is also a property responsible for the diversity seen in cell responses to nsPEF.

A double layer in biological systems is the surface where two different phases of matter are in contact, as it is in electrolytic systems, but with several notable distinctions. Certain cell types have a glycocalyx, which is a highly charged layer of transmembrane macromolecules attached to the cell membrane. It functions as a barrier between a cell and its extracellular environment, mediates cell-cell interactions, and protects the cell membrane from direct physical forces and stresses, assuring membrane integrity. The glycocalyx can be modeled as a polyelectrolyte layer with a volume spread electric charge [101]. However, in reality, biological surfaces including proteins, macromolecules and cells carry various chemical groups with different dissociation constants, which give them diverse electric charges at physiological pH. The resulting constant ion exchange between cells and their liquid environments means that the two are not in equilibrium. Further, this sets up a difference in electric potential between the cell interior (cytoplasm) and external liquid environment known as the transmembrane potential [102]. This potential in turn affects the structure of the double layer [103-106], and its susceptibility to an exogenous electric field, as illustrated in Fig. 2-5.

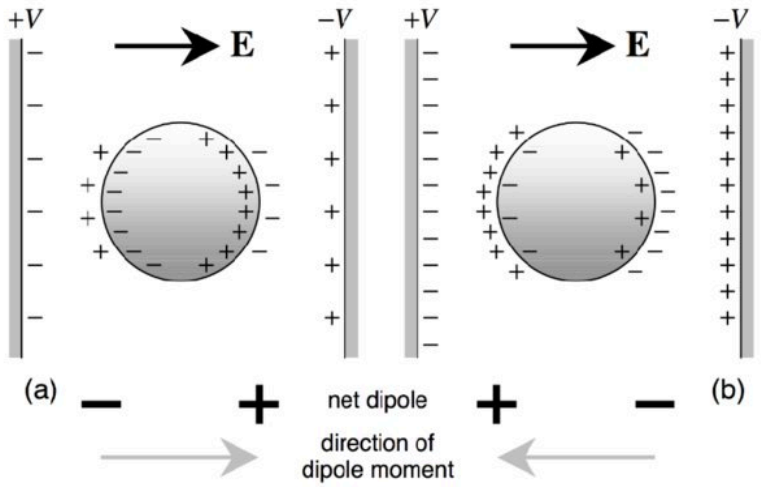

Fig. 2-5 Polarization of particles between parallel-plate electrodes if they have greater polarizability than the medium (a), and if the medium has greater polarizability (b). The direction of the net dipole is reversed for the two.

2.3.4 A model of unipolar versus bipolar nsPEF electropermeabilization

The design of optimum nanosecond electric pulse biomedical technologies capable of delivering focused pulsed electric fields to a target tissue area requires an understanding of how nsEPs shape the electric field in complex biological systems, and of how biological responses scale with the electric field and type of pulse delivered. These are in addition to considerations of electrode material, geometry and arrangement. The many existing models are aimed at understanding the physical mechanisms, rather than establishing a quantitatively accurate model.

For CANCAN to work there must be a significant biological difference between the spatial unipolar and bipolar responses. Electrode shape and the according distribution of individual charges are central to the effective implementation of CANCAN, but so is understanding the relationship between electric field strength and biological response. As nsEP BPC was discovered fairly recently, a comprehensive picture of bipolar nsEP potency is lacking. Potency is defined here as the electric field strength it takes to elicit the maximum biological effect. Due to BPC research emphasis on the pulse waveform and as BP nsPEFs were generated in most related experiments by parallel plate-or-needle electrode systems, the pulse number, repetition frequency, amplitude, width or sequence was varied while the electric field value was typically kept constant. As there is an electric field maximum for each phase of the BP nsEP studied versus one in the case of a UP nsEP with constant amplitude, the electric field referred to here is based only on the latter amplitude as a positive control variable.

A few studies nonetheless examined BPC using various endpoints *in vivo* and *in silico* at more than three nsPEF magnitudes for a general relationship to be assumed. Two independent studies were published on intracellular calcium concentration in response to varying nsPEF exposure magnitudes for both UP and BP nsEPs [58, 59], but direct comparisons are confounded because the researchers used different repetition frequencies and post-exposure measurement times. The first of these also compared YP1uptake against a range of nsPEF values, while the other compared PI uptake. Despite different endpoint markers and a limited range of values, a few common observations could be made: 1) UP responses in uniform fields are generally higher than BP responses; 2) responses to both pulse types are not linear below 10 kV/cm; and 3) a fluorescence signal saturation point occurs at higher fields for relatively shorter pulse widths. The lower limit of detection (LOD) is less clear as there are too few data points, especially for nsPEF values below 5 kV/cm.

For both UP and BP nsEPs, electropermeabilization as measured by PI and YP1 uptake has been shown to increase with increasing pulse number applied [83, 107]. Despite limited BPC data [6], a non-linear relationship below some critical electric field E_c can be attributed to sub- or incomplete permeabilization, above which is a linear response range whose slope depends on the potency of the exposure, followed by a saturation point that measures the maximal biological effect that an electric field can produce, or efficacy. These dynamics are illustrated in Fig. 2-6 for a notional investigation of membrane permeabilization, taking nsPEF magnitude as the abscissa and YP1 dye uptake, which has shown to be more sensitive to PEFs from UP than BP nsEPs, as the ordinate. The measure of the electric field magnitude that it takes to produce one half of the maximum effect is designated by EC_{50}, which stands for Effective Concentration at fifty percent efficacy in traditional pharmacological intervention.

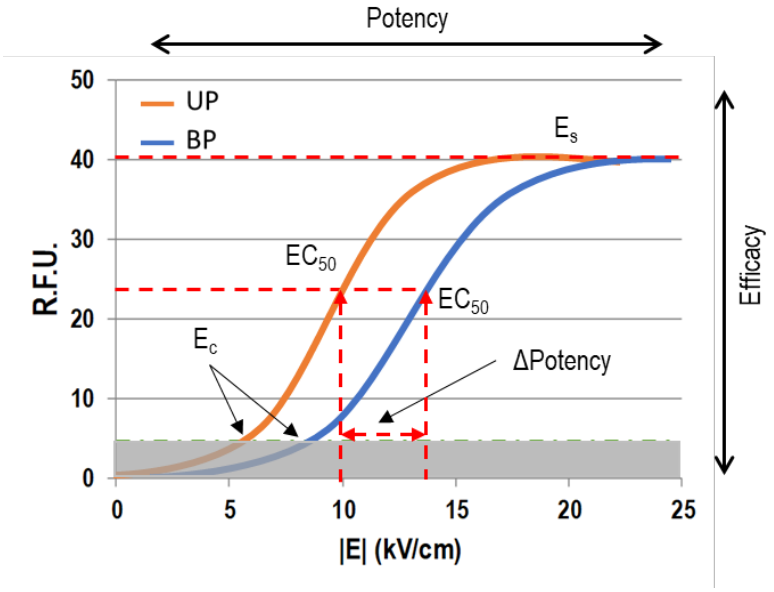

Fig. 2-6 Representative unipolar versus bipolar response curves under ideal conditions.

NsPEF exposures using parallel-plate or parallel-wire electrode geometries are popular because they generate a uniform electric field in the target area that allows for easy calculation of a discrete, absolute field strength |E| that correlates with consistent biological data, thereby simplifying analyses and minimizing error. This approach is insufficient for BPC analysis, however, when one considers that a bipolar pulse polarizes the electric field vector, introducing a temporal component to the biological response that is not easily accounted for by making direct correlation to a single electric field value. Ibey *et al*. [59] previously concluded that BPC

efficiency does not depend on the maximum electric field, but the ability to discern precisely how the vector field influences cancellation requires detailed investigation.

Producing a practical nsPEF system capable of delivering treatment that is safer and more effective than conventional approaches requires optimized methods to identify the precise exposure parameters that will selectively elicit the favored responses. CANCAN may be a revolutionary approach to deliver pulses with increased focal ability and potential for deeper targeting, but presents challenges due to requirements for more complex pulse shapes and precise synchronization. The ability to independently deliver tunable unipolar and bipolar pulses, previously a major capability gap and was addressed by Ryan *et al*. (2018) in preliminary work leading up to this dissertation [2]. Themes specifically dealt with here are common to nsPEF biotechnology development in general, but are particularly crucial given the above CANCAN requirements: 1) electric field characterization; 2) visualization of electropermeabilization; and 3) post-exposure quantitative analysis.

Based on the assumption that the relationship between electropermeabilization and nsPEF strength is sigmoidal [108] for both unipolar and bipolar nsEP stimulations, with the former having higher potency, it was expected that CANCAN would only be effective in the linear range between E_c and E_s. If the effect size difference between responses is too small, as might occur near electrodes where field strength tends to be higher, CANCAN may not occur. It is therefore necessary to delineate the conditions under which the magnitude of the effect size difference between the unipolar and bipolar response is sufficient for CANCAN. Unfortunately, limited data is available comparing bioeffects along an electric field gradient.

2.4 Current Empirical Literature Relevant to the Research Questions

2.4.1 Exposure systems for polar modulation of nsPEF responses

2.4.1.1 Pulsed power sources

One of the challenges of designing novel and effective nsPEF modalities rests with the increased complexity of pulse shapes and precision synchronization. Understanding the differential effects of typically square wave electric pulses of short, medium and long nanosecond duration requires scalable high voltage pulse generators with the properties of fast rise and fall times, powerful driving capability, and long lifetime. Schoenbach *et al*. [109]

ascertained that nanosecond pulse generators that could allow for experiments on intracellular electrical stimulation need voltage amplitudes at values sufficient to not only charge the plasma membrane, but the membranes of subcellular structures, and create pores. Nanosecond pulse generators rely on the energy stored in a capacitor, an inductor, or a combination of both, as in the case of a transmission line generator. Scalable square-wave high voltage (up to ~250 kV) nanosecond pulse generators are available with fast rise and fall times, powerful driving capability (up to terawatt power, millions of volts voltage, and tens of thousands of amperes current), and a long lifetime, and to date have tended to exclusively produce unipolar or bipolar pulse waveforms [110]. These may be categorized as sub-microsecond (1.2 μs-600 ns), medium-short nanosecond (300-100 ns), short nanosecond (100-10 ns) or sub-nanosecond (800-150 ps) and commonly employ either non-solid state or solid state circuitry, though typically the latter, in addition to requiring costly power supplies to produce electric fields of such high magnitude [111]. These types of pulse generators are well-suited to nsPEF studies on cell populations (e.g. suspended in cuvettes or a gelatinous medium). While not the general focus of most pulsed bioelectric systems, various feed types and connections are also used to ensure impedance matching between the pulse generator and biological load—biologics such as sugars, proteins, nucleic acids or related combinations of these, or cells and tissues—that absorb the energy from nsEPs. These tend to have higher impedances than blood, for example.

The need for a broader range of applications and the ability to overcome the limitations inherent in those systems, however, has already spurred next-generation nsEP power design. These newer designs are in part thanks to the use of voltage-controlled switching that MOSFETs offer, but commercially available power MOSFETs are commonly limited to 1 kV, so the output amplitude of a single-stage pulse generator does not exceed ~5 kV. To overcome this limitation, two different architectures have been developed that enable scaling of the output voltage. The first employs a solid-state Marx bank; the second employs a pulse transformer. Each type has its advantages: the first has a shorter trigger-to-output delay time and is capable of producing low-jitter pulses with a linear input-output voltage relationship, making it possible to adjust each individual phase (width, delay, amplitude); whereas, the pulse transformer is a simpler, ultrafast, dual resonance pulse transformer with fewer components and a linearly integrated primary stage [112]. Prototypes of both configurations have been designed, built, tested, and are currently being used to charge nsPEF exposure systems.

A custom-built solid-state pulser was used to drive the delivery of polyphasic pulses that would enable more efficient investigations of bipolar cancellation. The generator consists of a series of the fundamental module, which includes a capacitor and a MOSFET switch. A positive or a negative phase pulse module can be produced based on how the switch is connected. Stacking the modules in series can increase the voltage up to 5 kV. Multiple stacks in parallel can create multi-phase outputs. As each stack is independently controlled and charged, polyphasic pulses can be created to produce flexible and versatile pulse waveforms. The circuit topology can be used for high frequency unipolar or, bipolar, high frequency nanosecond burst pulse production, creating numerous opportunities for the generator in electroporation applications, tissue ablation, wound healing and non-thermal plasma generation. These details are elaborated in a recent publication [2], as are preliminary results from its use in testing nsPEF modulation of membrane effects in 2-D cultured CHO-K1 cells on an inverted microscope, part of which are summarized in the next section. For the current work, the pulse generator was adapted to accommodate six modules which, with an appropriate electrode design, would allow for the superposition of independently delivered polyphasic nsEPs and manipulation of the electric field, and therefore consequential cell response, in space.

2.4.1.2 Electrode design

Different electrodes are developed for specific treatment purposes. Electrodes invented for experiment *in vitro* commonly employ any of the following designs: sheet electrode and electrode cuvette; electrodes with high-speed fluorescence imaging system; electrodes with patch-clamp; and electrodes with confocal laser scanning microscopy. Electrodes invented for experiment *in vivo*, however, have consisted primarily of unipolar electrodes, five-needle array electrodes, a single-needle bipolar electrode, parallel plate electrodes, or suction electrode.

Studies [19, 49] of nanosecond pulse effects on tumors have commonly been carried out with commercial electroporation cuvettes, modeled as parallel-plate electrodes, where fringing effects are negligible and the electric field distribution is assumed to be homogeneous. In published and ongoing efforts directed at tumor therapy, however, needle-array electrodes are employed for which quantification of the electric field distribution is not as simple. Others include penetrating, two-needle (dipole) arrays, non-penetrating parallel ‘needles’ (Genetrode electrodes, Genetronics, San Diego, CA, USA), plate electrodes (Tweezertrodes, BTX, Hollister,

MA), balloon catheter-based electrode for delivery of DNA and electroporation, spoon electrode for vascular electroporation, caliper-mounted electrode plate electrodes, conformable defibrillator pads for electroporation, and multielectrode array [113].

The obvious limitations of the above approaches thus far are that the electrodes are inherently invasive and thus damaging to the tissue, or the exposure system is not clinically relevant. The approach studied here sought to overcome these by using a 3-D cell culture system paired with a planar electrode system that could bypass the need for invasive nsPEF exposure by demonstrating cell responses to a surface-level treatment, as well as the possibility of perpetrating a cellular response distal from the electrodes.

2.4.1.3 Verification of bipolar nsPEF modulation in CHO-K1 2-D cell culture

As part of a research group contribution, the author processed and analyzed phase-contrast microscope images of CHO-K1 cells exposed to a single 600 ns square wave monophasic or biphasic pulse (with and without interphasic delay) enabled by the polyphasic pulse generator to contrast biophysical responses, namely swelling and blebbing. Details of this study have been published. CHO-K1 (Chinese hamster ovary) cells cultured in F-12 K medium and mounted on the stage of an inverted microscope were exposed in 600 µl of culture medium at room temperature to electric fields ranging from 20 kV/cm to 60 kV/cm cells through a pair of 0.1 mm diameter tungsten rods. Images were acquired at 10× magnification and analyzed in ImageJ (Fiji distribution). Cell swelling was exclusive to a 20 kV/cm monophasic nsPEF; swelling and absent-to-moderate blebbing appeared for a 30 kV/cm; and blebbing was prominent for 40-60 kV/cm nsPEF exposures. Cell expansion appeared to peak at 40 kV/cm for the monophasic stimulation, but the blebbing response remained less under biphasic stimulation for all nsPEFs in Fig 2-7(b).

2.4.2 Electric field characterization

Based on the review of over 200 published articles on the electroporation of biological cells by nsEPs, it was found that “there is not enough emphasis on the determination and description of the electric field to which biological cells are exposed or they are not described in adequate detail” [27]. The strength and distribution of an electrode-generated electric field in a biological medium depends principally on five parameters: voltage applied, distance between

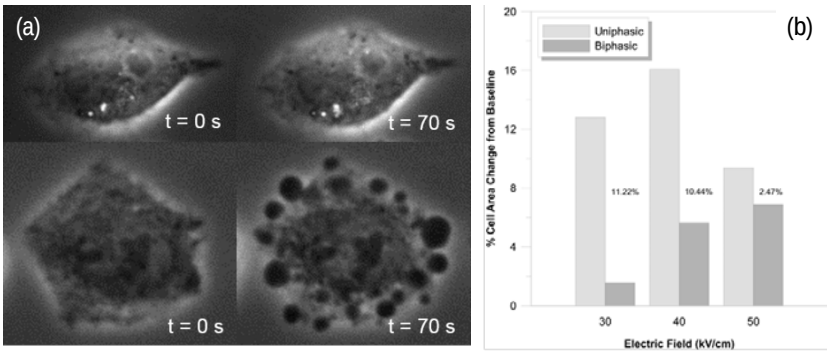

Fig. 2-7 Representative phase-contrast images of swelling and blebbing of adhered CHO-K1 cells due to a 600 ns pulse exposure. (a) Top: swelling from a 30 kV/cm nsPEF; Bottom: blebbing from a 50 kV/cm nsPEF. (b) 2D cell area difference in UP nsEP vs. BP nsEP exposure at t = 60 s, plotted as percent change from baseline (*t* = 0 s).

electrodes, electrode dimension and shape, tissue geometry and dielectric properties. For a square wave pulse, any biological effect of pulsed electric fields on cells depends on the pulse parameters of duration and number, as well as the electric field magnitude. The correlation between pulse duration and biological effects is such that multiple pulses are typically required for any application of nanosecond pulses, but their effects cannot be considered as simply additive [114]. Consequently, pulse parameter optimization has depended on educated guesswork and time-consuming experiments. Unlike pulse number, which is a discrete variable, the electric field is a continuous variable that has been discretized either for simplicity or from being inherently limited by the electrode system used to a uniform field.

As biological systems are inherently dielectric, the ability to predict where and how a nsPEF is being generated at or in a complex biological target is paramount to developing the precision-based medical nsPEF technology that CANCAN promises. To date, however, nsPEF studies have either been measured in uniform electric fields or in the linear region of an otherwise non-uniform field, ignoring effects closest to electrodes and limiting our understanding of the role of the electric field in BPC. The current study not only focuses on proximal responses specifically, but on a method to minimize them. This approach is supported by the use of modeling and simulation to approximate and visualize a non-uniform electric field distribution, which more complex electrode arrangements necessitate [115].

2.4.3 Visualization and spatial quantification of nsPEF electropermeabilization

The common use of primarily metabolic assays with optical spectroscopy has proved valuable as an indirect method of quantifying some effects of bipolar cancellation, but not the direct visualization of cell membrane permeabilization outcomes. Indirectly verifying the distribution of the electric field applied requires that biological effects from exposure are somehow observable. Tracer molecules such as YO-PRO®-1, FITC-Annexin V, FM1-43 and PI are commonly used in conjunction with fluorescence microscopy to visualize and spatially quantify nsPEF electropermeabilization in single or multiple adhered cells. Small ions such as Ca^{2+} are also used in PEF research to visualize the plasma membrane with fluorescent markers like Fluo-4, or Fura-2 [116]. Difficulties arise, however, in transitioning to more complex biological samples and systems. Parallel-plate electrode (cuvette) systems typical of high-volume cell suspension nsPEF studies, do not allow for observation of electropermeabilization, in addition to the fact that cells exposed to nsPEF in liquid suspension may be subject to rotational forces [117]. By comparison, a microfluidic electrode exposure design implemented by Oblak *et al*. [118] facilitated the direct visualization of dielectrophoretic differences in non-electroporated versus electroporated cells exposed to unipolar nsEPs at high and low frequencies in a non-uniform field.

In line with methods commonly for visualization, quantification of electropermeabilization fluorescence is typically performed in one of two ways. Vernier *et al*. [39] photometrically extracted pulse-induced changes to FM1-43 fluorescence intensity in human Jurkat T lymphoblasts after delivery of 4, 30 ns, 2.5 MV/m pulses from microscope images by defining and measuring pixel intensity over a cell region of interest (ROI). Other analytical methods have also been employed using differences in localization of membrane dye fluorescence patterns to compare cathodal versus anodal nsPEF electropermeabilization. For example, Valdez *et al*. [88] described dielectric polarization due to bipolar pulses of varied symmetries in individual cells by measuring a YP1 fluorescence profile across the cell membrane [88]. The majority of these studies have been in adhered single or small clustered cells so are naturally of particular value to investigations of membrane biophysics, but they do not account for differences in cell and tissue dynamics known to exist *in vivo*.

Membrane responses to nsPEFs have, nonetheless, been studied in larger cell populations using similar quantification methods. For example, an agarose gel-based 3-D tissue model with

stereomicroscopy was successfully employed in studies by Muratori *et al*. [4, 5]. In these studies, non-uniform nsPEF induced cell death by unipolar pulses from a pair of electrode probes were visualized by stereomicroscopy and quantified by measuring average PI fluorescence over a 2-D ROI between the electrodes. However, the area measured excluded the high-field regions closest to the electrodes and averaged a large area that accounted for 50% of the electrode gap distance, effectively obliviating the electric field gradient and insight into spatial-intensity dynamics in favor of a discrete value. By comparison, Chen *et al*. [119] used three different blunt-end wire electrode configurations to perform limited 2-D nanosecond electric field mapping of YP1 uptake fluorescence in monolayer cultured Jurkat cells. In the most recent example of related work, Gianulis *et al*. [120] reported only limited electric field data of YP1 fluorescence in 3-D cultured cells, which was only for a line profile.

For the present work, a combination and enhancement of the approaches used in these studies was applied in order to visualize and quantify nsPEF electropermeabilization. Fluorescence due to YP1 uptake in 3-D cultured cells was captured using stereomicroscopy, then multiple regions of interest were defined that spanned the full inter-electrode distance, to include the high-field area, in addition to beyond the electrode boundaries. A more refined electric field was obtained by numerical simulations performed in the time domain, which was overlaid with the florescence images to provide a more precise and continuous description of the relationship between electric field magnitude and electropermeabilization response across a gradient than previously reported.

2.4.4 Analysis of nsPEF outcomes

The multitude of parameters involved in efforts to demarcate effective parameters within which BPC operates, and nsPEF in general, has generated a plethora of data-generating opportunities. The downside is that this exploratory incentive has minimized the emphasis on analysis and outweighed the need for a more systematic assessment necessary to formulate more useful conclusions regarding BPC outcomes. These are largely inferred from statistically significant *in vitro* “exposure-response” differences between a negative (sham) or positive (unipolar nsEP) control and categorical variable (e.g. 50% BP nsEP). Few analytical approaches have considered, for example, the practical significance of these differences, validated models, or integrated findings into a larger system. The acquisition of comprehensive unipolar and bipolar

nsPEF response data for electrodes with complex geometry would enable spatial prediction of biological outcomes. As it stands, there has been no investigation of bipolar cancellation in a 3-D biological environment that spatially examines non-uniform electric field intensity distribution and can simultaneously be visually quantified.

2.5 The Quadrupole as an Ideal Electrode Arrangement for CANCAN

Two arrangements of a four-electrode array were considered to validate CANCAN as a proof-of-concept for a bipolar cancellation application. In the first, the electrodes are co-linear (*i.e.* reside on the same line) (Fig. 2-8(a)), while in the second, they are coplanar (*i.e.* reside in the same plane) (Fig. 2-8(b)). In either arrangement, any combination of high-voltage and signal ground electrodes can be selected depending on the location and strength of the electric field and corresponding biological response desired. The orientation of the dipoles and relative amplitudes of the h.v. pulses delivered dictate the position and strength of the resulting unipolar response. A "pure" quadrupole describes the ideal condition where the h.v. electrodes of opposing dipoles are charged to the same amplitude. Due to the temporal and spatial variation inherent in nanosecond pulse delivery, this is only one of multiple conditions applied in this study. For descriptive simplification, any use herein of the term "quadrupole" is solely in reference to the four-electrode arrangement, and not the specific distribution of electric charge due to the presence of four equal monopoles.

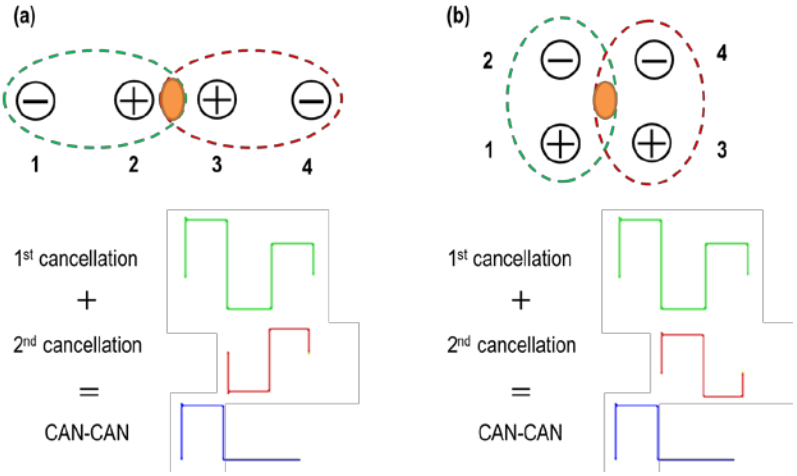

Fig. 2-8 Cancelation-of-cancelation (CANCAN) concept.

Fundamentally, a linear electric quadrupole is created by superimposing two electric dipoles of opposite orientation so that their positive charges overlap, with the central source containing twice the charge as the outer sources. The first electrode configuration considered for CANCAN is a modified linear quadrupole, where instead of a single $2q$ charge element at the center, the charges are separated by some gap, d_g, into two electrodes. The electric field in this case is represented analytically from Coulomb's law by vector addition of the fields such that cells placed in the field between the outermost electrodes would experience a force in the direction of the cathodal electrode. If the anodal electrodes are charged to the same voltage, opposing dipoles are created such that the electric field between them is cancelled. Synchronizing delivery of a matching pulse at the second phase of a polyphasic pulse as in Fig. 2-8(a) then means that cells located at the quadrupole center are exposed to a unipolar electric field based on the magnitude of the voltage from the first phase of the initial polyphasic pulse.

Gianulis *et al*. [121] recently validated bipolar cancellation in the linear system and demonstrated CANCAN between the interior electrodes by superposing nsEPs of various phases. However, effects were minimal, and a stronger effect is needed to be of practical use. This one-dimensional set-up makes for reliable, linearly directed nsPEFs that make exposure-response comparisons fairly simple and direct, but its practical use is negated by a target area that is limited to a narrow band. Further, the planar electric field region between high-voltage and ground electrode pairs is not unlike that of parallel wires, excepting that an agarose medium with high cell concentration and other dielectric components introduces capacitance and complex impedance factors. Outcomes based on the current studies using this system are relevant only to invasive applications. The planar quadrupole arrangement tested in this work improved upon the linear design by providing a two-dimensional, non-invasive exposure area with multiple sites for electrode activation and field generation, with potential for ablative application if penetrating needle electrodes are used to expand a surface area exposure to a volume of tissue.

The coplanar quadrupole was the configuration chosen for this work as it provided a two-dimensional area in which a linear, non-uniform electric field could be created, manipulated and quantified with minimal computational complexity [122]. As Fig. 2-8(b) shows, the quadrupole is created by aligning the four electrodes as if on the corners of a square. In the ideal form, dipole pairs are anti-parallel so that their positive charges are at opposite ends of the longest axis, which would create a null electric field at the axial center where the opposing vector fields are

generated. Applying the CANCAN method, adjacent electrodes (e.g. #2 and #4) are sequentially stimulated as in Fig. 2-8(a); only the cancelling pulse waveform is inverted due to the different vector orientation of the electric fields. Cells present in the perimeter gaps between electrodes would experience a bipolar nsPEF, whereas cells occupying the axial center of the quadrupole—the effective zone, where anti-parallel fields are superposed—are exposed to a unipolar nsPEF.

As with the linear quadrupole model, the superposition of electric fields in the coplanar quadrupole from selectively charging and grounding the electrodes in various combinations can create fields of differing magnitudes, and thus corresponding biological effects, at various inter-electrode positions depending on the direction and intensity of the individual fields created by the independent delivery of nanosecond pulses. The coplanar quadrupole system, however, offers significant advantages over the linear system. First, the 2-D arrangement increases the exposure area for practical application. Second, it moves the effective zone away from electrode surfaces to a distal target zone. Third, multiple site selection for active and ground electrodes provides options for the size of nsPEF area capable of being created. While only a pilot study was performed as part of this work, taken together, the above features advanced the concept toward a basic prototype to make spatial manipulation of nsPEFs possible. The production of a remote unipolar nsPEF (and its biological response) at a location then becomes possible when the delivery of appropriate pulse waveforms in the quadrupole configuration is effectively synchronized.

CHAPTER 3

RESEARCH DESIGN

The key objectives of this dissertation were to quantify and analyze the association between electric field strength, pulse polarity, electrode grounding and electropermeabilization in the 2-D plane perpendicular to the applicator end of coplanar quadrupole electrodes. The research design employed included the spectrum of descriptive, correlational, quasi-experimental and experimental quantitative approaches. NsPEF electropermeabilization was measured after application of unipolar and bipolar nsEPs to cells in a semi-solid gel suspension to facilitate better understanding of the effect these have on changes in cell permeabilization. Because nsPEF electropermeabilization responses are known to correspond linearly with the electric field generated in/at the biological target under an ideal set of nsEP conditions [3], electropermeabilization served as the biological endpoint, with green fluorescence due to cell uptake of the nuclear dye YO-PRO-1® tracer molecule serving the response variable. This chapter details the engineering and biological approaches taken in pursuit of the stated objectives. Section 3.1 provides an overview of the exposure system, including description of the exposure system components and experimental set-up. Section 3.2 provides cursory characterization of the pulse types and waveforms, including verification of the maximum applied voltages and corresponding Fourier transforms. Section 3.3 describes the general experimental methods and rationale for biological validation, along with the level of significance that will be used to accept or reject the hypotheses. The chapter concludes with a short summary.

In a scientific study, a pilot study may precede the central observation to correct any problems with the instrumentation or in the data collection techniques. In a quantitative study such as this one, a non-commercial instrument requires a pilot study to validate the effectiveness of the instrument and the value of the questions in which the right information can be elicited to answer the primary research questions. Most nsPEF studies are based on biological responses to the dipole electric field induced by a UP or BP nsEP applied to a single electrode with a signal ground (reference) electrode, where $V = 0$. The custom-built, flexible modular nanosecond pulse quadrupole electrode system employed in this study was modified from an earlier version, whose electrical characterization and validation of its ability to produce BPC in a microscopic

monolayer cell culture exposure to dipole electrodes was published in [2]. Described briefly in Chapter 2, the work served as a pilot study to demonstrate that further modification of the modular pulser to support a quadrupole electrode configuration could enable a broader study of bipolar cancellation in 2-D. The additional multipole expansion from the common dipole configuration thus allowed for the relationships above to be quantified in a non-uniform field under various *in vitro* exposure conditions, and for the potential for remote biological response modulation to be evaluated in 2-D. This in turn allowed for yet another pilot study to be conducted as part of the current work to test the instrument for its ability to elicit stronger distal electropermeabilization responses relative to the charged electrodes, and apply early results to support future refinements to both instrumentation and approaches to CANCAN toward the realization of remote nsPEF stimulation.

As BPC in space is being studied here for the first time, the approach to answering the research questions are in some cases exploratory. Otherwise, where sufficient knowledge exists regarding UP and BP nsPEF electropermeabilization, the null hypothesis is generally that the unipolar response is greater than the bipolar response where the amplitude absolute value of the second BP phase is <60% of the first. As detailed in Chapter 2, bipolar cancellation has been shown to peak when a biphasic bipolar nanosecond electric pulse has a second-phase (φ_2) amplitude roughly 50% of the first, but until now has only been studied one-dimensionally between a high voltage and a single ground electrode for a discrete electric field value. The first objective for this section was to validate findings in research published to date by applying asymmetric amplitude bipolar pulses with varied ground electrode configurations and compare results at select points in the 2-D plane. The objective here was thus to test this hypothesis by characterizing the BP spatial-intensity response relative to the UP response. With information at these discrete points in the plane, the final objective in this section was to examine the relationship between the unipolar electric field and bipolar cancellation response for the strongest cancelling pulse, to include developing a basic model for BPC that can be applied by researchers to estimate the electropermeabilization response for specified phase amplitude ratios.

To test the hypothesis that BPC efficiency is dependent on amplitude symmetry in space, cell responses to dipole-activated bipolar pulses were assessed at key points in the quadrupole plane: the axial center (A); the inter-electrode equator (B); and proximal to the h.v. electrode (C). Cell samples were exposed to nsPEFs generated by asymmetric-amplitude biphasic bipolar

pulses whose second (negative) phase amplitude was either 25%, 50% or 70% of the first. The objective for this section was to examine the relationship between the monophasic electric field and BPC response for a 50% BP nsEP due to its proven efficiency. Because the magnitude of the field is based off the peak applied voltage, there are two nsPEF maxima for a single bipolar outcome (YP1 uptake). Expressing the BP nsEP as a fraction of the UP nsEP allows for comparison of electropermeabilization based on the distribution of |E| for the first BP nsEP phase, which also represents the field for the UP nsEP.

Finally, this dissertation addresses analytical gaps by applying effect size statistics and linear regression analysis where appropriate to facilitate 2-D spatial analysis with greater predictive clarity. Regression analyses were performed to validate the fidelity of the dynamic cell permeabilization response pattern to the modeled electric field distribution and establish a quantitative framework with which to build predictive models of spatial cell permeabilization and bipolar cancellation. However, time and equipment constraints meant that, in some cases, sample size was too small to ensure statistical power was high enough. In these cases, rather than limit post-exposure analysis to tests of statistical significance, tests of practical significance were performed to measure the size differences of electropermeabilization effects between the pulse modes. These data were then used to generate simple mathematical models to describe bipolar cancellation.

3.1 Exposure System

Given that the complexity of studying nsPEF in a 2-D, non-uniform field with multiple pulse types left multiple avenues for analysis, the experimental portion was kept simple, relying on a single set-up and biological response endpoint. Fig. 3.1 presents an image of the three principal components of the modular quadrupole electrode system: the pulsed power generator, the quadrupole electrode applicator, and the 3-D tissue model. A benchtop electrical interface with copper D-sub pin connections (Digi-Key Electronics, Thief River Falls, MN) is used to allow manual switching of channel inputs between desired electrodes, which is independently enabled by a function generator. Resistors totaling 100 Ω in series ensure impedance matching between the pulse generator and biological load.

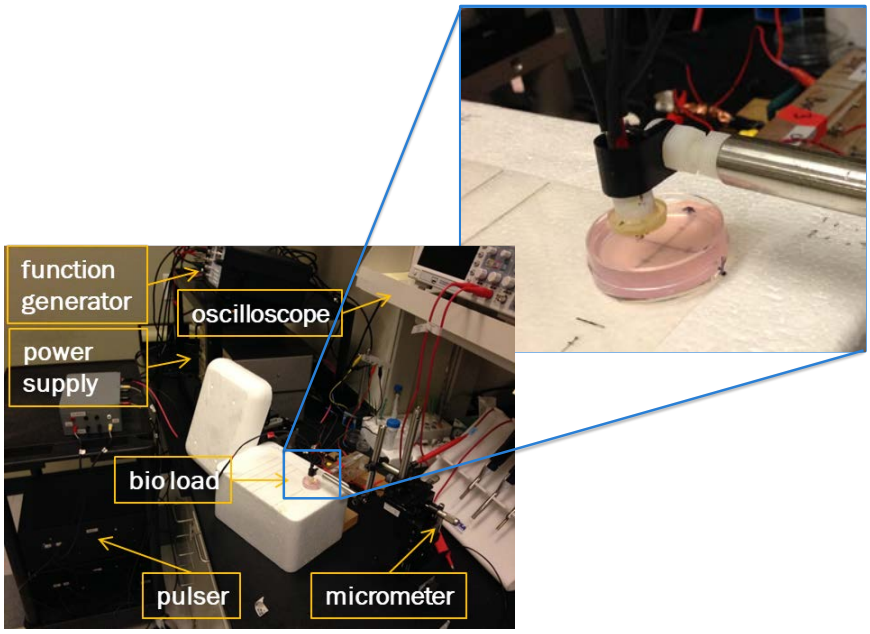

Fig. 3-1 Modular nsPEF exposure system. Pop-out shows the quadrupole electrode applicator with 3-D cell culture.

3.1.1 Modular nanosecond pulse generator

The high-voltage pulses necessary to deliver flexible nsEPs to the quadrupole electrode applicator were created by means of a modular nanosecond pulse generator that this author and others described in a recent publication [2]. It consists of a series of the fundamental module, which includes a capacitor and a MOSFET switch. Each module is responsible for the production of a positive and/or negative phase pulse. Stacking the modules in series can increase the voltage up to 5 kV, and multiple stacks in parallel can create multiple phase outputs. Each black box in Fig. 3-2(a) contains one or two stacks whose basic circuit is shown in Fig. 3-2(b), with each assigned to a specific channel and corresponding alphabetic designator (A-E). Because each module is charged by separate positive and negative DC sources and independently triggered, nearly any type of pulse can be created with or without a specified delay inserted between phases. The voltage and pulse duration can also be differentially adjusted. These features provided the flexibility this study required to produce versatile high frequency unipolar and bipolar nanosecond burst pulse waveforms of various pulse amplitudes and phase numbers.

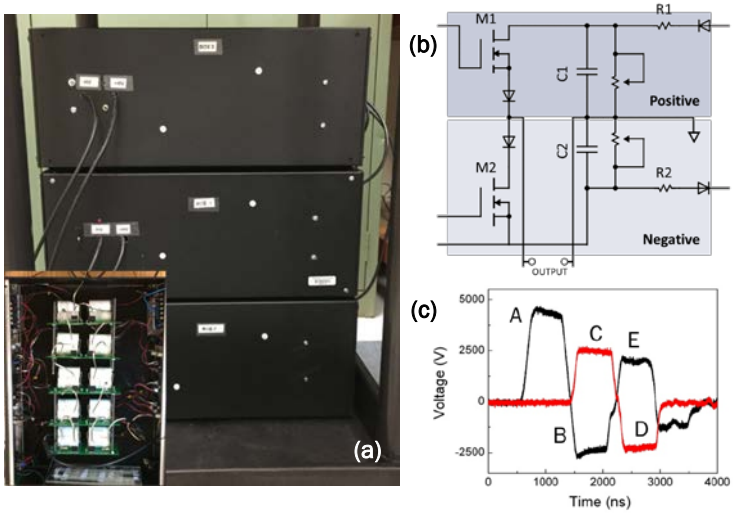

Fig. 3-2 Polyphasic nanosecond pulse generator. (a) 3 stacked modules; (b) basic circuit of the fundamental module (capacitor plus MOSFET switch) with positive and negative phase capacity; and (c) maximum source output voltage waveforms.

The input voltage is controlled at the power source for all channels, although Channel E is connected through a potentiometer, which serves as a variable resistor. While the positive and negative power sources may in theory supply respective voltages of up to 5 kV and 3 kV, the peak possible amplitude for each channel is limited by voltage dividing resistors connected through an external box (not shown). When measured across a 100 Ω load resistor, a 10% drop is seen between the charging voltage and actual voltage, which may be due to cross-coupling in the stacks across modules through the switches' parasitic capacitances. This limits the maximum positive charging voltage to 4.5 kV. Each of the five phase module channels thus has a maximum pulse amplitude (3-2 (c)) pre-determined by the resistors and limited by the positive and negative output voltage maxima as determined by the pulse capacity of the modular generator.

3.1.2 Pulse characterization

On a basic level, an electrical pulse can be characterized by its shape. Rectangular wave pulses have their amplitude at the peak voltage delivered from the power source and a duration measured by the time, τ_{FWHM} (full width at half maximum). Since most custom-built devices are not perfectly rectangular, τ_{FWHM} can best be calculated by first defining the rise (τ_r) and fall (decay) times (τ_f) and the maximum amplitude A_{max} of the pulse. Here, A_{max} refers to the overshoot voltage, whereas the amplitude encompasses the pulse plateau, and is defined by the

average of the voltage values ranging from the overshoot value to roughly where *dV/dt* drops by more than 10%. As in [123], rise time refers to the time required for the voltage to rise from 10% to 90% of the pulse amplitude. Similarly, fall time refers to the time it takes for the voltage to decrease from 90% to 10% of the amplitude value. Both times depend on the load impedance, which may vary with time, while the steady state value of the plateau region is also an important requirement for driving loads, in particular biological [123, 124]. Fig. 3-3 illustrates the waveform shape with $\tau_r \approx 120$ ns and $\tau_f \approx 75$ ns for a sample pulse. Although the pulse waveforms used for this research may be qualitatively described as quasi-rectangular or even asymmetrically trapezoidal, given that τ_r and τ_f are each <25% of τ_{FWHM}, in this work they are simply referred to as rectangular.

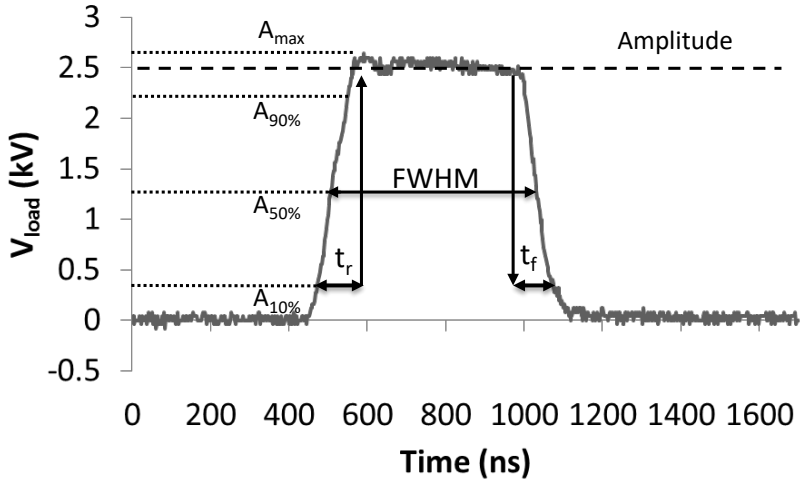

Fig. 3-3 Representative experimental waveform from a 600 ns unipolar pulse delivered at 2.5 kV to one quadrupole electrode with one grounded.

3.1.3 The Three-Dimensional Quadrupole Electrode Design

A linear quadrupole configuration of wire electrodes was previously suggested [125] as an ideal design for applying the principles described above to study the possibility of nsPEF spatial manipulation of bioeffects. Quadrupole conducting rod arrangements have long been used for applications in mass spectrometry [126, 127]. By applying either alternating-current (AC) and direct-current (DC) combined or AC-only voltages to four parallel rods of circular or

hyperbolic cross section, a dynamic electric field can be created to selectively filter gas-phase particles of a variety of or specific mass-to-charge ratios, which are axially ejected from the quadrupole center to a detector. The voltages are applied to the conducting rods in such a way that two opposing rods have the same voltage, while the other two have a voltage with opposite sign (+ and –, respectively). The voltages applied can be adjusted to manipulate the oscillations, and high voltages are not needed.

The operational principle behind manipulating charged particles by means of a dynamic electric field generated by a linear quadrupole is not all that far removed from what this work seeks to achieve using the same type of configuration. Rather than generate oscillating low-voltage electric fields to focus traveling gas-phase ions, the nanosecond quadrupole electrode system was designed to enable spatial manipulation of the electric field generated by high-voltage DC-powered pulses in order to create a localized response in a biological target. The response itself is based in part on the electrical properties of cellular charge carriers (ions and molecules) found in the cell membrane and intracellular space (cytoplasm). Depending on the spatial response desired, the nanosecond application may involve delivering a pulse to one or two working electrodes while the other electrodes are either floating or grounded.

The basic quadrupole electrode design used in this work is depicted by the model in Fig. 3-5. It consists of four blunt-end cylindrical-rod electrodes arranged at the corners of a notional square. Conceptually, this arrangement could allow for the treatment of a volume of tumorous tissue. The quadrupole electrode applicator consists of four blunt-end stainless steel solid wire conducting rods equidistantly spaced (“gap distance”, d_g) 1 mm apart, arranged in a square configuration. They are bound in place by a 3-D printed cylindrical Teflon housing, each having a radius, *a*, of 0.5 mm. Any one or more of the electrodes could serve as the high-voltage or grounded electrode.

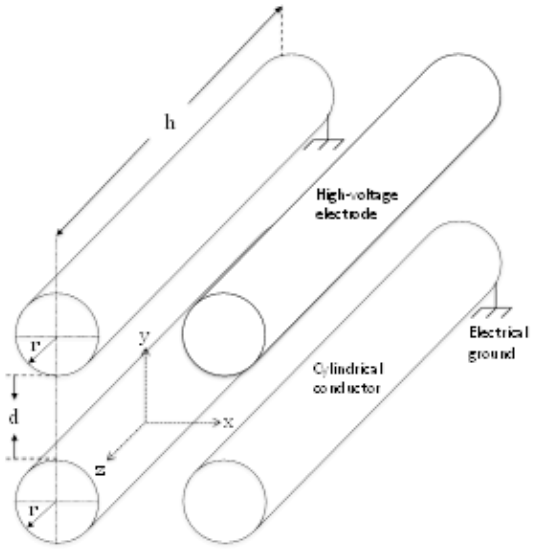

Fig. 3-5 Perspective plan of the planar quadrupole electrode arrangement in space (to scale).

As Fig. 3-4 shows, the applicator includes a disc-shaped plastic interface between the feed and operating end, which is simply a milled 35 mm culture dish insulated by an epoxy resin. This served simultaneously as a safety and functional barrier (from liquid immersion), as well as a physical marker to guide electrode placement for *in vitro* experiments. At the exposure end, the electrodes protrude at a height, *h*, of 5 mm past the housing. They are voltage-fed from the modular nanosecond pulse generator through the housing by contact stranded wires held in place with heat-shrink tubing (Fig. 3-1).

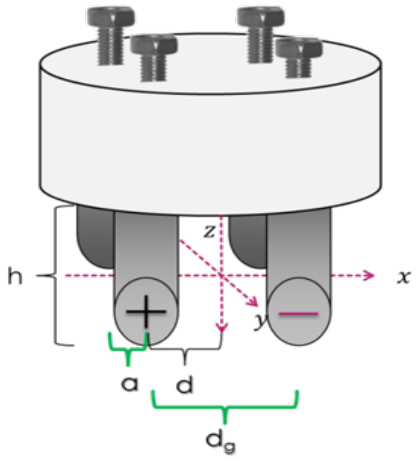

Fig. 3-4 Illustration of quadrupole electrode applicator.

3.1.4 3-D cell culture system

A Chinese Hamster Ovary (CHO-K1) immortalized cell line from the American Type Culture Collection (ATCC® CCL-61™, ATCC, Manassas, VA) was selected for all proposed nsPEF exposures. Cells with passage numbers between 12 and 26 were propagated on average over ~48 hours at 37°C with 5% CO_2 in air in Kaighn's Modification of Ham's F-12 Medium (ATCC 302004, Manassas, VA) supplemented with 10% fetal bovine serum, 2-mM L-glutamine, and 100-U/mL penicillin/streptomycin before being transferred to a 3-D tissue culture system.

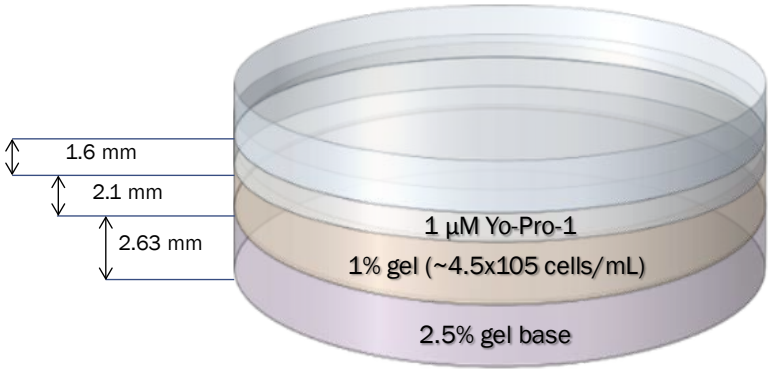

Fig. 3-6 3-D cell culture (tissue model).

Each 3-D tissue culture system was comprised of a 35 mm culture dish containing a 2.5% agarose gel base layer, followed by a 1% agarose cell culture layer, then a 1 µM buffer-dye layer. As a method was needed that could provide both visual and quantifiable data to measure and compare biological responses, the uptake of cell membrane impermeable green fluorescent nuclear dye YP1 was used to confirm positive membrane permeabilization as the biological outcome of exposure, and indirectly, spatial distribution of the electric field.

3.2 Electrical Characterization

3.2.1 Pulse parameter selection

The pulses delivered during biological validation experiments were either UP, BP or a synchronized combination of these (CANCAN). The Channel A waveform was chosen as the UP nsEP reference and positive control as it allowed for the highest possible amplitude and thus cell permeabilization response with which to compare all other exposure conditions. A second phase

was required to produce a bipolar pulse, so Channel B was paired with Channel A and adjusted at the negative voltage power source to modify the amplitude of the second phase. Since negative input voltages could not exceed 3 kV, it was not possible to produce a symmetric-amplitude BP nsEP without resorting to a lower energy pulse, which would limit the analytical range available for comparative study.

600 ns unipolar and 1,200 ns (↑600↓600) asymmetric-amplitude bipolar pulses with second phases approximately 25%, 50% or 70% of the first phase were selected for this work. As revealed in published research cited in Chapter 1 and in work recently completed by Gianulis *et al*. on the linear quadrupole system, 600 ns duration pulses consistently permeabilize cells, even at low amplitudes and pulse numbers. To maximize the likelihood of measurable cell permeabilization with YP1 uptake for all proposed exposure waveforms, a per-phase pulse width of 600 ns was thus selected as the first independent variable that was kept constant across all experiments. The second was pulse number *N*. As test experiments conducted at higher pulse numbers (100 or more) resulted in voltage breakdown at the electrodes and bubbling in the gel, an *N* of 50 pulses was chosen for all experimental conditions. The final parameter constant was a pulse repetition rate of 10 Hz, which ensured that cells would neither sit too long in PBS/YP1 or at room temperature prior to pulsing, nor be exposed to light at length post-exposure. For BP exposures, the listed waveforms were chosen: 1) due to pulse generator limitations on amplitude matching between positive and negative phases; 2) to ensure a sufficient magnitude spread for predictive modeling while setting reasonable limits on experimental requirements; and 3) to enable some comparison with data from the few published studies available that used similar bipolar cancellation parameters.

3.2.2 Electrical signals

Pulse waveforms were captured during biological experiments using two high voltage connected to a 2-channel, 200 MHz Hantek oscilloscope (DSO5202P, Qingdao Hantek Electronic Co., Ltd., Shandong, China), which served to measure and record the output (applied) voltage at the load. The applied voltage is determined relative to a reference electrode, which in this case is the grounded electrode. Pulse waveform traces were exported to a USB flash drive in .csv format. Characterization of system voltage data was performed to inform experimental design and electric field computations. Baseline waveforms at test amplitudes were initially

acquired using a 1X Dulbecco's Phosphate Buffered Saline (PBS) load, which has an electrical conductivity of 1.3 S/m at room temperature. For a charging voltage of 4.5 kV, comparison of input and output voltages in the conductive medium revealed a 46% loss. This reflected mismatched impedance that limited the maximum voltage that could be applied during biological validation experiments. Voltage waveform data was subsequently recorded during every experiment and used in numerical analysis of the electric field for each exposure type. Fig. 3-7 (a) shows typical UP and BP nsEP traces. Corresponding voltage amplitudes calculated by phase are provided in the experiment Chapters 5-7.

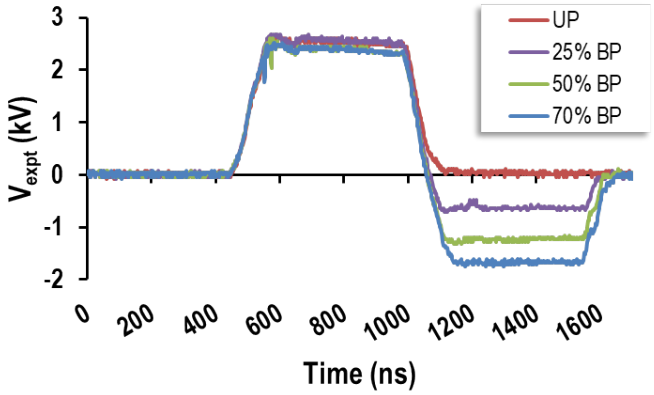

Fig. 3-7 Example of a 600-ns pulse delivered by a high-voltage pulse generator measured at the biological load.

3.2.3 Frequency Analysis

Fast Fourier Transform (FFT) frequency spectra for the UP and BP voltage waveforms used and shown in Fig. 3-7 are plotted in Fig. 3-8. The Discrete Fourier Transform (DFT) of time domain signals was carried out using the FFT implementation in the MS Excel® Data Analysis toolbox. The frequency composition of BP nsEPs differs from both UP nsEP and longer-pulse exposures. As specifically illustrated in Fig. 3-10, the frequency content of the BP pulse shifts to >1.1 MHz. The circuit model of the cell predicts that higher frequencies are less effective at permeabilizing the plasma membrane. As such, with inherently higher frequencies and less energy at lower frequencies, nsPEF exposures from BP pulses were predicted to be less effective than UP pulses.

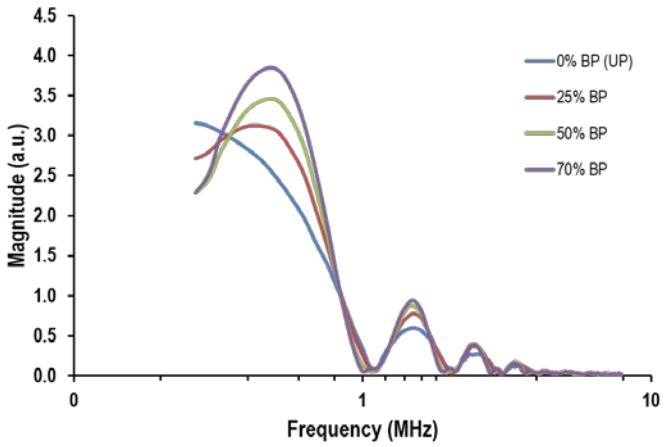

Fig. 3-8 Log-transformed frequency spectrum of the voltage signals in Fig. 3-7 computed by performing a Fast Fourier Transform and normalized.

3.3 General Methods – NsPEF Exposure, Data Collection & Analysis

3.3.1 NsPEF exposure protocol

After settling upon the pulse parameters, it was necessary to establish a protocol that could be employed for all exposures. For each experimental objective, selective activation of reference and ground electrodes was implemented according to the scheme in Fig. 3-6.

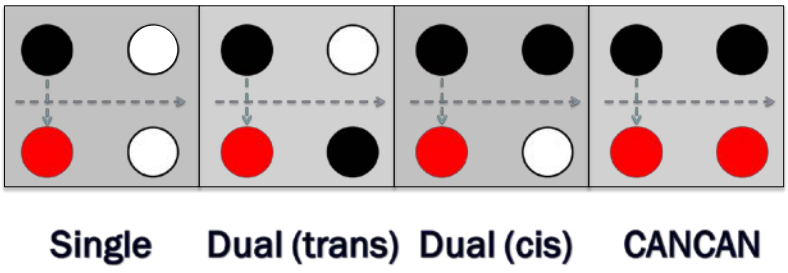

Fig. 3-9 Quadrupole electrode activation scheme for all conditions. From l-r: single ground (UP or BP); trans-dual ground (UP or BP); cis-dual ground (UP or BP); and CANCAN. Red: reference; black: ground; white: floating.

As Fig. 3-10 shows, after numerical simulations confirmed sub-permeabilization electric field magnitudes at locations distal from the activated electrodes, it was deemed possible to include four equally spaced exposures—allowing for a sham and positive control as well as two

test conditions—in one dish. To assist with electrode placement, the circumference of the Teflon housing, whose diameter was nearly equal to the inner radius of the dish, was used to guide the applicator with the micrometer perpendicular to a 4-quadrant grid, which was affixed to the platform below the translucent dish.

Each experiment proceeded as follows:

1. 3-D cell culture samples are prepared.
2. Prior to exposure, 1.5 mL dye mix is added to each dish and left to stand at room temperature for 5 mins.
3. Electrode applicator is lowered until electrodes have penetrated ~2.5 mm through the culture layer to the base layer.
4. Applicator is raised until electrodes are level with the top of the culture layer.
5. Four exposures are performed following a clockwise pattern, beginning with a sham control.
6. After 15 minutes, cell sample is moved to the stereomicroscope for imaging.

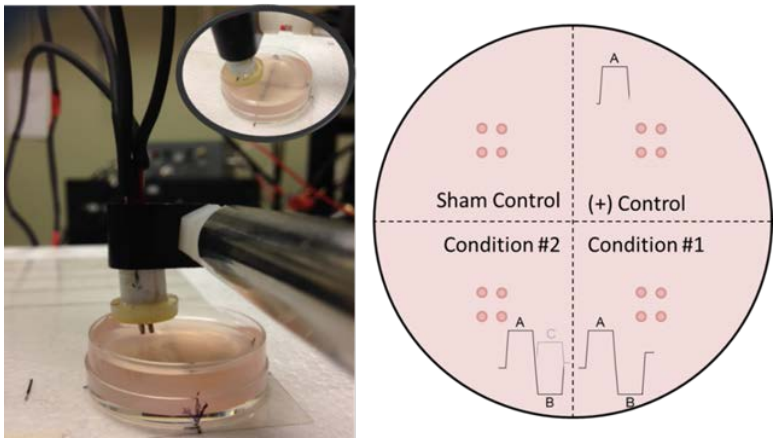

Fig. 3-10 Sample set-up for 3-D biological experiments.

3.3.2 Data Acquisition

Much of the following describes general techniques that were employed. Modifications or substantial departures from these specific to a given analytical approach are detailed in the description of results in the next chapter.

3.3.2.1 Electric field data collection

1-D line plots of the electric field solution were plotted from a 2-D cut plane of the 3-D model normal to the electrode surface (applicator end), minus 0.1 mm. Measurements were taken in this plane rather than in the plane perpendicular to the applicator end to reduce the likelihood of obtaining inaccurate results due to bending of the field lines at the electrode edges, an effect known as fringing. The field strength was recorded at various positions as in Fig. 4-5.

3.3.2.2 Sample images

2-D stereomicroscopy was used to visualize YP1 fluorescence in the immediate area encompassing the quadrupole electrode exposure. Imaging was performed using an Olympus SZX16 fluorescent binocular stereomicroscope (Olympus America, Hamden, CT) in conjunction with an Olympus 1.6× objective lens (NA 0.44). 1000×1000 pixel images were acquired by a Hamamatsu C9100 EM-CCD camera using NIS Elements microscope image acquisition software (Nikon Instruments, Inc.) at a resolution of 0.26 μm/pixel at 100 Hz (bright field). YP1 positive cells were excited by an X-Cite 120 Q Microscope Metal Halide Fluorescence Light Source (Lumen Dynamics/Excelitas Technologies Corp., Waltham, MA) at 200 Hz (GFP/FITC filter set: Excitation = 479 nm; Emission = 522 nm; Dichroic mirror: 497 LP).

3.3.2.3 Fluorescence data

The following general technique was applied as an initial processing step to acquire fluorescence data to enable post-processing quantification and spatial comparison of YP1 uptake between nsEP experimental parameters. A user-defined rectangular region of interest (ROI) was manually constructed in each image to measure the average fluorescence intensity at the locations specified in Chapter 2 or along a linear intra-electrode path. Dimensions of the ROI are 0.25 mm × 1 mm from the h.v. to ground electrode, or 3 mm × 0.25 mm between h.v. and ground electrodes bisecting the quadrupole. Each defined ROI was added to the ROI manager in the FIJI image processing package of Image J (NIH, Bethesda, MD). An example of this method is shown in Fig. 3-13.

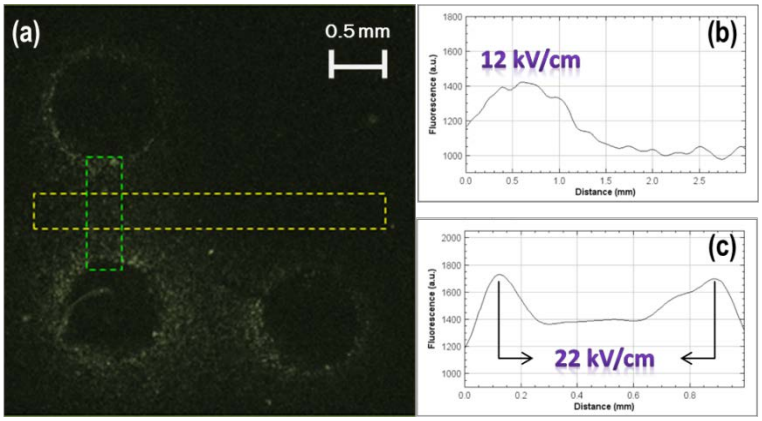

Fig. 3-11 Fluorescence image processing. YP-1 uptake from a trans-grounded UP pulse applied at 1.5 kV (a) and; post-filtered plots of intensity averaged from ROIs in the x-direction (b, yellow dashed) and y-direction (c, green dashed).

3.3.3 Data Processing and Analysis

3.3.3.1 Electric field, electrical signal and image data processing

Time-resolved values of the electric field approximation acquired *in silico* by averaging over the total pulse duration were plotted to make comparison with the experimental data straightforward. The peak voltage applied for each nsEP condition was measured by taking the mean of the plateau values from the waveform trace amplitude. Since the voltage excitation signal entered in CST Studio was set at 1 kV and because the electric field scales linearly, the experimental applied voltages could be used as a scaling factor against the *in silico* results to calculate the corresponding electric field distribution.

Post image acquisition analyses were performed using FIJI and Microsoft® Office Excel (Microsoft Corporation, Redmond, WA). All acquisitions represent 16-bit TIFF grayscale images. After sampling multiple filters (Fig. 3-14), a Gaussian blur (σ) was selected to reduce high frequency noise [128] in all quantified images, which is higher at lower relative cell concentrations. Background pixel data were subtracted to remove or reduce low frequency noise due to auto-fluorescence and ambient light. As sham exposures were performed in the same dish and were shown during troubleshooting to exhibit no YP1 uptake even after impressing the electrodes, absolute fluorescence was calculated by subtracting pixels measured from sham exposure images at the same inter-electrode ROIs from the same ROIs in the test sample images.

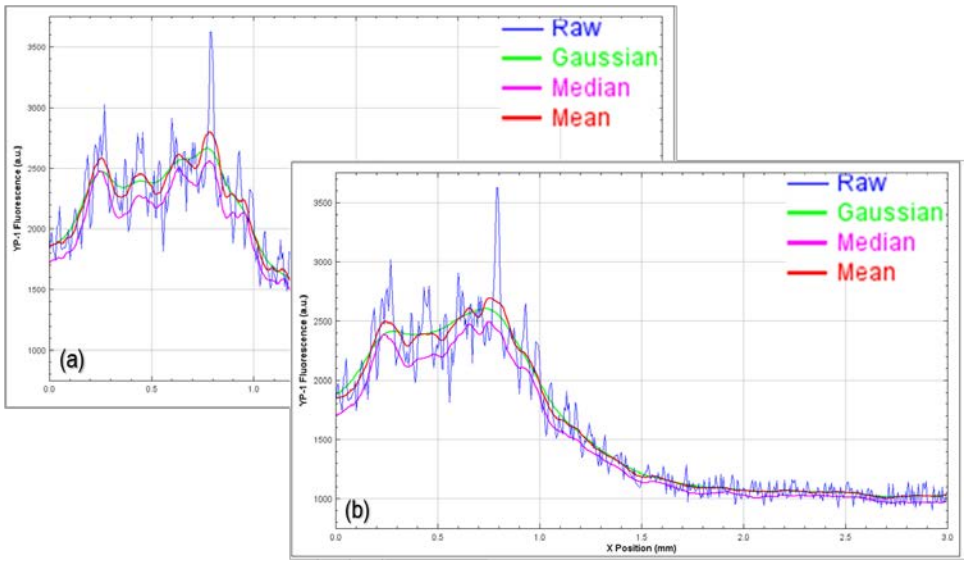

Fig. 3-12 Sample plots for various 8-pt (a) and 12 pt (b) filters applied to YP-1 fluorescence profiles of cells exposed to 600 ns pulses applied to a single quadrupole electrode at 2.5 kV.

Although ImageJ allows real-time identification of *x* and *y* coordinates, sample dishes were not aligned to an exact position on the stereomicroscope, leading determination of the exact midpoint between electrode impressions, for example, to be somewhat arbitrary. To reduce the influence of occasional outliers (for example, the presence of a cell or small clump of cells whose membranes were likely damaged during preparation), a square ROI was drawn around the outlier with a radius no longer than twice the outlier radius before the Remove Outliers feature in FIJI was applied.

3.3.3.2 Image data analysis

Preliminary data showed that YP1 uptake occurs on a gradient along with the electric field distribution. Data were either smoothed continuous or discretized, depending upon the type of analysis, the latter by averaging intensity across generally <0.1 mm in order to compare spatial-intensity relationships across pulse types at various inter-electrode positions of interest (P_i). For most analyses a YP1 line signal was created from fluorescence averaged within an ROI between h.v. and ground electrodes, or equatorially across the center, bisecting the quadrupole.

3.3.3.3 Statistical analysis

With the exception of CANCAN pilot experiments, data from a minimum of $n = 3$ independent experiments were included for all analyses. “Independent” here, for the case of *in vitro* samples, means cells tested under repeated experimental conditions were sub-cultured on different days at passage numbers ranging between 12 and 26. Cells replaced after late passage may in some cases have come from a separate frozen seed stock.

Two types of control variables were used depending on the type of analysis considered. The first was the negative (“sham”) control, included in every experiment (dish), which underwent the same procedures as other minus actual nsPEF exposure. The other is a positive control against which other exposure types were compared; for example, a unipolar pulse to analyze bipolar cancellation efficiency. Only one response (dependent) variable was considered: YP1 fluorescence, measured at 15 minutes post-exposure. Explanatory variables are electric field, waveform type, and position (point in the electrode plane). It is important to make the distinction here between a truly independent variable and explanatory variable. This is because the electric field generated for bipolar pulses is both vector-dependent and time-dependent and it is not yet known whether the cellular response also depends on other factors (e.g. pressure transients).

Data sets included in analyses are: 1) unipolar nsEPs at three input voltages (1, 3, and 4.5 kV); 2) asymmetric bipolar nsEPs of three different second-phase widths (approximate ϕ_2/ϕ_1 percent ratios of 25, 50 and 70); and 3) CAN-CAN synchronized nsEPs for biphasic/monophasic and triphasic/biphasic waveform combinations: 1). Simulation data are discrete and fluorescence data are continuous, unless the latter are discretized or categorized for specific types of spatial analyses. Descriptive statistics are presented as mean +/− SEM for *n* independent experiments unless otherwise specified.

Statistical analyses, which were largely performed using the Data Analysis tool in Microsoft® Office Excel (Microsoft Corporation, Redmond, WA), consisted of an unpaired two-tailed *t*-test when comparing the means of two groups. A *p*-value less than 0.05 was considered statistically significant. For the purpose of hypothesis testing, although the electric field in a quadrupole is non-uniform and *n* was typically small ($\lesssim 6$), given that most data was discretized, most distributions were assumed to be normal.

3.4 Conclusion

This chapter provided an overview of the research design for the dissertation, with emphasis on apparatus, technical and operational specifications, *in vitro* experimental techniques, *in silico* determination of the electric field approximation, and methods selected for data analysis. In the following chapter, results of modeling and simulation as well as biological validation experiments, are presented. Specific parameters or variations on some of the above methods only generally described are also detailed.

CHAPTER 4

ANALYSIS OF THE QUADRUPOLE ELECTRIC FIELD

The ultimate biological application for nanosecond electric pulses (nsEPs) relies on delivering an electric field of adequate intensity to the location where the expected effect is needed. Numerical simulations of the electric field distribution produced by the quadrupole electrode system were computed to provide the dosimetry for biological validation. Numerical analysis of the electric field formed by the delivery of a unipolar or bipolar nanosecond pulse or from applying the CANCAN technique was performed in the time domain in CST Microwave Studio. In order to map the electric field from a defined pulse to the biological response to nsPEF exposure, both the multimodal quadrupole electrode system and the 3-D tissue sample were first modeled in CST before implementing the finite integration technique to solve the given system of equations relevant to the structure. Additional information such as the position and connectivity of the electrical feed, numerical parameters, initial and boundary conditions and time step were defined externally and read by CST during execution. Finally, the solution was written to a plain-text output file used for post-processing.

4.1 Introduction

One of the fundamental challenges of electric field determination in integrated electrical-biological systems modeling and analysis is addressing the inherent complexity of working in a three-dimensional (3-D) environment. Unlike in the point charge model of a quadrupole, where the electric field is based on the summation of charges arranged in discrete units, if there is a continuous charge distribution over a conducting body, as is the case with electrodes used to deliver a nsPEF, the magnitude of the electric field must be integrated over the entire charged surface. This becomes an extremely complex endeavor, made more so by tissue dielectric considerations. However, when one takes advantage of the geometric symmetry inherent in common electrode shapes, the mathematical approach to field strength and distribution assessment becomes more straight-forward.

In the quadrupole electrode arrangement, if the origin is taken to be at the center of the square (between the rods), three planes of symmetry would need to be considered in the

approach to the electric field analysis in 3-D: the *xz* plane perpendicular to the *y*-axis that bisects the top and bottom dipole pairs; the *yz* plane perpendicular to the *x*-axis that bisects the left and right dipole pairs; and the *xy* plane perpendicular to the *z*-axis (axial center) that forms a cross-section of all four electrodes. However, in this work, the target region/area of interest is specifically the two-dimensional area bounded by the quadrupole electrode periphery at what would constitute the "applicator" end of the electrodes for an nsPEF technology that operates at a tissue surface. Analyses are thus confined to the *xy* planar region delimited by the outermost edges of the four electrodes. The axial symmetry of the quadrupole design used in this work allows for the 3-D electromagnetic problem to be initially approached using a 2-D model, thus significantly reducing the burden of calculating electric field values. It also supports numerical analysis and experimental validation of a non-uniform 2-D electric field distribution in a biological sample based on the delivery of different pulses to different electrodes, results for which are presented in the next chapter.

In the interest of simplifying electric field analysis and to take step toward assessing the potential for remote nsPEF biomodulation using the current electrode design, the geometric symmetry of the quadrupole electrode model is exploited to obtain simple expressions from the dipole to quadrupole expansion to obtain the maximum electric field. By utilizing this well-known approach, exact analytical formulas are obtained for the electric field as presented in the following section in terms of the electrostatic potential at the boundary of cylindrical electrodes, which can be used to estimate the same for the surrounding space and otherwise applied to the analysis of electromagnetic problems and computer simulations of condensed-matter media.

4.2 Theory

As there are two lines of geometric symmetry in the 2-D cross-sectional model of the nanosecond quadrupole electrode design —each one along the *x* and *y* axes—an algebraic expression exists that allows for simple calculation of the electric field near to the electrode edge. The field is produced by a uniformly distributed charge per unit length, λ, on each electrode. However, for the purposes of this work, it is assumed that each electrode's length, defined as height, *h*, is much greater than the gap distance, *S*, between adjacent electrodes so that the effect of fringing fields around the electrode ends can be ignored. Consequently, there is no component of electric field in the *z*-direction [121]. The rod electrodes under evaluation can be considered as

infinitely long compared to the wire diameter (1 mm) and inter-electrode regions being measured (< 0.1 μm^2). Therefore, treating the electric field distribution as a two-dimensional problem allows for some simplification of electric field calculations.

To find the maximum electric field, the geometry of the electrodes must be considered. Superposition can be used in electrical theory to simplify a circuit with multiple inputs and power sources, but calculating the vector field value at any inter-electrode point in this dynamic 3-D system cannot be accomplished using analytical methods. Despite the complexities of determining the electric field distribution in a biological medium between quadrupole electrodes under multiple time-variant pulse parameters, an analytical solution can be obtained for a constrained set of conditions. Some common electrode designs used in biomedical applications have elementary dimensions that can be described analytically to simplify the model for the purpose of calculating the electric field [129].

4.2.1 Analytical solution for the maximum electric field in parallel dipole cylindrical wires

One of the electric field geometries that can easily be derived from Gauss' law and is a foundation for the electrode geometry used in this work is the axial rod-rod model, which is equivalent to the sphere-sphere model when taken in two dimensions to represent the cross-sectional area. Theoretical investigations of the electric field strength in rod-rod (singularly, "cylindrical wire") model configurations have previously been conducted by multiple authors using known formulas [130-132]. In order to investigate the accuracy of the model electrode system, they provide an analytical basis, along with the annotated illustration shown in Fig. 3-5, against which results from the numerical simulation can be compared later in the chapter.

For the case of two thin parallel conducting rods of any diameter D, separated by a distance, 2*S*, from the center of a reference conductor to the center of the proximal conductor, two electric field quantities may be defined: the maximum field strength E_{max} at the rod edge and the mean value of the field strength $E_{mean} = V/d$, where d is the shortest distance between the conductors and the second is to a ground. These two quantities allow for a 'field efficiency factor' (originally proposed by Schwaiger) to be defined:

$$\eta = \frac{E_{\text{mean}}}{E_{\text{max}}} = \frac{V}{dE_{\text{max}}} \tag{4-1}$$

where η equals unity or 100 per cent for a uniform field. It approaches zero for an electrode with an edge of zero radius. The factor η is a pure quantity, however, and so only applies to electrostatic field analysis. In a more complex electrode arrangement, E_{max} may appear at any point on an electrode, not necessarily coinciding with the points providing the shortest gap distance, *d*.

The field distribution along the flux line may be calculated for the highest density, *i.e.* between the electrodes, where the field strength is highest. The flux line is that which lies directly between the dipole electrodes through the points normal to each curved surface. Assuming a total potential difference or voltage of *V* between them, the potential $\Phi(y)$ along this line starting at the point normal to the inside edge of the first electrode where $y = 0$, is given by $\Phi(y) = +V/2$. The field strength $E(y)$ can instead be expressed in terms of the gap distance, *S*, noting that the field distribution is symmetrical to $y = S/2$, using the following formula [130]:

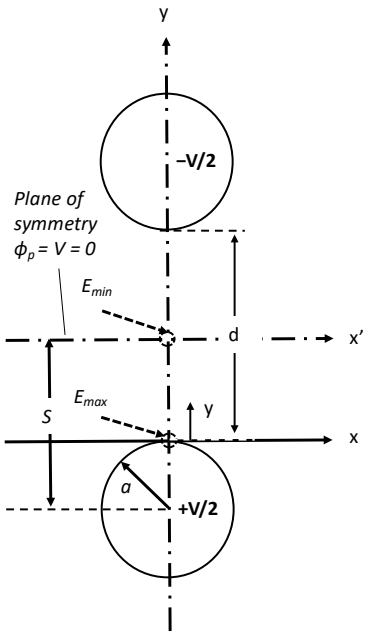

Fig. 4-1 A schematic of the 2-D electrode geometry of the cylindrical wire dipole, for which there exists an analytical expression for the mean and maximum electric fields.

$$E(y) = \frac{d\Phi(y)}{dy} = \frac{V}{x} \cdot \frac{\sqrt{\left(\frac{x}{2 \cdot a}\right)^2 + \left(\frac{x}{a}\right)}}{\left(1 + \frac{y}{a} - \frac{y^2}{a \cdot x}\right) \cdot \ln\left(1 + \frac{x}{2 \cdot a} + \sqrt{\left(\frac{x}{2 \cdot a}\right)^2 + \left(\frac{x}{a}\right)}\right)}\ , \tag{4-2}$$

where, *a* is the radius of the electrodes and *x*, *y* are the coordinates of the first electrode, while the coordinates of the second are (0,0). The field distribution between two cylindrical conductors can be more easily considered by relating equation (4-2) with the maximum field intensity E_{max} for $y = 0$. This ratio becomes:

$$\frac{E(y)}{E_{\max}} = \frac{1}{1 + \frac{y}{a} - \frac{y^2}{aS}} = \frac{a}{a + \left(1 - \frac{y}{S}\right)}\ . \tag{4-3}$$

For all values $y/S << 1$ the parallel conductor is of diminishing influence. As the minimum value of *E* is reached for $y = S/2$, the ratio E_{min}/E_{max} becomes:

$$\frac{E_{\min}}{E_{\max}} = \frac{1}{1 + S/4a}\ . \tag{4-4}$$

If the relationship is defined by the distance from the midpoint to the center of the electrode instead of by gap distance, *S*, where $y = d\text{-}a$, (2-4) becomes:

$$\frac{E_{\min}}{E_{\max}} = \frac{1}{1 + d - a/2a} = \frac{1}{1 + d/a}\ . \tag{4-5}$$

Because the wires are assumed to be infinitely long and to have zero resistivity, the electric field is independent of the *z*-coordinate. The maximum electric field strength occurs where $y = 0$, thus:

$$E_{\max} = \frac{-V_1\sqrt{d + a}}{a\sqrt{d - a}\ln\left(\frac{d}{a} + \sqrt{\left(\frac{d}{a}\right)^2 - 1}\right)}\ , \tag{4-6}$$

when defined by the coordinates, (*x*, *y*) to be at the electrode midpoint, or:

$$E_{\max} = \frac{V}{S} \cdot \frac{\sqrt{\left(\frac{S}{2 \cdot a}\right)^2 + \left(\frac{S}{a}\right)}}{\ln\left(1 + \frac{S}{2 \cdot a} + \sqrt{\left(\frac{S}{2 \cdot a}\right)^2 + \left(\frac{S}{a}\right)}\right)}, \tag{4-7}$$

when defined [132] by the gap distance. With parallel cylindrical conductors as in Fig. 4.11 [135] (p. 222), cylindrical fields are more uniform for the same ratios of gap distance and radii.

If the two electrodes are designated as V_1 and $-V_1$, the potential difference between them is $2V_1$. Thus, if the potential is defined as V, the equation should be changed to 0.5V. For an applied voltage, V, the exact maximum electric field between cylindrical dipole electrodes can then be determined algebraically by:

$$\mathrm{E_{max}} = 0.5\mathrm{V}\sqrt{d + a} \,/\, \left[a\sqrt{d - a}\ln\left(\frac{d}{a} + \sqrt{\left(\frac{d}{a}\right)^2 - 1)}\right)\right]. \tag{4-8}$$

4.2.2 Applying the dipole analytical solution for E_{max} to quadrupole cylindrical wires

The relationship described by 4-7 is consistent in two-coordinate systems, so if two or more cylindrical electrodes are at the same potential with reference to a ground, a solution of the field distribution is possible by the complex variable technique (i.e. conformal mapping), and is applied to define the maximum electric field in the case of four conducting cylindrical wires as illustrated in Fig. 4-2 [132] (p. 221).

Assuming the electrodes carry potentials $\pm\phi_0/2$, the result is a 2-D potential field

$$\phi(x, y) = \frac{\phi_0(x^2 - y^2)}{2r_0^2}. \tag{4-9}$$

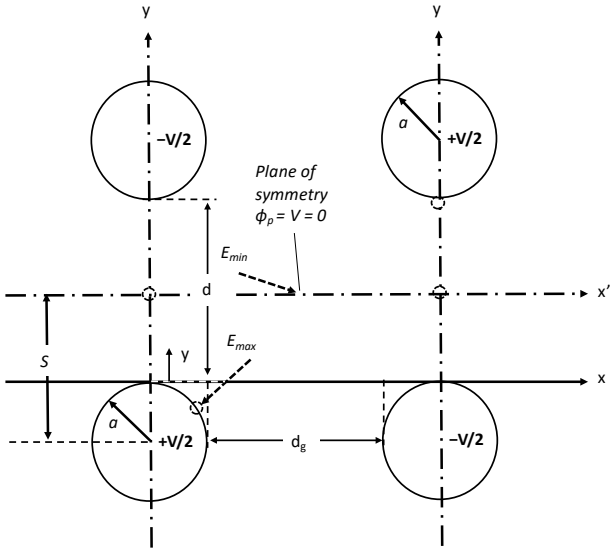

Fig. 4-2 A schematic of the 2-D electrode geometry of the cylindrical wire quadrupole, for which there exists an analytical expression for the mean and maximum electric fields. Each electrode is equidistant from its adjacent electrode, separated by some inter-electrode gap distance, S.

As in the case for the dipole configuration, the potential between the anti-parallel wires in the quadrupole configuration, for applied voltages of equal magnitude, is $\phi(y) = \pm V/2$. The region of maximum electric field, E_{max}, in the *x*-*y* coordinate plane of this configuration now shifts due to the influence of the nearby conductors. At the center, $E_{(0,0)}$ is equal to 0 kV/cm if the voltage applied to each of the electrode pairs is the same and the distance between each of the outer electrodes is also the same. For an applied voltage, V, the maximum coplanar electric field can then theoretically also be determined by (4-8). This value can then be compared with the results of numerical analysis for equivalent electrode radius and distance quantities, which is demonstrated at the end of this chapter.

4.2.3 Numerical analysis of the electric field in a quadrupole electrode model

The electric field strength distribution inside an insulating (*i.e.* biological or model system) material is a key determining factor influencing the breakdown voltage under high voltage stress. [1-3] As such, investigating the field strength distribution in non-uniform electric fields, such as those in rod-rod arrangements, is of great importance for the design and dimensioning of high voltage biomedical equipment. Direct experimental measurement of the high voltage field strength in small electrode gaps is difficult, however, and not very accurate.

The action of inserting a given sensor, especially near the active electrode, may be cumbersome or prohibitive at a given sensor-gap size ratio, and even when possible, perturbs the field, thereby affecting the measured result.

In electromagnetic theory, solutions of Poisson's equation are common for various geometries that have high symmetry. Along with the finite difference method, the finite element method is the most frequently used numerical method to solve Poisson's or Laplace's equation. Even absent a dielectric medium, however, mathematically analyzing air gap electric field models using Laplace's and Poisson's equations for general 2- or 3-dimensional fields, although more accurate, may nonetheless be laborious and time consuming. Numerical approximation, on the other hand, is capable of solving complex conditions both accurately and rapidly.

As was shown above in the point charge model of the electric quadrupole in 2-D, which consists of alternating positive and negative charges arranged on the corners of a square, calculating the field at a location in the plane with respect to the four charges can be accomplished through discrete mathematical analysis. When those charges are represented in 3-D, however, calculation of the in- or out-of-axis electric field becomes more complex. Solutions to more complex problems require software computing.

Numerical approximation of the electric field associated with a cylindrical quadrupole electrode model has been achieved using derivation or appropriate computational software [133]. Accomplishing the aims in Chapter 1 required an approximation of the absolute electric field value associated with the unipolar and bipolar nanosecond pulses of various phases delivered to one or more quadrupole electrodes. As the focus was on time-dependent electromagnetic fields that are mainly capacitive (electro-quasistatic) with negligible radiation and propagation effects, the quasi-static quasi-electrostatic *in silico* model was employed to study the distribution of the electric field from the quadrupole at the surface of a biological tissue and its magnitude at the peak amplitude of the pulse.

The model and simulations were implemented using commercial 3-D electromagnetic simulation software, Computer Simulation Technology (CST) Microwave Studio (CST Studio Suite v2016/7, Dassault Systèmes, Framington, MA), [134]. The full set of Maxwell's equations provides a general description of electromagnetic fields. Various levels of approximation based on these equations can be applied to different problems in order to reduce the complexity of the mathematical explanation. CST Studio employs the Finite Integration Technique (FIT) for its

general purpose transient solver, which relies on an algorithm considered to be computationally equivalent to of the Finite Difference Time Domain (FDTD) method for the particular case of a time-stepped scheme using Cartesian grids [135]. The FDTD method has earned widespread recognition among researchers because it makes spatial and temporal discretization of Maxwell's equations possible by a forward Euler method [136]. This computational approach is suitable for the simulations performed in this research because it solves directly for the vector as well as absolute electric field strength (|E|), which is the aspect of interest. Further, because it computes in the time domain, all frequency components of the input signal can be accounted for in a single simulation.

However, the major limitation of the FDTD approach is that the computational mesh is a uniform, square grid. While this promotes high accuracy by promoting fast computation, it creates 'staircasing' at curves in the model. As a key component of this work was to determine the electric field nearest the curved edges of cylindrical electrodes, a much denser grid technique is necessary. The Finite Integration Technique (FIT) is a generalized finite difference scheme for the solution of Maxwell's equations. CST implementation of the FIT generates a non-uniform hexahedral grid [137], which partially mitigates the staircasing effect and enhances resolution at sharp or rounded edges, but since extremely small mesh steps can lead to long simulation times that require considerable computing power, this does not completely overcome the problem. As this discussion section of this chapter explains, it may be necessary to note values that represent the maximum computed electric field value within the vicinity of the target position (*i.e.* the nearest adjacent grid along the electrode surface containing the highest computed value). The use of non-rectangular grids, such as trapezoids, is not available for the time domain solver [138].

The importance of linear systems is that they are relatively easy to analyze mathematically, with many applicable mathematical techniques (*e.g.* time domain computational methods that employ Maxwell's equations, such as FIT, and frequency domain linear transform methods, such as Fourier). Exact solutions to Maxwell's equations, however, only exist for special geometries such as spheres, spheroids, or cylinders, so approximate methods are generally required. When biological materials are exposed to a moderate to high frequency range pulsed electric field, the distribution and magnitude of the endogenous field can be simulated by solving Maxwell's equations for given boundary conditions.

There are a few reasons for choosing to complete electric field analysis in the time domain (TD) versus frequency domain (FD). While FD approaches require relatively less computational expenditure and are well suited to, for example, analyzing electrical and other devices at power frequency, non-sinusoidal, non-smooth (*e.g.* rectangular pulse) excitations would require a Fourier transform to be applied in order to make use of FD methods for each spectral component of the signal. If more than a few frequency points need to be considered, many FD simulations would thus be required to achieve sufficient accuracy. TD methods are useful in the quasi-stationary regime in electric diffusion problems, such as where there may be a nonlinear dependence of the electric conductivity σ(|E|) on |E| in a material. Further, as the biological validation performed in this work was limited to end-point analysis, necessitating a static time point measurement of the electric field, consideration had to be given to allow for, at a minimum, qualitative analysis of the spatial-temporal changes to |E| when a rectangular bipolar pulse or multiple synchronized pulses were delivered to one or more electrodes. Therefore, the use of TD methods was decidedly more appropriate given the complexity of the current numerical solution process [135].

4.2.4 Governing equations underlying the quasi-electrostatic model

To begin a description of the quasi-electrostatic model requires a brief overview of the key equations governing the electrostatic model. $\vec{E}(x, y)$ is the electric field at a point, which is the force per unit charge. Electric field is a vector, having magnitude and direction. In a 2-D Cartesian co-ordinate system it has components along the *x* and *y* axes, E_x, and E_y, such that the coplanar components of the electric field are given by

$$E_x = -\frac{\partial \phi(x, y)}{\partial x} \tag{4-10}$$

$$E_y = -\frac{\partial \phi(x, y)}{\partial y}. \tag{4-11}$$

A static electric field (vector) can be deduced from a gradient of some scalar function, denoted here by $\phi(r)$, and called a scalar electric potential. The electric field is then given by the

negative gradient of the scalar potential, which can be written to define the relation based on equations (4-10) and (4-11):

$$\vec{E} = -\nabla\phi(x, y), \tag{4-12}$$

where the gradient operator, ∇, is given by

$$\nabla = \frac{\partial}{\partial x}\hat{\imath} + \frac{\partial}{\partial y}\hat{\jmath}, \tag{4-13}$$

and where $\hat{\imath}$ and $\hat{\jmath}$ are unit vectors in the *x* and *y* directions, respectively. This allows one to find the electric field between two or more cylindrical systems.

Based on the law of conservation of charges, where *J* is the electric current density (in amperes per square meter), the governing equation for electric potential can be written as

$$\nabla \cdot J = \nabla \cdot (\sigma(T) \cdot \nabla \cdot \phi) = 0. \tag{4-14}$$

In free space where there are no charges, $\vec{E}$ must satisfy this law such that for static electric fields due to charge distributions:

$$\nabla \cdot \vec{E} = 0. \tag{4-15}$$

Basic electrostatic field theory may be applied to most practical applications involving homogeneous, isotropic materials at power frequency or impulse voltages, but with direct or slowly alternating voltages, effective general application of the theory is greatly impeded by conduction phenomena [132]. Consider, for example, a saline solution that contains various ionic species. When these are exposed to electric pulses, the electric potential (voltage difference) becomes a solution to the quasi-electrostatic equation:

$$\nabla \cdot (\sigma\nabla\phi) = 0, \tag{4-16}$$

where σ is the electrical conductivity of the fluid. The electric field distribution in the numerical model is thus generated by solving the governing equation [139]:

$$-\nabla \cdot \left(\sigma\left(\vec{E}\right)\nabla\phi\right) = 0, \tag{4-17}$$

where $\sigma\left(\vec{E}\right)$ is the electric field dependent electrical conductivity of the tissue, where σ may be highly dependent upon time due to relaxation phenomena, temperature and/or field intensity.

Biological tissues are largely composed of water, free ions such as Na^+, K^+, Ca^{2+}, $C1^-$, and a wide variety of proteins. This composition makes the dielectric properties of the tissues like those of saline solutions, which are characterized by an important dielectric loss factor at low frequencies (less than 3 GHz) [140]. The dielectric effect of cells suspended in a culture medium must then factor into the field analysis, as biological tissues induce capacitive effects due to their cell membrane structures [141]. This means that, for a lossy biological dielectric medium, σE_x and σE_y must be subtracted. As there is no direct way to model dielectrically complex biological materials to predict the distribution and magnitude of an endogenous electric field generated from nanosecond pulses, some general assumptions of conductivity and permittivity were made in the numerical analysis of the planar quadrupole electric field in experimental biological media.

4.3 Approach

4.3.1 Modeling the dipole and quadrupole in 3-D

Before modeling the entire nsPEF exposure system, simple dipole and quadrupole electrode models were created *in silico* in order to numerically assess the accuracy of the analytical solution for E_{max} in a 2-D and 3-D system, as well as spatially quantify the electric field distribution in 2-D in response to a nsEP exposure. Fig. 4-3 illustrates the basic planar quadrupole electrode model, which consists of four cylindrical electrodes modeled as perfect electrically conducting (PEC) finite wires of radius, a = 0.5 mm and length, l = 5 mm, in a cube domain.

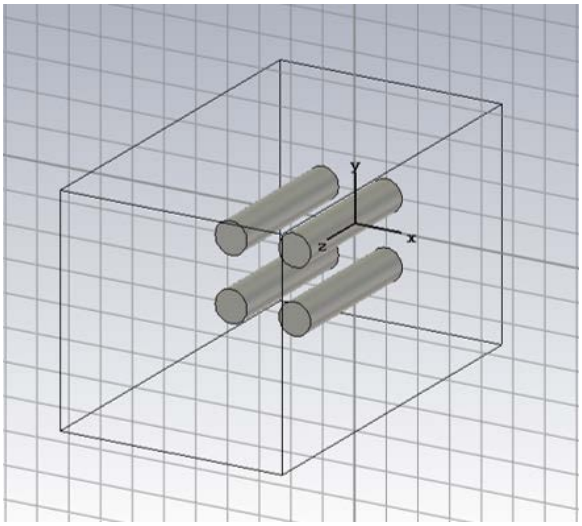

Fig. 4-3 Basic model of the planar quadrupole electrode arrangement.

4.3.2 Simulation parameters

The accuracy and performance of a simulation depend heavily on the quality of the mesh describing the structure. A homogenous locally refined mesh (see Fig. 8a) was applied to ensure consistency and to increase computational precision at curved edges of the model, each of which are geometrically and materially equivalent. Mesh formation parameters were set to the values listed in Appendix 2, with refinements added. Each structure was excited by one (dipole) or two (quadrupole) discrete ports (Fig. 4-4(b-c)) used as a feeding point voltage source excited with a constant voltage amplitude at the termination of a notional coaxial transmission line.

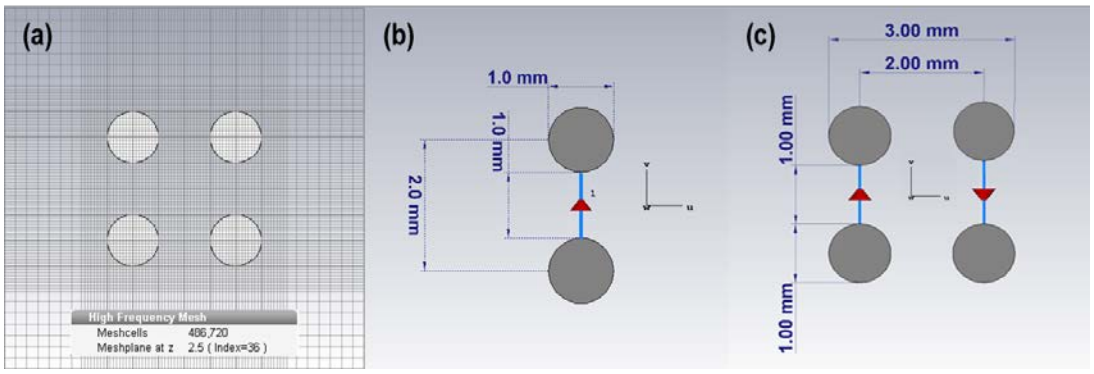

Fig. 4-4 Sample refined mesh in the planar quadrupole model (a) and discrete port configurations in the dipole (b) and planar quadrupole (c) models.

A discrete edge port consists of a perfect conducting wire connecting start and end points, which here are the points at the intersection of the flux line and the h.v and ground electrodes at the feed end, and a lumped element in the center of the wire. Since discrete ports were used, the boundary condition *Open (Add Space)* was applied in all directions, with an estimated reflection level of 1 x 10^{-4} mm and added absolute distance of 2 mm. The boundaries of the cube domain are considered a soft boundary condition, resulting in a nulled field at the cube boundary. In transitioning from a 1-D theoretical to 2-D numerical analysis, solutions for the electric field were obtained by executing both the electrostatic (Es) and transient (Ts) numerical solvers in the dipole and quadrupole arrangements in CST MWS. Each electrode pair was activated with the same potential difference. In the Es simulation, the charged electrodes were defined in the dipole by +500 V and 0 V (ground) potentials, and in the quadrupole by +500 V and 0 V potentials at each alternate electrode. In the Ts simulation, a +1000 V rectangular unipolar excitation signal (120 ns rise, 600 ns plateau, 75 ns fall) was applied to one (dipole) or two (quadrupole) electrodes according the discrete port scheme described by Fig. 8b-c, while the other electrodes were at ground potential (0 V). The latter describes a ‘pure’ quadrupole, which is axially asymmetric in the given cylindrical coordinate system. Each solution was computed in a vacuum.

4.3.3 Electric field data collection

Based on the model Cartesian coordinates, 1-D line plots of the electric field solution along the *x* and *y* axes were extracted from: 1) a 2-D *xy* cut-plane of the 3-D model bisecting electrodes, and; 2) at 0.1 mm above the applicator end. Measurements were taken at this position rather than coplanar with the applicator end to reduce the introduction of a greater error in accuracy that would arise due to staircasing at model curves, despite applying hexahedral mesh edge refinement. Absolute electric field values were quantified from the line plots at the five target intra-electrode positions (A-E) shown in Fig. 4-5.

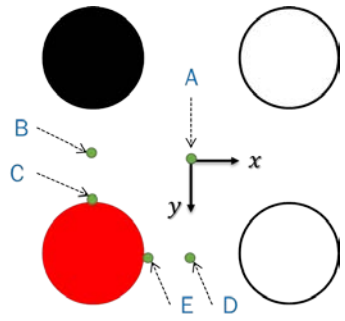

Fig. 4-5 Target points in the plane where inter-electrode electric field strength values are measured. Electrode scheme: red (h.v.); black (ground); white (floating).

4.3.3.1 Modeling the quadrupole system for numerical analysis of nsPEF exposure

To approximate the magnitude and distribution of a nanosecond pulsed electric field under experimental conditions, an *in silico* exposure system that expands the basic model described in Chapter 2 was designed. As Fig. 4-9 illustrates, it consists of up to four distinct 3-D geometric components: the electrodes; the cell sample container; a conductive layer; and a dielectric layer. In computing the electric field at the interface of two materials and at metal surfaces, a similar problem to that encountered at curved surfaces occurs in simulation. To avoid this, yet still ensure a reasonable degree of both accuracy and model fidelity to a surface-type treatment modality, the model electrodes were aligned perpendicular to the surface of a 3-D cell culture model with the blunt end of the electrodes placed just inside (0.25 mm) the tissue layer at the interface between the two dielectric layers. Both media are contained within a 35 mm round cell culture dish modeled as an open-top loss-free Teflon cylinder. The conductive layer and dielectric layer represent a 1X PBS solution containing YP1 and cell suspension in a 1% agarose gel medium, respectively. The upper layer has a conductivity, $\sigma = 1.5$ S/m, while the bottom tissue layer has a relative permittivity, $\varepsilon_r = 77.6$ and conductivity, $\sigma = 0.24$ S/m [142].

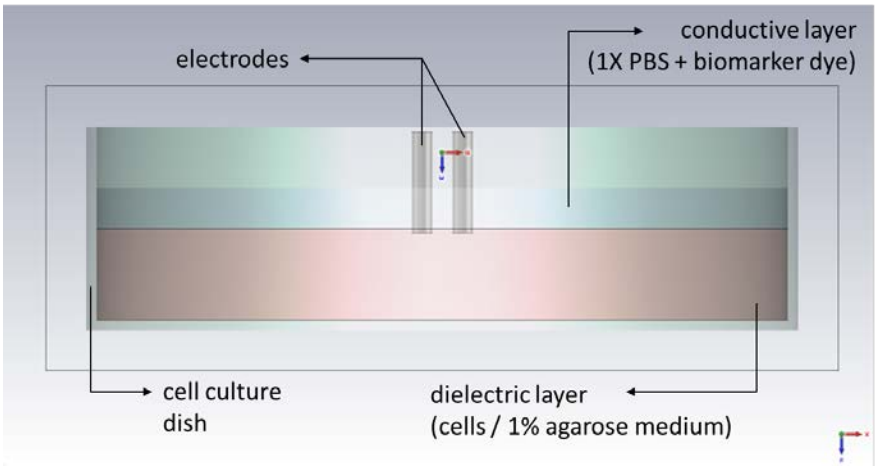

Fig. 4-6 CST Microwave Studio structural model for biological exposure simulations.

The mesh and boundary conditions were the same as those applied in Chapter 2. Optimized pulse waveforms based on those acquired from experimental observations (as in Fig. 4-5) were initiated in CST Studio. This was done by setting the rise (120 ns), fall (75 ns) and plateau (600 ns) durations for a rectangular unipolar pulse in the signal library, exporting the ASCII file, and then modifying the data in Excel to create new ASCII files of the bipolar waveforms to import into the library. For each simulation, a +1000 V, a nanosecond pulse or set of pulses was delivered to the 3-D model as the desired ASCII-defined excitation signal. These were applied via discrete port to one (for unipolar and bipolar pulses) or two (for CAN-CAN) electrodes, while at least one other electrode was left floating. The one or two remaining had an applied voltage of 0 V (ground potential). The various port configurations required for each type of condition are shown in Fig. 4-7.

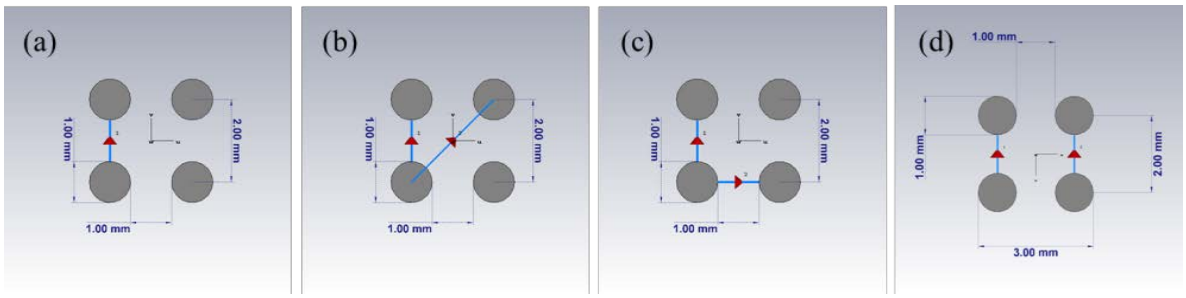

Fig. 4-7 Discrete port array for various excitation configurations: (a) single; (b) trans; (c) cis; and (d) CAN-CAN. The arrow points away from the high-voltage electrode to the grounded electrode.

4.4 Results & Discussion

As there was no visually discernable difference between the electrostatic solver and transient solver images of the 2-D electric field distribution in the bisecting plane of the 3-D models, representative images of the dipole and planar quadrupole configurations resulting from the Es are shown in Fig. 4-8. The color scale bar is clamped to the highest electric field value in kilovolts per centimeter (kV/cm) measured on the flux line between any two dipole electrode pairs. What is immediately obvious from the quadrupole image is that the electric field tends to zero at the center, where the superposing of the anti-parallel electric field vectors produced by the adjacent dipoles cancel each other.

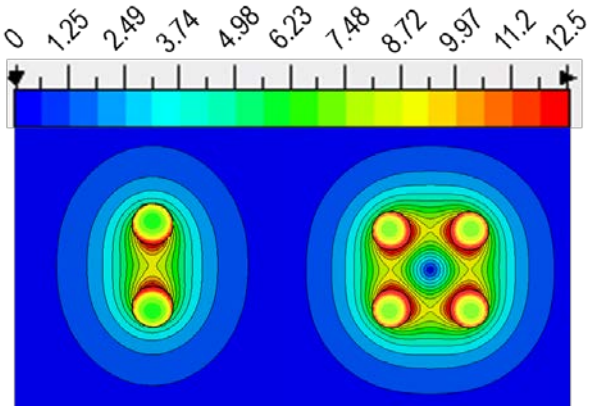

Fig. 4-8 Contour plots with isolines of the electric field gradients (in kV/cm) at the cross-section mid-way along the length of the electrodes.

Theoretical results for the maximum electric field and simulated results for E_{max}, as well as the remaining target points specified in Fig. 4-5, are given in Table 4-1 for both electrode arrangements. The purpose was to use the E_{max} value calculated from the well-known analytical formula (2-8) describing the maximum electric field intensity between co-linear and coplanar cylindrical wires as a reference to easily test the overall accuracy of the *in silico* model and advanced mesh simulation results. E_{max} was calculated as 13.15 kV/cm with constants d and V equal to 0.1 cm and 1 kV, respectively, and 0.05 cm for the radius a. These dimensions equal those of the actual electrode structure used in this work.

Table 4-1 Electric field values in kV/cm at target points for unipolar nsEP excitation of a single electrode

	AIR								
		Dipole				Quadrupole			
	Analytical	Electrostatic Solver		Transient Solver		Electrostatic Solver		Transient Solver	
Position		*Mid*	*End-0.1mm*	*Mid*	*End-0.1mm*	*Mid*	*End-0.1mm*	*Mid*	*End-0.1mm*
A	—	3.69	2.91	3.66	2.88	0.00	0.01	0.00	0.00
B	—	8.79	7.61	8.79	7.61	8.67	7.46	8.68	7.46
C	13.15	12.42	15.10	12.43	15.10	12.58	15.34	12.58	15.35
D	—	3.15	3.13	3.18	3.17	8.68	7.46	8.68	7.46
E	—	6.39	10.16	6.45	10.23	12.56	15.66	12.56	15.65

4.4.1 Verification of the analytical vs. numerical solution of the electric field

Although E_{max} was taken to be the value measured at the point on the flux line just before touching the electrode (the electrode edge point coordinate +/- 0.01 mm), the solvers returned slightly different values for E_{max} in the plane. Upon closer inspection of the model, these values were found to reside along the curved edge of the electrode ends proximal to where the flux line meets the PEC surface. The following standard formula was applied to determine the degree to which the simulated values deviated from the exact value for E_{max}.

$$\% \text{ Error} = (|\text{Simulated} - \text{Theoretical}| / \text{Theoretical}) \times 100$$

These percentages are reported in Table 4-2, where position C was previously defined and position C* represents the otherwise unspecified position in the 2-D plane corresponding to the maximum electric field value determined by the solver. The E_{max} values extracted from the 1-D (flux) line plot and those returned by the solvers in both dipole and planar quadrupole configurations indicated percent errors, rounded to the nearest whole number percent, as low as 1% and as high as 6%.

Table 4-2 Percent error for E_{max} for measurements made on the flux line vs. solver-specified

	Dipole				Quadrupole			
	Electrostatic Solver		Transient Solver		Electrostatic Solver		Transient Solver	
Position	*Mid*	*End-0.1mm*	*Mid*	*End-0.1mm*	*Mid*	*End-0.1mm*	*Mid*	*End-0.1mm*
C	5.57%	14.81%	5.49%	14.81%	4.35%	16.64%	4.35%	16.71%
C*	0.90%	39.14%	0.97%	39.30%	4.62%	42.95%	4.62%	43.02%

Because the theoretical formula for E_{max} assumes infinitely long electrodes and that the measurement is taken at the midpoint, the accuracy of the reported values must consider the short length of the modeled electrodes (0.5 cm), in addition to the roles of solver (spatial and temporal) resolution (*e.g.* how the perfect boundary approximation (PBA) algorithm computes) and user-applied simulation parameters (*e.g.* mesh grid and sub-model boundary definitions). The assumption clearly deviates at position C for measurements proximal to the rod ends and fails according the solver-identified maximum in the same plane for C*. These suggest that, although <6% simulation deviation from the theoretical value seems reasonable, for relatively simple cylindrical rod-rod geometries, a smaller deviation is expected and suggests the need for additional refinements to simulation parameters in order to increase computational accuracy.

4.4.2 The unipolar pulsed electric field

All unipolar pulse simulations involved applying the 600 ns excitation signal in Fig. 4-9, which was modeled on the experimental UP nsEP characteristics, to one cylindrical conducting rod (wire electrode) in the quadrupole system model. Simulations were run to compute the electric field strength and distribution for a 1 kV unipolar pulse excitation delivered to one quadrupole electrode while an adjacent electrode was at ground (0 kV), as well as to compare the effect of adding a second ground connection to the electrodes. Also, in order to assess the effect on the field of having inactive electrodes near to active and reference electrodes, an additional simulation was performed on a dipole electrode model.

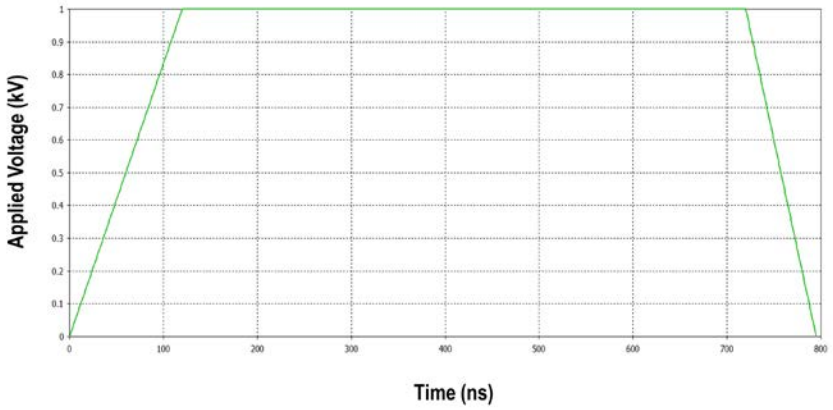

Fig. 4-9 600 ns excitation signal

In order to visualize the fields produced under these conditions as well as the effects of varying the ground electrode configuration, contour plots with isolines for these conditions are shown in Fig. 4-10. Accompanying legends show which electrode is high-voltage (red), grounded (black) or floating (white). The color scale bar on the left is clamped to the highest electric field value (kV/cm). The effect of nearby conductive material on the electric field distribution is immediately apparent. Despite that the same excitation parameters are applied, the presence of the conductive wire rods in close proximity to the active quadrupole electrode pair distorts the electric field distribution (Fig. 4-10(b)) that is regularly concentric about the electrodes in the dipole arrangement (Fig. 4-10(a)). In the cis-dual configuration (Fig. 4-10(c)), the ground electrodes lie on the same side of the *xz* plane. Here, the applied voltage and inter-electrode proximity is enough to induce local charging of the floating electrode and create and electric field that is distributed around the entire quadrupole, with the potential difference set up across the axial center (*z*-axis) creating a stronger field around the second ground electrode and even pulling some of the field such that the field strength is reduced along the periphery of the h.v. electrode, relative to that formed in the same area in Fig. 4-10(b). In the trans-dual ground configuration (Fig. 4-10(d)), the field distribution is largely limited to the region around the three active electrodes, with a broader maximum field localized around the h.v. electrode and oriented toward the axial center.

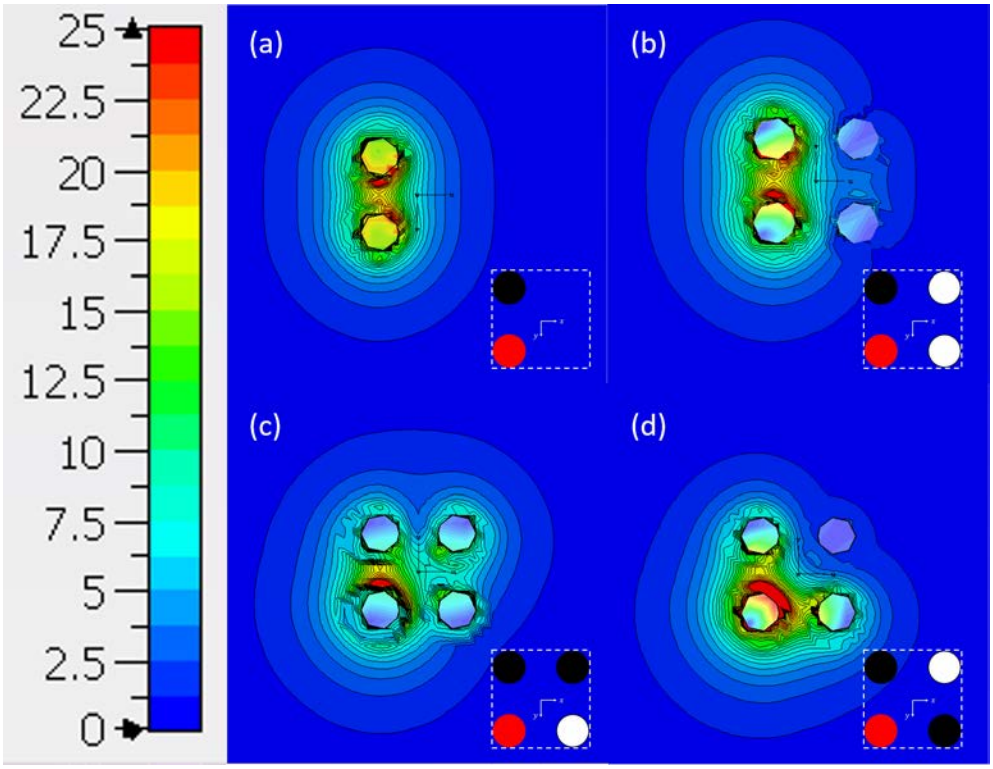

Fig. 4-10 Contour plots of the electric field for different 1 kV nsEP activation schemes: (a) dipole electrodes (b), and; single (c) dual cis- (d) and dual trans- electrode activation in the quadrupole.

Since the electric field scales linearly with the applied voltage, the spatial electric field value was simply calculated by multiplying the experimental applied voltage against the results from the 1 kV excitation signal. To compare the biological effect of exposure to the electric field generated by nanosecond pulses delivered to quadrupole electrodes, field measurements were acquired at and compared between discrete points. These (A-E) were specified in Chapter 1 and restricted as this study was primarily concerned with the electric field strength and biological effects at the h.v. electrode or at the axial center of the quadrupole.

To discretely quantify and analyze the electric field distributions shown in Fig. 4-2, absolute values were captured for each inter-electrode position and plotted (Fig. 4-3). As theory predicted in Chapter 2 and as Fig. 4-2 illustrated, E_{max} occurs proximal to the high-voltage electrode at points C and E. With a single ground, E_{max} is ~13 kV/cm at C. With a cis-dual ground, E_{max} also occurs at C, but is slightly higher at 14 kV/cm. With a trans-dual ground, E_{max} is ~15 kV/cm at both C and E. The only point at which the field does not appear to be affected by the number or position of any ground electrode is at B, where it is a consistent 8 kV/cm.

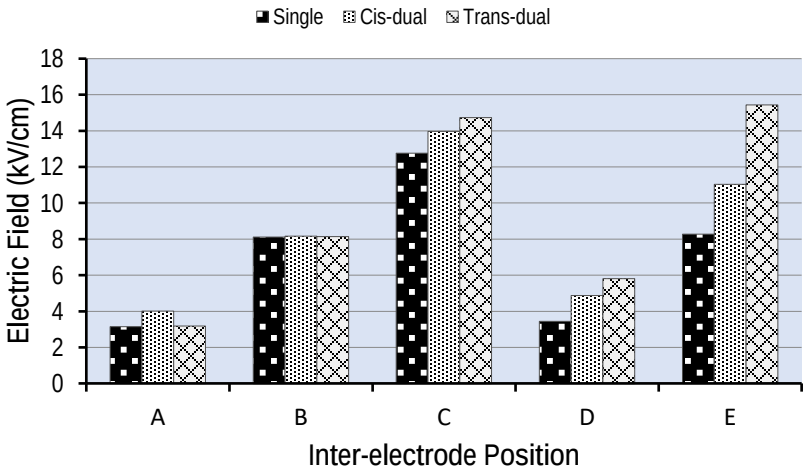

Fig. 4-11 Electric field strength at various inter-electrode positions for an applied voltage of 1 kV.

To visualize and further quantify the electric field distribution for the above parameters in 2-D, line plots were generated along the *x*- and *y*-axes coplanar with the quadrupole applicator end (Fig. 4-4). In the current model, the *x* and *y* values of -1.5 mm and 1.5 mm in Fig.4-2(b) and (c) are points on the periphery of the quadrupole. For a single ground excitation (light blue), the electric field at B, between the h.v. and ground electrodes, is lower (~7 kV/cm) than for the dual ground configurations. It also appears to be lower than when measured from the *y* direction (~8 kV/cm) at this same position, in contrast with Fig. 4.3. At the axial center, A, the field along the line (a) is ~2.5 kV/cm. Further, at the model electrode boundaries in (b), the maximum field is balanced between them at ~13 kV/cm. This is despite the apparent computational discontinuity, likely caused by decay of the excitation signal energy from absorption by the nearby discrete ports, which are treated as transmission lines, and occurs as the time domain signal is numerically propagated throughout the computational volume. Alternatively, it may be due to incomplete localized mesh calculation at the curved metal surface. While E (c) is at the edge of the same electrode as C (a), the maximum field there is only ~8.2 kV/cm. This is unsurprising given its position 90° away from the ground electrode along the circumference toward the proximal floating electrode. Finally, although D is positioned the same 0.5 mm distance away from the h.v. electrode as B is, there is less influence by the ground electrode such that the electric field at D is only ~3.5 kV/cm. However, the difference in magnitude between points B and C and between D and E is about the same (~4.7 kV/cm).

When a second, distal ground electrode is defined (“cis-dual”, green), the electric field at the axial center, A, is nearly doubled at ~4 kV/cm. At B, the field is ~8 kV/cm when measured in both the positive *x* and *y* directions. In the cis-dual ground configuration, the maximum electric field is increased at C by at least 1 kV/cm relative to that resulting from UP pulse excitation in the single ground configuration. The electric potential here is influenced by the adjacent as well as distal ground electrode, producing a higher electric field (~14 kV/cm) than at E (~11 kV/cm). Additionally, one can see how the added electrode causes a localized increase in the field profile (a) between the second ground and floating electrodes.

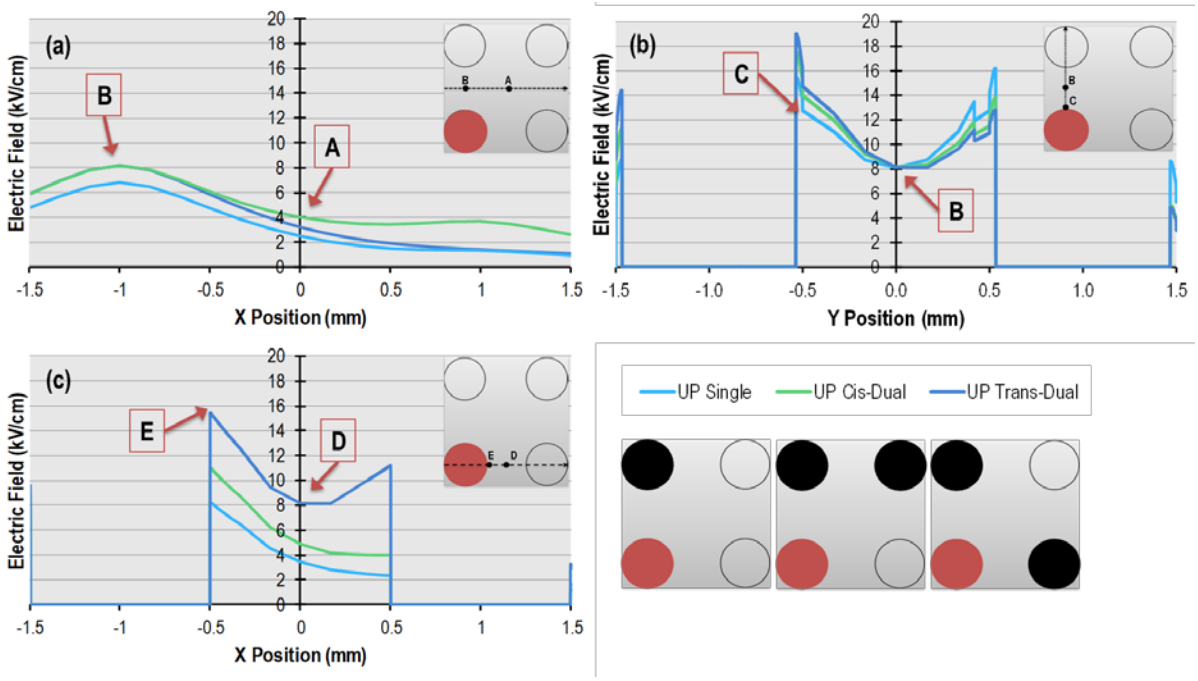

Fig. 4-12 Line profiles of the inter-electrode quadrupole electric field for three different ground configurations of a unipolar pulse applied at 1 kV: single (a); cis-dual (b) and cis-trans (c). Inset images mark biological response points of interest and direction of line profile plots. Bottom right image cluster shows, l-r, configurations corresponding to (a-c) with high voltage (red) and ground electrode (black) positions.

Unsurprisingly based on the diagonal symmetry of the trans-dual grounded electrodes relative to the h.v. electrode, the electric field is the same at points B and D (~8 kV/cm) as well as at points C and E (~16 kV/cm). Also notable is that the values at the latter positions are twice that for C in the single ground configuration, consistent with the 2X linear scaling factor that applies for a symmetric addition of a second ground. Adding a second ground adjacent to the h.v.

electrode clearly increases the maximum electric field otherwise produced with only a single ground. However, it should be noted that, while only the field at positions in the half of the quadrupole arrangement that include the h.v. electrode are quantified in this work, the line profiles suggest a relative decrease in the field strength near the ground electrode corresponding to the increase at the opposing h.v. electrode.

As field strength can be calculated from a single applied voltage for any point in the 2-D electric field that has already been obtained, three peak voltage amplitudes from unipolar pulse experiments – 0.6 kV, 1.7 kV and 2.5 kV – measured from pulse oscilloscope traces, were multiplied by the spatial electric field values calculated from *in silico* results for each ground configuration to approximate the experimental electric field distribution. The values at each of the five positions of interest are listed in Table 4-3. Given a unipolar nsEP applied to one electrode in a quadrupole arrangement in a moderately dielectric material, the maximum attainable electric field for an applied voltage of 2.5 kV is 38.61 kV/cm, calculated near the high-voltage electrode with a trans-dual ground; the minimum field is 1.89 kV/cm calculated at the axial center with a single ground for an applied voltage of 0.6 kV.

Table 4-3 Unipolar pulse absolute spatial electric field for three ground configurations (in kV/cm).

Position	0.6 kV			1.7 kV			2.5 kV		
	Single	Cis	Trans	Single	Cis	Trans	Single	Cis	Trans
A	1.89	2.41	1.92	5.36	6.83	5.44	7.89	10.04	8.00
B	4.87	4.91	4.89	13.81	13.90	13.85	20.30	20.44	20.37
C	7.66	8.39	8.84	21.70	23.76	25.05	31.92	34.94	36.84
D	2.08	2.93	3.49	5.88	8.31	9.90	8.65	12.22	14.56
E	4.97	6.62	9.27	14.08	18.76	26.25	20.71	27.59	38.61

4.4.3 The bipolar pulsed electric field

In the UP nsEP case, the excitation signal was modeled on the experimental pulse so that its frequency could be validated and because the CST signal library contained a tunable unipolar rectangular pulse. In the bipolar case, numerical analysis was performed for only the single-ground connection using the same general method as for unipolar pulses. Since the emphasis here was on the spatiotemporal value of the electric field at the peak amplitudes of the pulse phases, a rectangular bipolar excitation signal with a second phase amplitude that was half of the

first was created from exported unipolar signal data having a shorter phase duration and rise and fall times (80 ns and 1 ns, respectively), then imported as an ASCII file. Next, the spatiotemporal vector electric field was computed for a simulated bipolar pulse applied at 1 kV. The resulting values were then scaled based on the recorded experimental voltage amplitudes and new values similarly calculated for a 25% and 70% bipolar pulse (Table 4-4).

At the voltage amplitudes calculated for the unipolar pulse and both phases of the bipolar pulses, the electric field vector in the *x* direction (E_x) is ~0 kV/cm at the axial center of the quadrupole ('A'), between the high-voltage and grounded electrodes at their midpoint ('B') and at the edge of the former ('C') on the same line as B. There is otherwise a positive *x* component between the h.v. and adjacent floating electrode. Given that the 2-D analysis of the quadrupole model is for electrodes whose cylindrical cross-section is in the *xy*-plane of a Cartesian coordinate system, where the high-voltage electrode lies in the top-left quadrant, relative to the grounded electrode, the electric field vector in the *y* direction (E_y) for the 0% BP nsEP (UP equivalent) is predictably negative.

Table 4-4 Spatiotemporal electric field (in kV/cm) from a bipolar pulse with a 2.4 kV first-phase amplitude.

	φ1		*φ2*					
Position	**0% BP**		**25% BP**		**50% BP**		**70% BP**	
	E_x	E_y	E_x	E_y	E_x	E_y	E_x	E_y
A	0.0	-7.6	0.0	-2.0	0.0	-3.9	0.0	-5.1
B	0.0	-19.5	0.0	-5.1	0.0	-10.1	0.0	-13.2
C	0.0	-30.2	0.0	-7.9	0.0	-15.6	0.0	-20.5
D	7.6	-2.0	2.0	-0.5	3.9	-1.0	-1.5	-1.3
E	19.9	-0.1	5.2	0.0	10.3	-0.1	-13.4	-0.1

Irrespective of pulse type, the absolute maximum electric field value occurs at the same inter-electrode position, C, as predicted theoretically for E_y, and increases with increasing amplitude by phase. For any of the bipolar nsEPs, with only the single adjacent ground in the quadrupole electrode configuration, E_y is lowest and remains at 0 ± 0.1 kV/cm at E, the edge of the high-voltage electrode, at 90° from C and facing a floating conductor. E_x at this position, however, is much higher in each case. A notable observation from these numerical approximations is that, whereas E_x is positive for both the unipolar case and for both the 25%

and 50% bipolar cases, the vector field turns negative when the BP nsEP second phase is 70%.

4.4.4 Simulation of the CANCAN electric field distribution

Numerical simulations of the electric field distribution produced by the quadrupole electrode system were computed to provide the dosimetry for the experimental study and to validate the CANCAN concept. To validate that the superposition of two pulses with synchronized phases of opposite polarity produce regions of electric field that are distinctly unipolar and bipolar, a representative CANCAN exposure was modeled whereby excitation signals were delivered to two adjacent wire cylinder quadrupole model electrodes while the other two opposing conductors were at 0 kV (ground). A 2+1 (bipolar plus unipolar) CANCAN model was implemented. The 100/50% bipolar pulse was a biphasic waveform with the first phase (φ_1) amplitude set at 1 kV and the second (φ_2) set at 0.5 kV. The unipolar pulse was a monophasic waveform with a 0.5 kV amplitude. Excitation by the latter was delayed so that delivery of the positive and negative 0.5 kV phase signals was synchronized.

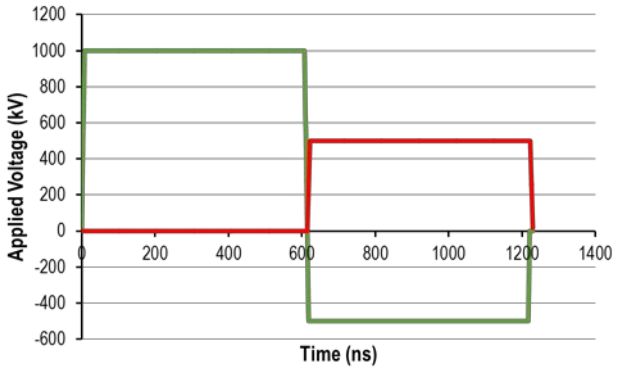

Fig. 4-13 CANCAN using bipolar and unipolar excitation signals

As in the bipolar case, the numerically approximated electric field values were scaled based on the voltage amplitudes measured at the load for each positive and negative phase applied. These are given in Table 4-5.

Table 4-5 Spatiotemporal absolute electric field for a 2+1 CANCAN (100/50%) applied at 1 kV and 0.5 kV.

Position	φ1	φ2
A	2.4	0.0
B	0.1	3.9
C	0.4	8.1
D	4.8	7.8
E	3.9	3.8

4.5 Conclusion

This chapter described the fundamental physical and electromagnetic foundations that make possible the study of the electric field distribution in a 2-D electrode system. The principle of superposition and rationale behind approaches to investigating an electric field distribution when moving from 1-D to 2-D systems are specifically addressed, namely regarding how the simple circular geometries presented by the 2-D representation of dipole and quadrupole cylindrical electrodes allow for an exact calculation of the maximum electric field. This foundation then provided the input for the creation of basic electrode models that could be used to support a first-order approximation of the electric field intensity at any point in a plane using numerical simulation software that employs the Finite Integration Technique. Calculation of the analytical formula for E_{max} based on the design used for *in vitro* simulation described in later chapters revealed a value of 13.15 kV/cm, which assumes infinitely long wires uniformly charged to 1 kV. Initial simulations conducted in air on both dipole and quadrupole models returned values within 6% of theoretical (dipole) and within 5% (quadrupole) when measured along the flux line in the perpendicular bisecting plane between 0.5 cm long electrodes. The key parameters of the applied mesh formation have been investigated in order to ensure accuracy and yet keep the demand for computing power and time low. These tests have shown that the application of the selected mesh, material environment and boundary conditions has produced simulation results that are in good agreement with primary theoretical expectations, but require further optimization to ensure a higher degree of certainty (reliability) in modeling electric field results when a biological medium is incorporated to reflect experimental conditions.

CHAPTER 5

QUANTIFICATION OF CELL PERMEABILIZATION AFTER UNIPOLAR NSPEF EXPOSURE

5.1 Introduction

Chapter 4 allowed for the visualization and numerical approximation of the electric field distribution. To characterize and quantify the electropermeabilization response to unipolar nsPEFs generated by a quadrupole electrode exposure system and compare them to the calculated field, three objectives were specified: 1) define the critical electric field (E_c) required for membrane permeabilization; 2) spatially delineate the degree of electropermeabilization for a range of applied voltages; and 3) relate the electropermeabilization response pattern to the electric field distribution.

5.2 Approach

Relating the electric field to the cell permeabilization response first required determining a set of UP nsEP parameters that could produce a detectable signal in the 3-D *in vitro* system. As multiple studies have alluded to a critical electric field threshold (E_c) for nsPEF electropermeabilization and other bioeffects, the first task was to determine a precise E_c for cells exposed in a 3-D tissue model. This was accomplished by exploiting continuous response data across the non-uniform electric field generated by charging a single electrode grounded at an adjacent electrode in the quadrupole to capture the earliest point at which electropermeabilization occurs. By employing the formula (5-1) and applying a conservative threshold statistic, it was hypothesized (H_{1a}) that a lower Limit of Quantification (LOQ) could be determined in relation to the sham control such that fluorescence values above that threshold would be considered a ‘true’ nsPEF electropermeabilization response. The *Ec* was then found by mapping the point at which the LOQ crossed the plot of YP1 fluorescence to the electric field line plot. To ascertain the relationship between applied voltage and degree of electropermeabilization, a set of voltage parameters was tested to produce a range of electric field values that would produce a commensurate fluorescence spectrum from YP-1 uptake that could be used to manage

expectations of spatial responses in subsequent experiments, and as a qualitative indicator for further investigation.

To quantify the electropermeabilization response to unipolar nsPEFs in a quadrupole electrode exposure system, three objectives were specified: 1) define the critical electric field (E_c) required for membrane permeabilization; 2) spatially delineate the degree of electropermeabilization for a range of applied voltages; and 3) relate the electropermeabilization response pattern to the electric field distribution. The electropermeabilization threshold is defined as the lowest local electric field value that elicits a fluorescence response. To obtain a rough estimate of E_c, one reference electrode was activated with high-voltage unipolar nsEPs of various amplitudes while an adjacent electrode was grounded. A 1 mm x 5 mm ROI was drawn on the fluorescence image acquired from the 0.6 kV single ground nsEP exposure across the quadrupole's bisecting line (*x*-axis) after 10-point Gaussian blur image filtering, without background subtraction. The following formula for the Line of Quantification (LOQ) was then applied to determine the electropermeabilization threshold:

$$LOQ_{MP} = \mu_c + z \cdot \frac{\mu_c}{\sigma_c}, \tag{5-1}$$

where μ_c is the mean sham fluorescence, z is the z-score statistic, and μ_c/σ_c is the signal-to-noise ratio, represented by the mean divided by the standard deviation of the mean. The *z*-score selected was 1.96, which ensured that at least 97.5% of the values measured were above the averaged sham, or baseline (background), fluorescence.

To ascertain a starting point from which to begin assessment of bipolar cancellation in a non-uniform nanosecond pulsed electric field, it was necessary to determine the set of unipolar pulse parameters that would provide a detectable electropermeabilization response range within which to perform subsequent exposure-response analyses. To this end, three different pulse amplitudes were tested to form the baseline for delineating the nsPEF plasma membrane permeabilization response in the quadrupole system and the degree of linearity between the numerically determined electric field distribution and corresponding biological response. As 4.5 kV was previously determined to be the maximum effective output of the pulser, this was the

highest positive phase input voltage used, with two others selected at lower amplitudes (3 kV and 1 kV).

Having established the limits of fluorescence detection for the conditions specified, the next step was to quantify the relationship between the degree of electropermeabilization and magnitude of the nsPEF distribution. A major assumption of this research was based on the general hypothesis that there is a linear relationship between the absolute electric field value and YP1 uptake. A cursory comparison of the electric field values for the 1.7 kV and 2.5 kV UP nsEP conditions between points in the sample plane where fluorescence intensities were the same revealed that the corresponding field magnitudes were not the same. This observation prompted a look into whether the above assumption was valid in an *in vitro* 3-D tissue model for the applied voltages selected. The objective here was then to test the hypothesis (H_{1b}) that YP1 fluorescence and nsPEF intensity are linearly correlated. YP1 uptake was quantified at specific points in the quadrupole plane where the electric field strength was approximately equal. A linear regression of the response (in relative fluorescence units) to electric field strength (kV/cm) was performed in MS Excel using the *trendline* tool, with a significant result defined as at or below 5%.

To visualize the effect of grounding on YP1 uptake localization, one electrode was charged with unipolar nsEPs at three different voltage amplitudes for each of the three ground electrode positions described in Chapter 4. Based on those results, the degree to which charging voltage influenced response localization was then assessed to learn whether and how electropermeabilization depends on the spatial magnitude of the nsPEF. Results from a preliminary experiment using parallel plate electrodes suggested that at higher relative cell concentrations, dielectrophoretic effects may dominate and become a confounding variable. Single-cell nsPEF studies have otherwise demonstrated electrode polarity bias under certain pulse conditions, described as differences in the membrane concentration of ‘nanopores’ relative to each electrode pole [88, 143] and by respective charging and discharging effects on the cell, depending on the applied field [89]. Due to greater impedance in the 3-D culture sample relative to monolayer cell culture targets and the tendency of charges to accumulate on electrode surfaces, it was hypothesized that electrode localization of YP1 uptake depends on the magnitude of the applied voltage (H_{1c}). To test this secondary hypothesis, the symmetry of the unipolar response between the h.v. and ground electrodes was assessed.

The inter-electrode distribution of YP1 fluorescence was specifically examined from the positive high-voltage electrode ("anode") and ended at the negative terminal or ground electrode ("cathode") side of the cell surface area. After applying a 10-pt Gaussian blur to the stereoscopic image of exposed cells in FIJI, using MS Excel, maximum dye fluorescence was identified within 0.25 mm of the h.v. or ground electrode for each unipolar pulse amplitude. The mean fluorescence intensity for ten pixels encompassing the peak values at each electrode pole was calculated, representing 62.5 μm ($1\ \mathrm{mm}/160\ \mathrm{pixels} \times 10\ \mathrm{pixels}$) of the inter-electrode profile.

To quantify the spatial distribution of YP1 fluorescence, a polarity ratio was established whereby post-exposure YP1 fluorescence was averaged across 25% of the data proximal to the "*anode*" and "*cathode*" sides of the cell culture surface and their sums were divided such that:

$$R = \frac{\sum(A_{F\{0.6,\ 1.7,2.5\}})}{\sum(C_{F\{0.6,\ 1.7,2.5\}})},$$

where A_F and C_F reflect YP1 uptake at the anode and cathode, respectively. If the ratio was greater than one, then this would demonstrate that YP1 uptake across the cell culture surface primarily occurred at the anodal electrode; if the ratio equaled one, then YP1 uptake did not favor either pole; if the ratio was less than one, then YP1 uptake favored the grounded or cathodal electrode. These relationships are expressed below using the above terms.

$$R > 1;\ \sum(A_F) > \sum(C_F)$$
$$R = 1;\ \sum(A_F) = \sum(C_F)$$
$$R < 1;\ \sum(A_F) < \sum(C_F)$$

Because cells behave differently in 3-D and dielectric differences may affect local cell responses, a secondary hypothesis was that electropermeabilization favors the high-voltage electrode (H_{1d}). To test this, YP1 uptake was compared between a single working and single ground electrode to determine if cells cultured in a tissue-like environment respond as they do in a monolayer. The significance of the difference in magnitude between anodal and cathodal responses to nsPEFs produced for each voltage amplitude was measured by applying an *F-test*

for variance before selecting and performing a *two-tailed t-test* at a 0.05 alpha level of significance to compare responses at each pole.

5.3 Results & Discussion

5.3.1 YP1 uptake after UP exposure

Before quantifying the relationship between applied voltage and degree of electropermeabilization, the first step was to identify which UP nsEP parameters could produce a detectable signal in the 3-D in vitro system. Based on the cited literature as well as test and evaluation, the set of voltage parameters comprising 1 kV, 3 kV and 4.5 kV charging voltages produced applied voltages of 0.6 kV, 1.7 kV and 2.5 kV at the biological load. These were enough to elicit the small range of low-to-high YP1 fluorescence seen in Fig. 5-1.

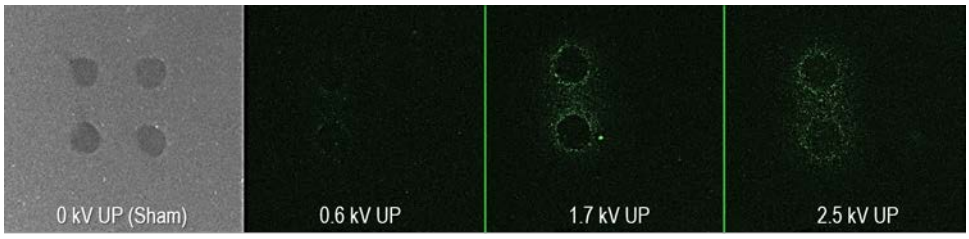

Fig. 5-1 Sample brightfield and YP1 fluorescence images from cell exposure to a dipole electrode nsPEF by unipolar pulses delivered at three different voltages to the quadrupole system.

5.3.2 Defining the electropermeabilization threshold

Based on the mean of three experiments, the LOQ was calculated to be 1020.67 fluorescent units, a value that also appeared upon visual inspection to depart sufficiently from the baseline value. If x = 2.5 mm is taken to be the axial center of the quadrupole in a Cartesian coordinate system, where the outermost edges of the active electrodes in the quadrupole align with x = 1 and x = 2, the intersection of the fluorescence profile plot and the LOQ occurs at x = 1.75 mm. When cross-referenced with the simulated electric field data for a 0.6 kV pulse, the electric field at this position is 1.11 kV/cm and is considered E_c in this configuration. Notably, if the same fluorescence value read at position x = 1 mm, which is the outer edge of the quadrupole, that value is 2.83 kV/cm.

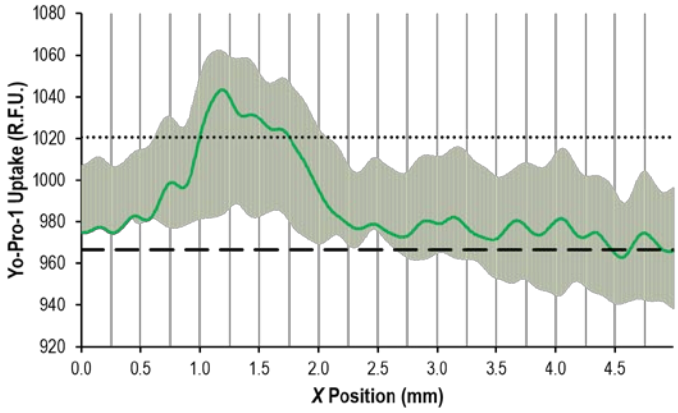

Fig. 5-2 Critical electric field threshold for electropermeabilization. Green line represents mean YP1 fluorescence ± SD (shaded area, n = 3) for a single ground 0.6 kV unipolar nsPEF exposure.

5.3.3 Connection of a secondary ground spatially modulates UP nsPEF responses

Representative fluorescence images after threshold application and color overlay are presented in Fig. 5-3 for all unipolar exposures, illustrating the general distribution pattern of electropermeabilization as well as the influence of ground electrode configuration. The pattern of YP1 uptake illustrates that, with a single ground, the floating electrodes did not substantially influence the local field enough to induce permeabilization up to V_{app} of 2.5 kV. When electrodes on both sides of the h.v. electrode are grounded, YP1 fluorescence is hardly visible around the electrode imprint sites at V_{app} = 1.7 kV but is then visible around both and strongest around the circumference facing the h.v. electrode. When the second electrode is grounded diagonally across the plane, the field is insufficient for all applied voltages to induce dye uptake across the axial center, but uptake can still be seen around the distal ground electrode. Minimal YP1 uptake can be seen for a 0.6 kV unipolar pulse, which is strongest at the h.v. electrode.

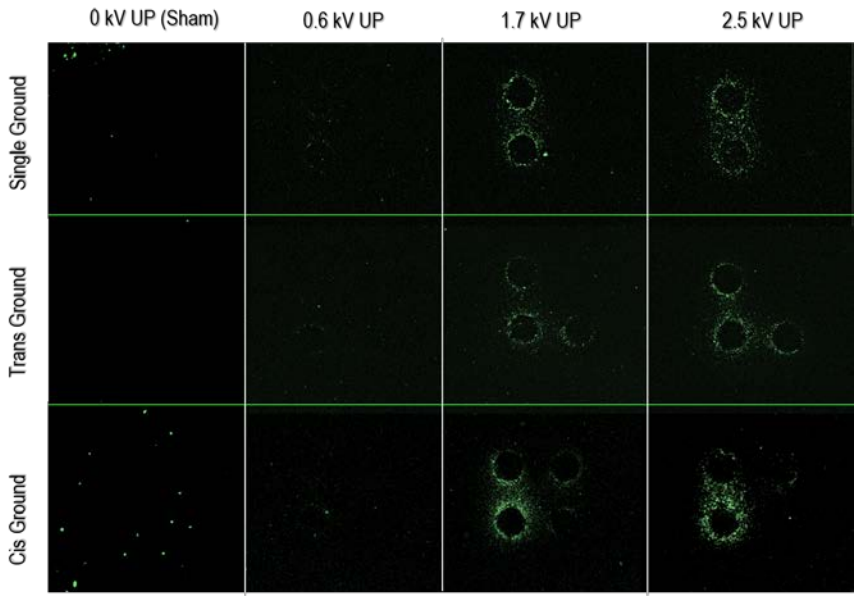

Fig. 5-3 Sample YP1 fluorescence images of cells exposed to unipolar pulses delivered at three different voltages to one quadrupole electrode, each with different ground connections.

5.3.4 YP1 uptake in the quadrupole plane is detectable over a range of applied voltages

At the sample load, the applied voltages were measured at approximately 2.5 kV, 1.7 kV and 0.6 kV, respectively. Line plots along the *x*-axis and *y*-axis are shown in Fig. 5-4 representing the average fluorescence due to YP1 uptake normalized to the sham (background) response for three independent experiments (n = 3). The fluorescence patterns in Fig. 5-4 align closely with the electric field distributions in Fig. 5-4 (a, b). Although electropermeabilization was induced at all three voltage amplitudes, YP1 uptake at the periphery of the quadrupole ($x = -0.1$ mm) is already present at the higher voltages (Fig. 5-4 (a)).

A Gaussian type pattern specifically occurred between active electrodes, peaking at point B, which corresponded at each applied voltage with electric field strengths of 4.9 kV/cm (0.6 kV), 13.8 kV/cm (1.7 kV) and 20.3 kV/cm (2.5 kV), as in Table 4-3. The highest overall fluorescence intensity occurred normal to the flux line at $y = \{-0.5\text{ mm}, 0.5\text{ mm}\}$, the interfacing edges of the ground and h.v. electrodes, where theory predicted E_{max} to occur. The corresponding electric field strengths at the h.v. electrode (point C) were 7.7 kV/cm (0.6 kV), 21.7 kV/cm (1.7 kV) and 31.9 kV/cm (2.5 kV). These results demonstrated that an applied voltage of up to 2.5 kV could induce YP1 uptake in gel-suspended cells. However, the moderate

YP1 response along the field gradient for a 0.6 kV pulse suggested that the lower threshold for electropermeabilization should be investigated, namely since Tables 4-3 through 4-5 indicate that the spatial electric field falls below 4.9 kV/cm in certain cases.

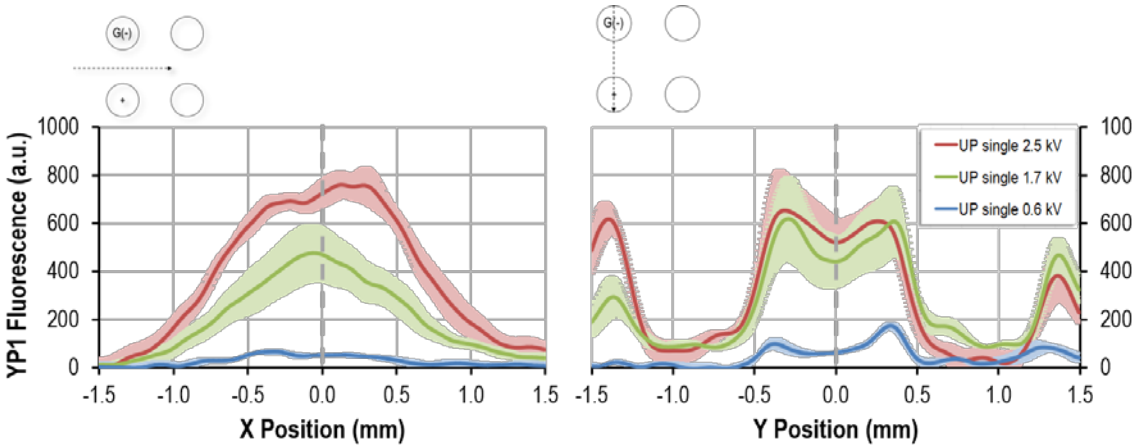

Fig. 5-4 Fluorescence profile of cells measured along the x-axis (left) and y-axis (right) after unipolar pulses were delivered to one h.v. electrode at different voltages with one adjacent electrode grounded. Data is presented as mean ± SEM (n = 3).

5.3.5 Electropermeabilization does not solely depend on the absolute electric field

Having unipolar nsPEF electropermeabilization data from three different applied voltages made it possible to compare YP1 fluorescence to the local electric field at a minimum of two positions. Similar pixel intensities were found with corresponding electric field values of 2.5, 4 and 10 kV/cm for each of the three applied voltages and plotted in Fig. 5-4. Since a 0.6 kV pulse was not enough to generate a 10 kV/cm field (see Table 1), response data was only available at the lower two field values. At points where the field was only 2.5 kV/cm, YP1 uptake was about the same for all voltages applied. Linear regression of the trendlines for the two plots, each having three electric field values for comparison, revealed a slope of 47.1 (R^2 = 0.998) for a 1.7 kV applied voltage, and a steeper slope of 59.9 (R^2 = 0.998) for the higher applied voltage of 2.5 kV. These differences were not statistically significant at $\alpha = 0.5$.

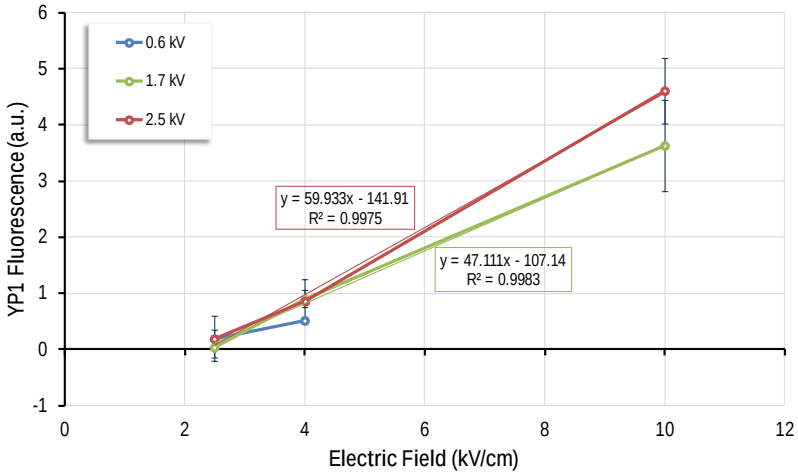

Fig. 5-5 Assessment of spatial linearity between single ground UP nsPEF strength and YP1 uptake.

5.3.6 Localization of UP nsPEF response depends on electrode polarization

While the magnitude of the electric field does not dictate the degree of electropermeabilization, its value is nonetheless influenced by other factors that may influence the biological response, such as electrode polarization. The ratios for each of the three applied voltages are plotted in Fig. 5-6. In general, as the applied voltage is increased, the electropermeabilization response tends to favor the cathode. This relationship between fluorescence polarity (y) and applied voltage (x) is curvilinear and fits ($R^2 = 1$) the second-order polynomial equation as indicated for voltage amplitudes between 0.6 and 2.5 kV.

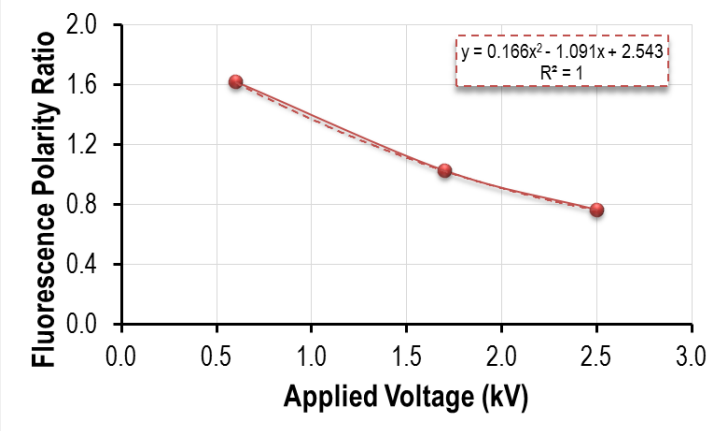

Fig. 5-6 Ratio of YP1 fluorescence due to electropermeabilization from single-ground unipolar nsEPs at the positive (anodal) versus negative (cathodal) electrodes.

Analysis revealed that exposure to UP nsEPs delivered to a h.v. electrode in the quadrupole arrangement with a single grounded electrode resulted in biased and unbiased YP1 uptake. At a 0.05 alpha level of significance, 0.6 kV UP nsEP exposure produced YP1 uptake with highly significant anodal dependence ($F = 4.03$; $p < 0.001$); the same exposure delivered at 1.7 kV revealed no significant polarity bias ($F = 1.23$; $p = 0.245$), whereas YP1 uptake revealed highly significant cathodal dependence ($F = 1.94$; $p < 0.001$) when pulses were applied at 2.5 kV.

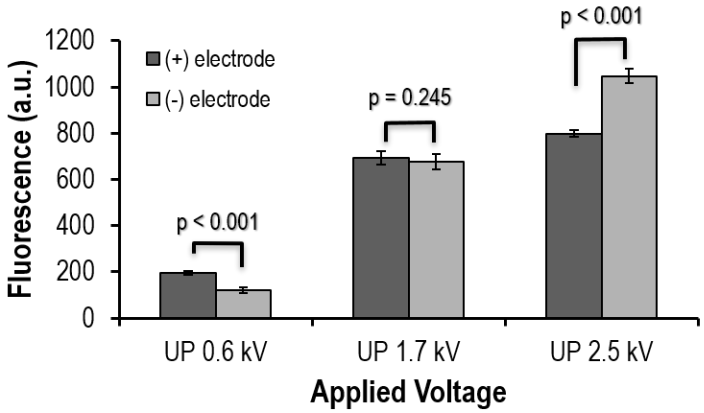

Fig. 5-7 Influence of electric polarity on Yo-Pro-1 uptake for single-ground unipolar pulses based on voltage amplitude. Statistical significance is set at $\alpha = 0.05$.

CHAPTER 6

QUANTIFICATION OF CELL PERMEABILIZATION AFTER BIPOLAR NSPEF EXPOSURE

6.1 Introduction

This study sought to build a quantitative basis to address how bipolar cancellation can be applied simply in a complex exposure system to reduce field intensity at the electrodes and enable focused, remote nsPEF biomodulation. This chapter describes the effect on YP1 uptake in cells in 3-D culture by pulsed electric fields generated using the modular nanosecond quadrupole electrode system. Experimental validation of the electric field distribution and of the efficacy of bipolar cancellation and CANCAN in the quadrupole configuration comprised the preparation of a multi-layer cell culture system, sample exposure to 50 pulses of a 600 ns unipolar or 1200 ns bipolar pulse delivered at 10 Hz, and descriptive, inferential and effect-size statistics on select inter- and intra-experimental results.

6.2 Approach

As bipolar cancellation has largely been studied in dipole electrode configurations, it was thought that a more complex electrode arrangement in the form of a quadrupole might provide insight into BPC mechanisms. The primary objective of Aim 2 was thus to validate BPC under comparable exposure conditions and add to recent findings regarding BPC in two-electrode systems by examining BP nsPEF electropermeabilization in the quadrupole system. To determine whether BPC occurs and identify how it manifests spatially in a non-linear electric field, asymmetric amplitude bipolar pulses were first applied to a single working electrode and grounded at one or two adjacent electrodes and visualized. As with the unipolar case in Chapter 5, stereo microscopic imagery allowed for a qualitative evaluation of YP1 uptake to consider whether factors such as incident field vector or electrode proximity might play a role not observable in two-electrode exposure studies.

Given that exposures occurring between the blunt ends of curved electrodes disperse the vector electric field, bipolar pulses applied in the same manner as unipolar pulses were expected to exhibit spatially dependent bipolar cancellation. To test the hypothesis (H_{2a}) that cancellation

efficiency spatially varies in a non-uniform field, YP1 uptake after single-ground quadrupole nsPEF exposure was thus measured at three inter-electrode points and compared with respect to the unipolar response at the same points. Pulses were delivered to one electrode; an adjacent one was grounded while the other two remained floating. To simplify the matter of measuring only a single endpoint (post-exposure YP1 fluorescence) for an interrogation that has spatiotemporal as well as directional components, BP nsEPs are reported in terms of the pulse phase amplitude ratio (φ_2/φ_1), but described as a percentage in the text. The same φ_1 input voltage of 4.5 kV was used in order to make reasonable comparisons with the results from UP nsEP delivery, which served as a positive control. This produced attenuated applied voltage amplitudes of 2.44 ± 0.06 kV. A 2-point Gaussian blur was applied to each post-exposure fluorescence image and ROI data were collected across the quadrupole's equatorial *x*-axis and between active electrodes along the *y*-axis. The fluorescence intensity value was obtained at points A, B and C for each pulse type. The amplitude of the UP nsEP was normalized to a value of '1', with its corresponding YP1 fluorescence value representing the 100% response.[1] The unipolar pulse was thus described by a phase ratio of '0' and the bipolar pulses by their appropriate decimal value.

After plotting results from the three BP nsEP types at the selected points, a curve fit analysis was performed to assess the linearity of the relationship between phase amplitude symmetry and electropermeabilization. Regression analysis was used to model bipolar cancellation dynamics as it gives information on the relationship between a response (dependent) variable and one or more predictor (independent) variables, such as confounders and risk factors, whose importance is determined through expanded systems analysis. The response variable here is, of course, YP1 fluorescence intensity, whereas the bipolar pulse phase ratio is the predictor variable. To provide a simple model that could be built upon to describe the general behavior of cell electropermeabilization under known cancellation conditions, a set of algebraic expressions was then established based on the spatial intensity values of YP1 fluorescence corresponding with each of the three bipolar pulse types. These expressions serve as a jumping-off point for further development of models to aid in predicting BPC in space.

---

[1] This only defines the positive control unipolar response by which subsequent bipolar responses are compared. It is not meant to imply 100% electropermeabilization.

To spatially assess BPC efficiency, YP1 uptake for UP compared to BP nsPEF exposures is illustrated and discussed relative to the anodal phase electric field. The algebraic expression was conceived of based on results generated from single ground UP (0%) and BP (25%, 50% and 70%) pulses at three inter-electrode positions, A-C, in Fig. 4-5. Because the goodness of fit and accuracy of conclusions depend on the type and quality of data used, it is imperative to use truly representative data that is properly compiled. Given that the underlying hypothesis of this dissertation assumes linearity between nsPEF strength and electropermeabilization response, the linear regression model was specifically employed here. It describes the linear relationship between response variable, *y* and predictor variable, x_i, where $i = 1, 2, ...n$, of the form

$$f(x) = \beta_0 + \beta_1 x_1 + \beta_2 x_2 + \beta_3 x_3 + \cdots + \beta_n x_n + \varepsilon \tag{6-1}$$

where β_0, β_1, β_2 and β_3 are regression coefficients (unknown model parameters), and ε is the error due to variability in observed responses. The *trendline* function in MS Excel was first used to visually compare different order polynomials and identify candidate models, limiting selection to those with $R^2 \geq 0.95$ regression coefficients for fitting the BPC data. A second-order polynomial appeared to fit each of three data sets best, which has the form:

$$y = \mathrm{a} + \mathrm{b}\varphi + \mathrm{c}\varphi^2 . \tag{6-2}$$

Bipolar cancellation has been shown to peak when a biphasic bipolar pulse has a second-phase amplitude roughly 50% of the first, but until now has only been measured one-dimensionally between one working and one ground electrode. Due to the plane-perpendicular application of the electrodes and non-linear fringing fields cells were exposed to, examining the role of polarization between only two electrodes was considered an important objective in determining BPC efficiency. The formation and breakdown of electrical double-layers due to charging and discharging between the high voltage and ground electrodes, which can affect the response of the cell sample as a dielectric medium. Electropermeabilization polarization, defined here as the alignment of cell responses to the cathodal or anodal electrodes, have been observed in single cells exposed to nsPEFs. Unipolar responses were shown to favor the anode; bipolar responses were balanced if symmetrical, whereas they favored the electrode corresponding with

the higher amplitude phase if asymmetrical [88, 143]. For this reason, it was hypothesized that YP1 uptake in the tissue model balances between cathodal and anodal electrodes under single-ground bipolar nsPEF exposure parameters prescribed for this work (H_{2b}). To test this, the BPC efficiency of the three asymmetric pulses was determined by comparing YP1 uptake at the high-voltage and the ground electrodes. The two polarity values were calculated by taking the average YO-PRO®-1 fluorescence from each half of the "anode" and "cathode" sides of the target sample area, defined by a 0.25 µm wide by 1 µm long inter-electrode ROI. Statistical analysis was performed using an unpaired two-sided *t*-test for differences in YP1 uptake at a 0.5 alpha level of significance.

Finally, to establish a foundation for the assumption laid out in Chapter 2 (see Fig. 2-6) that regions of higher cancellation are a pre-requisite to successful CANCAN, the bipolar nsPEF and YP1 fluorescence distributions are illustrated and analyzed along the regions between the h.v. (E2) and base floating (E3) electrodes with a cis-dual ground connection. This configuration was chosen to serve later in Chapter 7 as a basis of comparison for the successful example of CANCAN in the linear quadrupole. E2 was charged by a 3 kV UP or BP nsEP, which produced a 1.7 kV load voltage for the UP nsPEF and ~1.6/0.8 kV for the BP nsPEF.

6.3 Results & Discussion

6.3.1 YP1 uptake varies among asymmetric amplitude bipolar exposure regimes

Validating BPC with the current system seemed like a logical objective, but with multiple conditions, the question was how to approach interrogation. As results with UP nsEPs demonstrated that changing the ground configuration spatially alters nsPEF electropermeabilization, the first objective of Aim 2 was to image and compare features of inter-electrode and axial responses when a second ground electrode is added. To obtain a broader view of the response distribution, BP nsEPs were delivered with the first phase charged to 4.5 kV. YP1 fluorescence was captured under the same exposure conditions for different ground (top row) and pulse (left column) parameters as shown in Fig. 5-8. In the montage, features of localization and intensity of the YP1 signal are contrasted between conditions. A cursory qualitative review of the post-exposure fluorescence imagery from stereomicroscopy presented in Fig. 6-1 helped to home in on some immediately observable and contrasting features between responses to the different types of bipolar pulses and ground configurations.

The first thing that stands out is that, save for YP1 uptake by a few stray cells, likely due to damage caused during cell preparation, no clear pattern of fluorescence is present in the sham exposure images. This is crucial because it confirms that cells are not damaged by the act of impressing electrodes into the gel-suspended cells. When scanning across single-cis-trans, YP1 uptake for a 25% BP nsEP appears to localize primarily at the ground electrodes in the first two configurations, but be dispersed when the two grounds are side-by-side. For the 50% BP nsEP case, inter-electrode intensity appears to be overall lower than for the other two pulse types, with some localization seen around the h.v. electrode in the far-right frame. The opposite appears to be true for the 70% BP nsEP, with inter-electrode intensity being the strongest compared to all other BP configurations. However, fluorescence appears to be more distributed rather than strongly localized around a particular electrode.

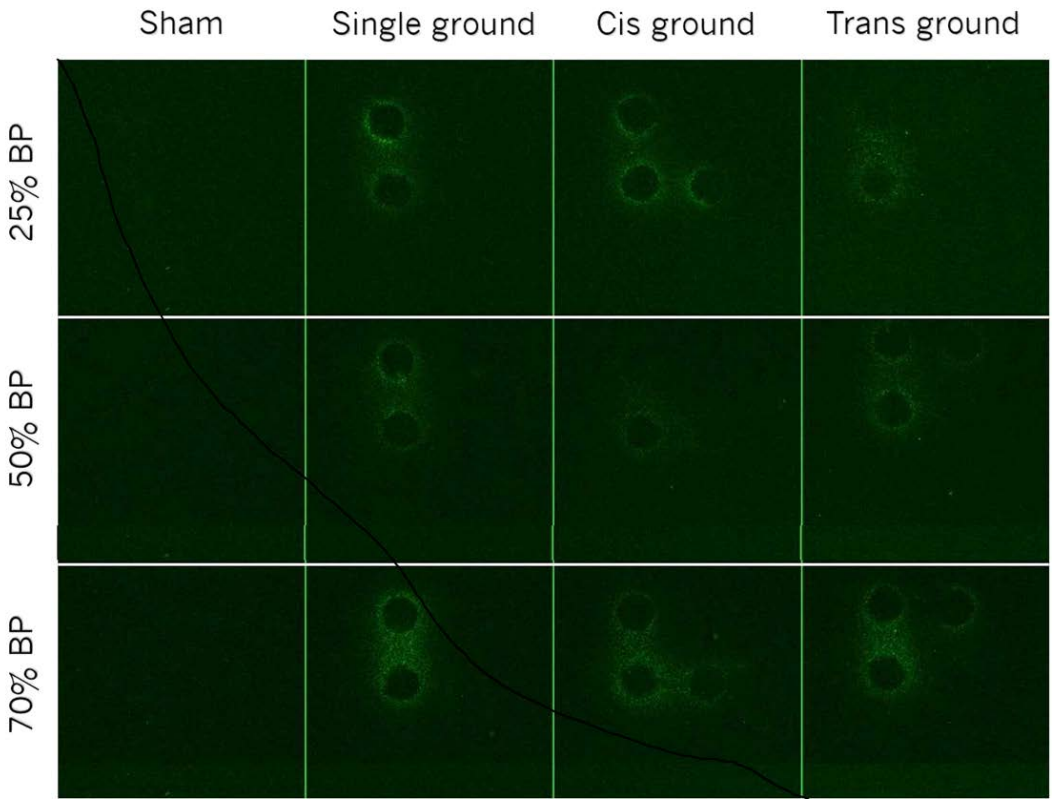

Fig. 6-1 Sample images of YP1 fluorescence after bipolar nsPEF exposure. Pulses were delivered to the bottom-left (h.v.) electrode. Rows show percent phase amplitude and columns show ground electrode configuration.

6.3.2 Spatial character of YP1 uptake differs between bipolar and unipolar exposures

One way to interrogate a possible role for the vector field on BPC was to evaluate electropermeabilization at different points in the field. Since quadrupole electropermeabilization occurred across a gradient that also included the influence of double-layer effects, YP1 uptake was measured at the quadrupole axial center (A), at the halfway point between the h.v. and ground electrodes (B), and at the h.v. electrode where E_{max} occurs. As Fig. 6-2 shows, YP1 uptake displays a similar response pattern at all three points in the quadrupole plane, with electropermeabilization decreasing for a 25% BP nsEP case to roughly 50-70%, relative to the unipolar response. This decreases a further ~15% when the second phase is 50% of the first, except at 'A', which is the axial center of the quadrupole. Here, the bipolar response *increases* by about the same magnitude. When φ_1 is 70%, YP1 uptake at all points increase relative to the 50% BP nsEP, but with each markedly different relative to the unipolar response. Proximal to the h.v. electrode, BPC occurs, with YP1 uptake at about 70% of that for the UP response. Between the h.v. and grounded electrodes, YP1 uptake is only ~5% higher, and for the 70% BP nsEP, YP1 uptake is much (75%) higher than that for the unipolar pulse.

6.3.2.1 Modeling bipolar cancellation

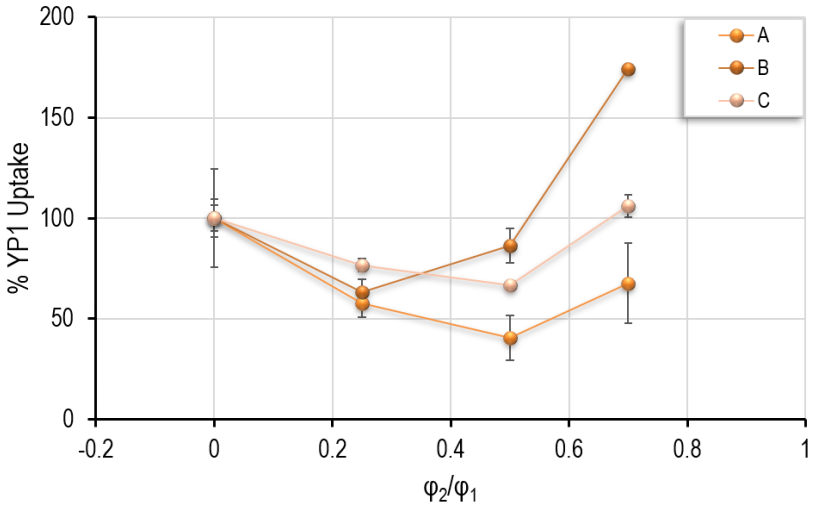

Fig. 6-2 Spatial-intensity plot of YO-PRO-1® uptake as a function of the bipolar pulse phase ratio. Cancellation efficiency is represented as the mean +/- SEM of n = 3 or 4 independent experiments.

The ability to quantitatively predict BPC is crucial to nsPEF technology design and development, yet it has been elusive to date. Elucidation of its mechanisms is partly limited by the fact that it has not been specifically demonstrated in high cell concentration samples or analyzed regarding the vector field. Although Fig. 6-2 showed that BPC differed spatially in magnitude, similar patterns relating YP1 uptake to the pulse phase ratio were observed. It was inferred from this that if electropermeabilization is proportional to the bipolar pulse phase amplitude ratio, then the relationship can be quantified to predict BPC in space for a given cell type. The objective was thus to formulate a quantitative model that might facilitate a simple algebraic description of BPC in terms of the pulse amplitude phase ratio for predicting spatial responses within experimental constraints.

Regression analysis is about determining how changes in the independent variables are associated with changes in the dependent variable. Coefficients tell you about these changes and *p*-values tell you if these coefficients are significantly different from zero. The model is meant to include the essential features of the relationship between bipolar nsPEFs and cell permeabilization and exclude superfluous details, only to the degree that the relationship can still be described with reasonable accuracy within experimental constraints.

The normalized value of YP1 uptake (y-axis), φ is the value of the second phase of the bipolar waveform as a fraction of the scaled unipolar waveform. The data for each of the plots shown in Fig. 6-2 were imported into the online software tool, MyCurveFit (MyAssays Ltd., England and Wales, #07089538). A Cubic Regression was then performed on each set, which returned the functional coefficients in Fig. 6-3 according to their sequence in (5-2), with respective error values given in Table 6-1.

Table 6-1 Bipolar cancellation goodness-of-fit analysis

Position	± Error		
	a	b	c
A	0.070	0.485	0.669
B	0.061	0.426	0.587
C	0.103	0.714	0.985

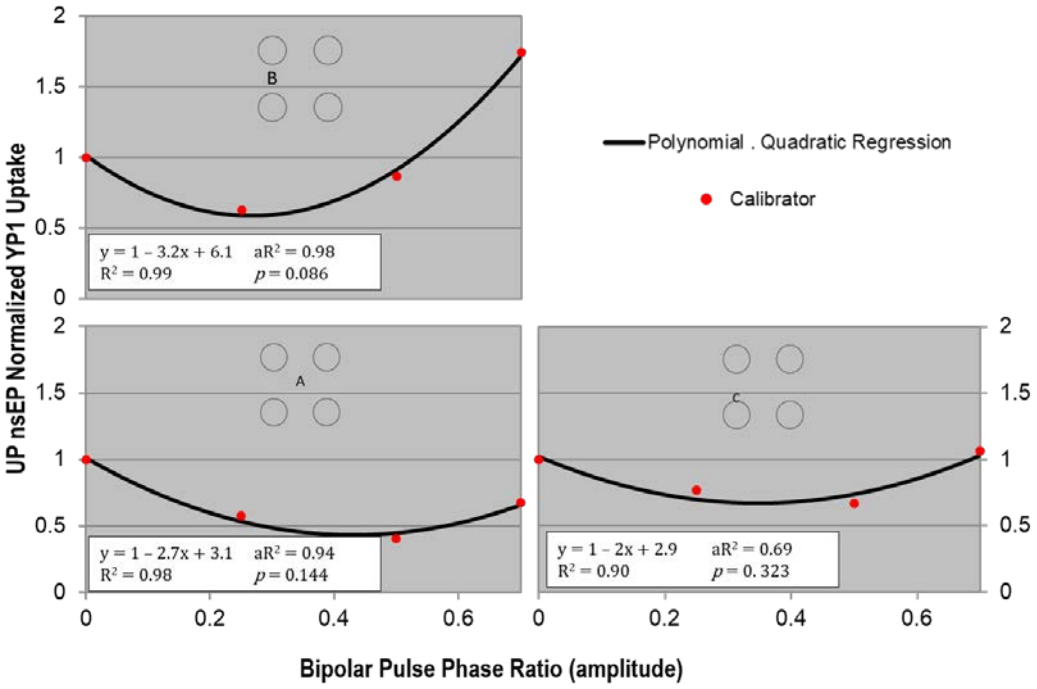

Fig. 6-3 Curve fitting using polynomial quadratic regression to model bipolar cancellation. Calibrator represents mean fluorescence data (n = 3) from Yo-Pro-1® uptake after exposure to a BP nsEP delivered by one working electrode grounded by one electrode in the planar quadrupole.

The $R^2 = 1$ value for all three expressions, corresponding to the calculated coefficients, suggests a very good fit between the model curve and the pattern of fluorescence for the BPC parameters studied and within the boundaries of the experimental data. The Durbin-Watson Statistic[2] (DWS) values shown indicate a moderate positive autocorrelation, or the degree to which a subsequent increase in the second phase will be positive if the previous is positive. As qualitative analysis also suggested, the coefficients at positions A and C are identical when rounded to the nearest tenth and suggest that response behavior can be predicted using the same model at these inter-electrode positions.

[2] The Durbin-Watson Statistic (DWS) is used to detect the presence of autocorrelation in the residuals of the regression. DWS values range between 0 and 4. A value close to zero indicates positive autocorrelation between residuals; 4 indicates negative autocorrelation, and a value around 2 indicates there is no significant autocorrelation.

6.3.3 Electrode polarization effects differ between unipolar and bipolar exposures

In addition to the discovery that there are spatial differences in YP1 uptake, considering also that unipolar responses showed anodal bias based on the applied voltage, it was necessary to similarly examine the possible differences in charging effects caused by electrode polarization when bipolar pulses are applied. Qualitative examination of the line created by averaging pixels across a rectangular ROI drawn around the flux line between the cathodal and anodal electrodes revealed that exposure to 50% BP nsEPs resulted in unbiased YP1 uptake. Similar to results from a UP nsEP delivery (Fig. 6-4 (a)), the YP1 uptake pattern for a 25% BP nsEP (Fig. 6-4 (b)) displayed cathodal bias but had an overall lower response. Fluorescence due to YP1 uptake from exposure to electric fields from 50% BP nsEPs (Fig. 6-4 (c)) appeared evenly distributed along the same pattern as the electric field gradient, with no polar bias. In contrast, when the second phase was 70% of the first (Fig. 6-4 (d)), not only was a slight reversal in maximum YP1 fluorescence localization to the "*anode*" detected, but fluorescence along the full length of the averaged inter-electrode region was higher overall for than for the UP response, with a roughness that was also more evident than in comparison to the other BP and UP nsEPs.

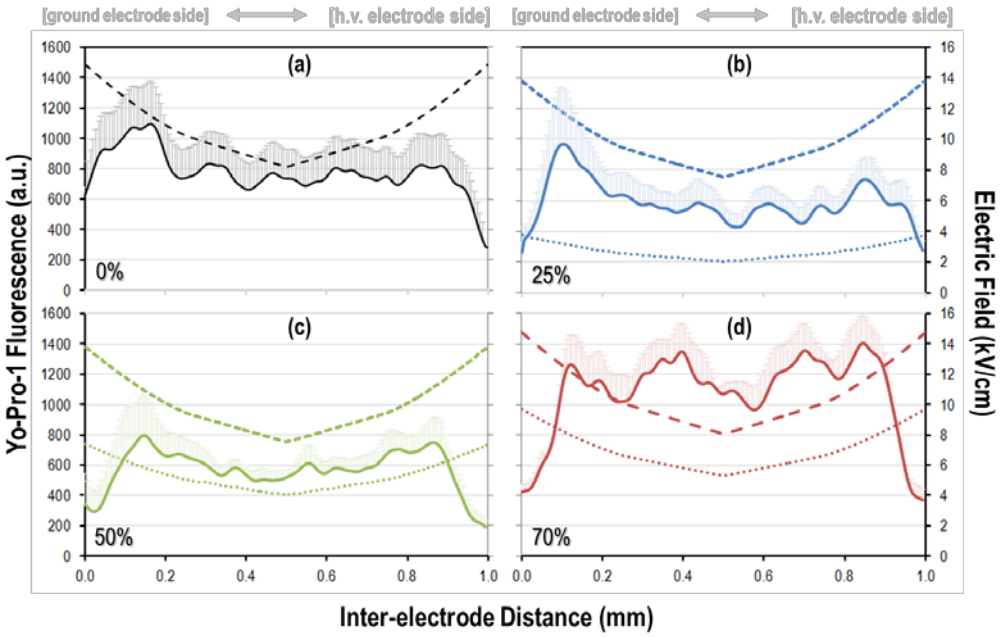

Fig. 6-4 Effect of electrode polarization on YP1 uptake. Each plot shows mean ± SEM fluorescence intensity (solid line) measured with 2-pt Gaussian blur filter along the flux line between the h.v. and adjacent grounded. The first (dashed line) and second phase (dotted line) |E| are shown for each UP (a) and BP (b-d) pulse charged to 4.5 kV. Pulse phase ratios are expressed as percentages.

When A_F versus C_F was compared, no statistically significant difference in response polarity was found for each asymmetric pulse type tested. This diverges from results of the linear quadrupole study [6], which clearly displays YP1 uptake, albeit reduced relative to the unipolar result with equivalent first-phase amplitude, favoring the "*anodal*" electrode. That the linear example employed embedded electrodes may account for this difference, as more cells would have been exposed to the stronger uniform field at the center region of the electrode. Of further contrast is the finding from Valdez *et al*. [64] during a study of asymmetrical width BP nsPEF exposures where "*anode*" dependence of YP1 uptake was present for a positive first-phase 900 ns pulse followed by a negative second-phase 300 ns pulse. The reverse was true (*i.e.* "*cathode*" dependence was present) when the phase widths were reversed. As of this writing, no similar studies were found regarding polarization effects on nsPEF electropermeabilization in single cells given an asymmetric amplitude bipolar pulse waveform.

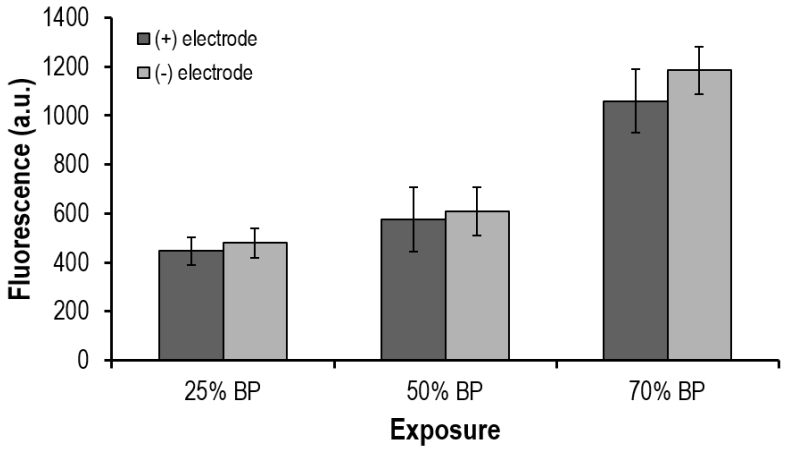

Fig. 6-5 Influence of electric polarity on Yo-Pro-1 uptake for single-ground unipolar pulses based on voltage amplitude. Statistical significance is set at $\alpha = 0.05$.

6.3.4 BPC efficiency and electric field distribution

Although it was important to quantify the exposure-response relationship at specific points in the quadrupole plane, it was thought that spatially characterizing the relationship between the |E| and electropermeabilization distributions for unipolar and bipolar nsEPs might reveal more about bipolar cancellation efficiency. Of specific interest were the base (E2/E3) and equatorial regions between the h.v. and floating electrodes as shown in Fig. 6-6. To focus on the

distal rather than electrode-proximal response, only the field and fluorescence values for the central 0.6 mm gap region were considered.

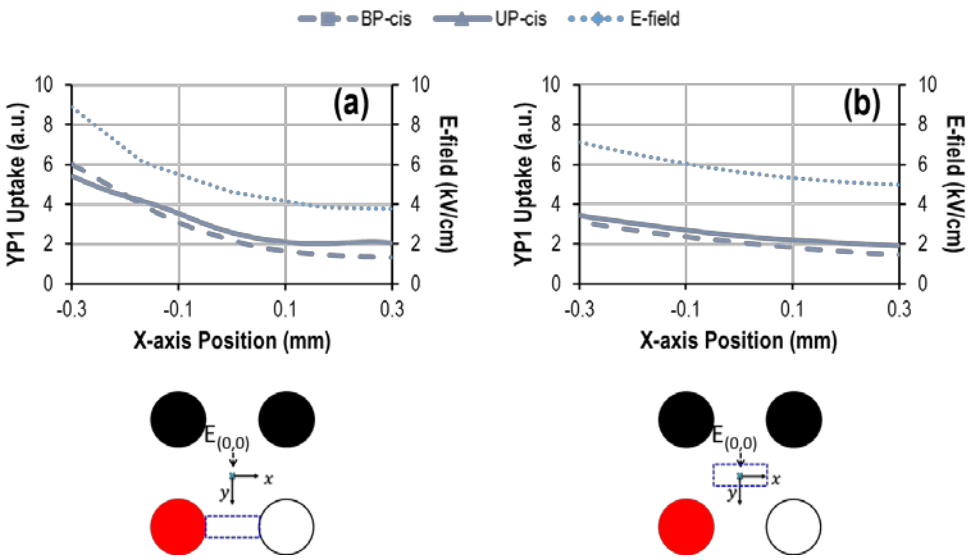

Fig. 6-6 Bipolar cancellation pattern at two different positions in the quadrupole plane for a 50% pulse.

The anodal phase electric field is strongest starting from the h.v. side of the quadrupole and weakens toward the rightmost side of the measured region over both ROIs. It is highest between E2 and E3 at ~9 kV/cm compared to ~7.2 kV/cm in the center region close to E1 and E2. On the opposite side of the quadrupole, the reverse is true. For the axial ROI, |E| is slightly higher at ~5 kV/cm than at the same vertical position between E2 and E3 at ~3.2 kV/cm. |E| is 0.5 kV/cm higher along the y-axis in the equatorial position than between E2 and E3.

In both regions, YP1 uptake from both UP and BP exposures generally follows the |E| distribution. Bipolar cancellation is evidenced by the dashed line falling below the solid line and is thus indicated across both regions, but it is mild. However, the UP response drops below that of the BP response approaching E2 in Fig. 6-6 (a), indicating electrical double-layer influence. Based on the finding that BPC was minimal in the target region, per the assumption illustrated by Fig. 2-6, it was expected that this would lead to poor CANCAN. Nevertheless, as both UP and BP responses generally follow the trajectory of the field, adjustments to the charging voltage or electrode shape or distance may allow for greater separation between the two to be achieved.

CHAPTER 7

CANCAN IMPLEMENTATION: A PILOT STUDY

7.1 Introduction

Gianulis *et al*. [6] successfully demonstrated moderate distal electropermeabilization by CANCAN using a linear quadrupole system. The goal of the final part of this study was to verify that spatial modulation of nsPEF electropermeabilization using the CANCAN technique is feasible in a coplanar quadrupole system. Proximal to the electrodes, electropermeabilization was expected to be eliminated or reduced relative to the quadrupole center. This is because reversing the electric field vector by delivering a subsequent pulse of opposite polarity initiates a local bipolar nsPEF response, which becomes increasingly unipolar approaching the axial center due to destructive interference of a second superposing wave caused by delivering an anti-polar pulse to an opposing electrode, demonstrating the potential for remote tissue stimulation. The study by Gianulis *et al*. demonstrated that two pulses, at least one of which is polyphasic, could be delivered independently by gel-penetrating electrodes such that the superposition of their electric fields produces relatively stronger UP nsPEF electropermeabilization in suspended cells between the two innermost electrodes of a linearly arranged quadrupole [6, 61]. In order to provide preliminary evidence for a more effective 2-D remote nsPEF biomodulation capability, a pilot study was conducted to test both theory and empirical data described in earlier chapters. The coplanar quadrupole electrode system was thus employed using the CANCAN technique and assessed for its effectiveness in creating a unipolar-equivalent nsPEF electropermeabilization response at the axial center. This was followed by an evaluation of the system and its ability to exploit bipolar cancellation to facilitate remote nsPEF electropermeabilization. Taken together, the information gleaned in this chapter serves to further the potential for the development of a non-invasive, 2-D remote nsPEF biomodulation capability.

7.2 Approach

The first objective was to identify feasible pulse modes for realizing CANCAN. The next was to apply synchronized pulses by independently charging adjacent electrodes such that the second, anti-polar (superposing) pulse began at the second phase. YP1 uptake was then

compared between regions closest to the electrode first charged and at the axial center. Although time and resource constraints did not allow for a full study, it was possible to pursue two main objectives toward the aim of implementing and quantifying CANCAN. The first was to determine a pulse application regime expected to produce visible YP1 uptake at the quadrupole center. The second was to demonstrate CANCAN by delivering the synchronized pulses and confirming whether and to what degree responses aligned with expectations.

Feasible pulse modes for realizing CANCAN were identified by sampling from the various pulse generator channels and adjusting the positive and negative voltage sources to ascertain which settings would align the synchronized phases best. Two regimes were constructed comprising a monophasic unipolar pulse synchronized with the second phase of a biphasic bipolar pulse (2+1) or a bipolar biphasic with the second phase of a bipolar triphasic pulse (3+2). Their respective representative waveforms are shown in Fig. 7-1 (a) and (b). Each was delivered to paired electrodes such that their superposition would sum to a unipolar pulse. The other two electrodes were grounded and voltages at the biological load were measured by two probes.

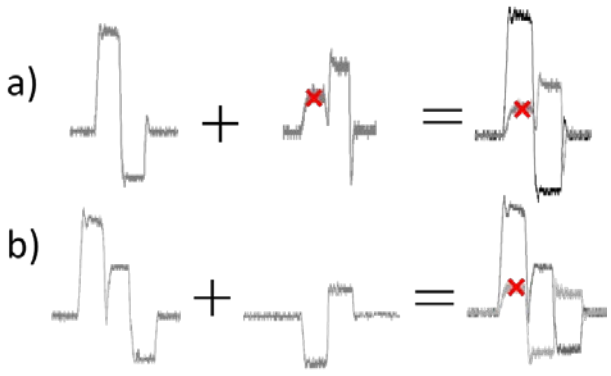

Fig. 7-1 Pulse waveform options for applying CAN-CAN: a) biphasic cancellation and b) triphasic cancellation.

The second part of this chapter and final aim of this research was to evaluate the current system for its overall ability to support remote biomodulation by nsPEF. Insights gleaned regarding bipolar cancellation characteristics of this system were incorporated along with spatial modeling of UP and BP nsEP transients to establish a means by which remote biological response might be achieved by applying the CANCAN technique using quadrupole electrodes.

within a given set of constraints. These illustrative models were then compared with results of published research on BPC studied in 1-D systems. A second objective was to conduct a spatio-temporal analysis of CANCAN from the perspectives of the vector field, pulse waveform dynamics and grounding configurations to gain insight into cancellation mechanisms and identify any patterns that might reflect the magnitude of the biological responses. Finally, the third objective was to quantitatively compare and contrast 2-D versus 1-D quadrupole electrode permeabilization by synthesizing and comparing experimental results from Aims 1-3 against those obtained from the related recent linear quadrupole study by Gianulis *et al.* [82] to verify parameters that could be optimal for manipulating proximal versus distal responses.

7.3 Preliminary Results

As with the unipolar and bipolar exposures, the phase duration, number, and repetition rate were kept constant for each contributing CANCAN pulse. Preliminary data was obtained for different peak amplitudes, number of phases and phase amplitude ratios. The pilot test was conducted using three pulse synchronization schemes based on these independent variables as listed in Table 7-1. For each set of CANCAN conditions, the phase one (φ_1) amplitude was used as a reference (100%), with each subsequent phase (φ_s) set as a percentage of the former. For ease of narrative description, exposures were defined as: CANCAN A (100/45%), CANCAN B (100/26%) and CANCAN C (100/41/27%).

Table 7-1 Peak amplitude for each synchronized CANCAN pulse

Pulse Phase	CANCAN A n = 3		CANCAN B n = 1		CANCAN C n = 2	
φ_1	1.35	—	2.26	—	1.42	—
φ_2	0.59	-0.63	0.43	-0.76	0.64	-0.53
φ_3	n/a	n/a	n/a	n/a	0.48	-0.29
	+	–	+	–	+	–

As it was with the unipolar and bipolar calculations, numerical approximations of the electric field were scaled based on the peak applied voltages for each phase. Unlike with CANCAN A, it was more difficult to match the magnitudes of the positive and negative

independent pulses during phase two of CANCAN B and C. Due to this limitation, superposition would result in incomplete cancellation during the second and third phases, so limited or no distal YP1 uptake was expected.

7.3.1 Proximal versus distal effect

Since it was possible to complete three independent CANCAN A experiments and since the synchronized second phases were well matched in opposing amplitudes, proximal and distal responses were considered first for this 2+1 combination. To confirm whether CANCAN A could reduce nsPEF electropermeabilization at the electrodes normally occurring with UP nsEPs, analysis of YP1 uptake were limited to two regions of interest (ROIs): a 1×0.25 mm rectangular area tangent to the interior edge of the first-charged electrode (E1) facing the quadrupole interior, and a 0.5 mm $\times$ 0.5 mm square area encompassing the axial center. NsPEF responses from a 3 kV first-phase charging voltage were measured at these two positions and plotted in Fig. 7-3 for the following conditions: single- and cis-dual ground unipolar, cis-dual ground bipolar and CANCAN A nsPEF exposure.

For the CANCAN A sequence, where a ~45% BP nsEP (↑1.35↓0.63 kV) was synchronized with a 0.59 UP nsEP, proximal YP1 uptake was 25.9% higher than for a 1.7 kV single-ground UP exposure, but on par with the cis-dual ground UP exposure. This contrasts with a cis-dual ground 50% BP pulse (↑1.6↓0.8 kV), the response to which was surprisingly ~15% higher at the reference electrode than it was for the UP pulse. As Fig. 7-2 (b) depicts, there was no significant difference in YP1 uptake between all exposures in the axial region.

To confirm whether a higher pulse amplitude or additional phase might be better at reducing nsPEF electropermeabilization at the electrodes and creating a distal (axial) response, and especially to assess the effects of incomplete cancellation, YP1 uptake in the same two regions was compared between all three CANCAN pulse synchronization regimes. Results from these are shown in Fig. 7-3. A relative CANCAN effectiveness score (rCCE) was defined to aid in quantifying this comparison as follows:

$$\text{rCCE} = \text{distal response} / \text{proximal response}$$

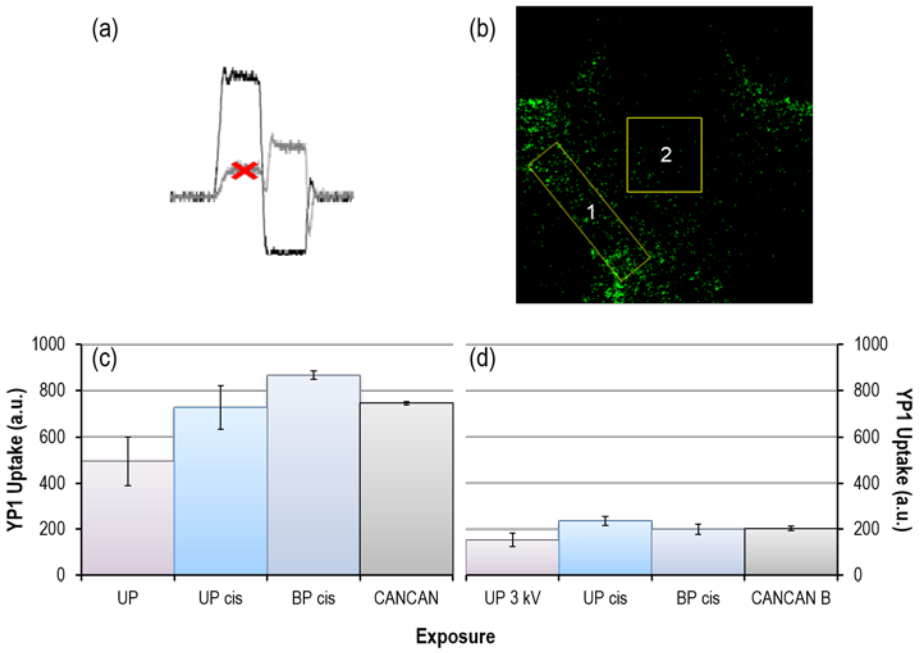

Fig. 7-2 Comparison of proximal and distal YP1 uptake for a CANCAN A (2+1) pulse synchronization.

The proximal response from one CANCAN B experiment, with its higher φ_1 amplitude at 2.26 kV and partly cancelled φ_2, had a score (0.58) twice that of the lower strength φ_1 CANCAN A equivalent (0.27). The CANCAN C scheme was the least effective with an rCCE score of 0.09.

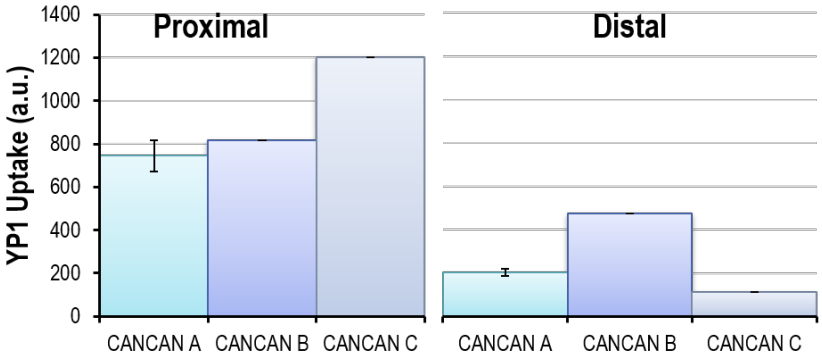

Fig. 7-3 Spatial analysis of fluorescence after application of CANCAN technique.

When the preliminary data from all three CANCAN approaches were compared, results suggested possible notable relationships between response localization and waveform character. While CANCAN A and B had similar synchronization regimes, the proximal responses were about the same despite the difference in φ_1 magnitude, yet the distal response was 57% higher for B. For CANCAN C, the proximal response was even higher than it was for B despite the lower φ_1 value, but YP1 uptake at the axial center was the lowest overall. Due to small sample sizes, additional experiments are necessary to confirm the accuracy and statistical significance of these early results.

7.3.2 CANCAN reduces UP uptake, but not at charged electrode

Based on unexpected results of high bipolar nsPEF responses relative to CANCAN A (Fig. 7-2), it was worth investigating whether the analytical approach used may have been insufficient. It was thought that if the proximal ROI measured along the center-facing part of the electrode was in fact drawn too long, then it was possible that pixel data otherwise confined to the flux line region between electrodes was erroneously being included. To test the hypothesis that CANCAN under certain conditions can produce an effective remote electropermeabilization response at different inter-electrode points in the quadrupole plane, YP1 uptake was measured and compared among cis-UP, 50% cis-BP and CANCAN A exposures between electrodes E1 and E2. The common φ_1 pulse charge amplitude was 3 kV. Statistical analysis of YO-PRO®-1 uptake 15 min post-exposure was determined with an unpaired two-tailed *t-test*, alpha = 0.05.

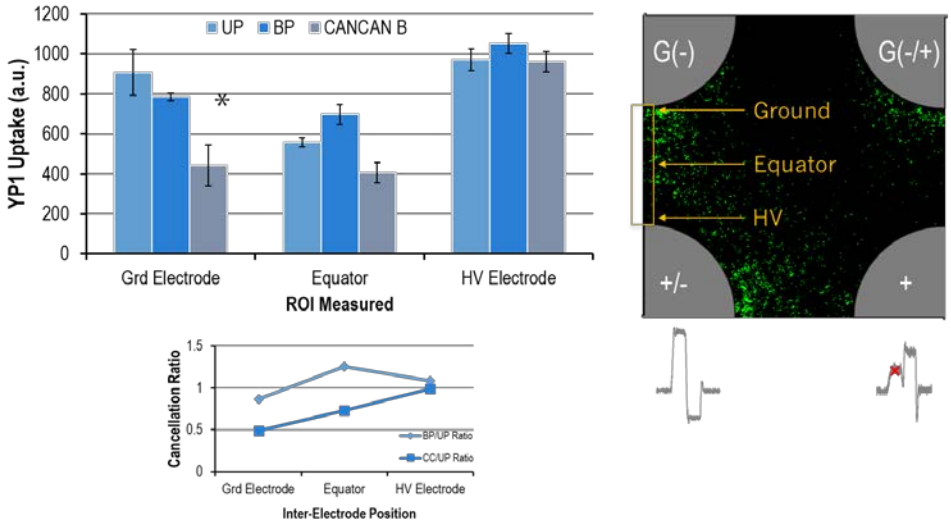

Fig. 7-4 Inter-electrode effect of CANCAN on electropermeabilization.

Significant reduction of YP1 uptake did occur ($p = 0.038$) nearest an electrode relative to the UP response, but it was the ground electrode rather than h.v. electrode. Though not quite statistically significant, the equatorial position indicates the higher relative BP nsPEF response ($p = 0.059$) observed in the first section of this chapter, as well as a lower relative CANCAN A response ($p = 0.053$). Differences in exposure types were not significant at the h.v. electrode.

7.4 Evaluation of Remote NsPEF Biomodulation

The long-range goal of this work is to be able to remotely stimulate a biological response to nsPEF. Two aspects of nsPEF were already investigated as part of this work. The ability to spatially manipulate nsPEF electropermeabilization was qualitatively and quantitatively explored by varying the ground connection of UP and BP nsEPs delivered to the tissue model by a planar arrangement of quadrupole electrodes driven by a pulsed power system. This first involved assessing the vector details of the electric field responsible for the spatial differences in the planar bipolar nsPEF responses. The purpose of this chapter is to build on the understanding acquired through these experiments to determine the feasibility of using the planar quadrupole exposure system as a non-invasive nsPEF delivery technique. The objective is then to consider the vector character of the electric field in more detail and assess it against the quality of spatial nsPEF electropermeabilization in the target tissue model. This would provide insight into how waveform polarity transitions over a field gradient may be reflected in cell responses.

7.4.1 Assessment of the role of bipolar cancellation efficiency in effective CANCAN

Bipolar cancellation efficiency was evaluated by quantitatively comparing and contrasting 2-D versus 1-D quadrupole electrode permeabilization by synthesizing and analyzing experimental results produced in this study along with those (published and unpublished) obtained from a related study by Gianulis *et al*. [121], who recently validated bipolar cancellation using a modified linear quadrupole electrode configuration driven by the same modular nanosecond pulse generator used in this work. As Table 7-2 describes, the linear system electrodes each had a larger radius than that for the planar system and were separated by twice the distance. This is important because it generally results in a more homogenous field. It must also be noted that the linear system tested BPC at the center of the electrodes, which were embedded in the gel-suspended cells, whereas the planar system tested the phenomenon at the

surface of the 3-D culture, where the electrodes were instead sitting in a PBS electrolyte. Since charging voltages were roughly the same in both studies, the effect on the above is evident in the electric field ranges produced, which was twice as high for the planar system. BPC trends found in both were in line with earlier studies reported in Chapter 2, in which BPC peaked at second-to-first-phase ratios of 20-60% for various exposure systems and biological markers used.

Table 7-2 Bipolar cancellation efficiency of a linear versus planar quadrupole system

	Linear Quadrupole	Planar Quadrupole
Gap Distance	• 2 mm	• 1 mm
Electrode Diameter	• 1.6 mm	• 1 mm
Max Electric Field Range	• $4 < \vec{E} < 20$ kV/cm	• $0.5 < \vec{E} < 40$ kV/cm
Max BPC By Φ_2/Φ_1 amplitude	• ~2-3 fold when 20-60%	• ~2-3 fold when 25-50%
Pulse Number, N	• For N $\leq$ 40 p, BPC not dependent on $\lvert\vec{E}\rvert$	• For N = 50 p, BPC not dependent on $\lvert\vec{E}\rvert$
Saturation	• $\geq$ 80 p, $\vec{E} \geq$ 12 kV/cm	• Not tested for >100 p

Fig. 7-5 illustrates the relationship between stimulation by the first-phase electric field of a 50% BP nsEP and electropermeabilization response using the linear quadrupole system. Fluorescence was measured between E2 and E3. Despite differences in electrode size and spacing between the linear and planar quadrupole systems and higher pulse numbers used in the linear study, it was still possible to compare responses based on the electric field values. The degree of bipolar cancellation in the linear configuration was clearly much greater across the E2-E3 gap than it is in the planar configuration (Fig. 6-6), especially at the anodal electrode.

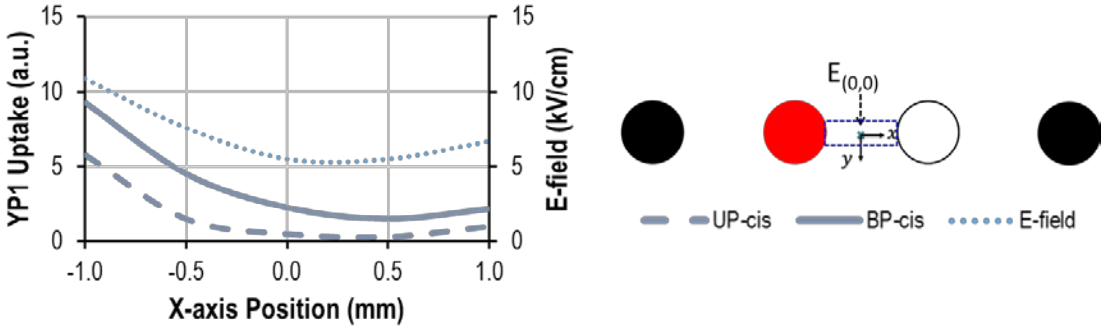

Fig. 7-5 Bipolar cancellation in linear quadrupole system exposure.

7.4.2 Vector field dynamics at select points in the exposure surface plane

The effect of independently delivering various pulse types in the same exposure was determined at key points in the 2-D plane. Results from Chapter 4 revealed similar, but distinct differences between unipolar and bipolar responses measured from the same exposure at different inter-electrode locations. To better understand such differences, *in silico* results were used to identify the 2-D vector and absolute (additive) field at specified points of interest across the exposure surface in order to assess the extent to which pulse polarity plays a role in the spatial dynamics of YP1 uptake. Although there were many possibilities in terms of where to examine the field, this investigation was limited to a circular ROI whose center was at the axial center of the quadrupole (Fig. 7-6 (a)), as this is the desired target CANCAN response location.

A 50% bipolar pulse has been shown in this work and in others to produce perhaps the strongest cancellation. This evaluation thus examines the case where a 50% BP nsEP with a 1 kV rectangular wave excitation signal is applied to E2, synchronized at the second phase with an opposite-polarity UP nsEP delivered to E3 at 0.5 kV to understand the nature and likelihood of electropermeabilization from nsPEF exposure under this condition at a given point in the plane. Fig. 7-6 shows that, counterclockwise starting from between E1 and E4, the absolute field rises briefly then drops to its lowest value between E3 and E4 before steadily increasing at points closest to E1 and E2, the electrodes activated with the initial pulse.

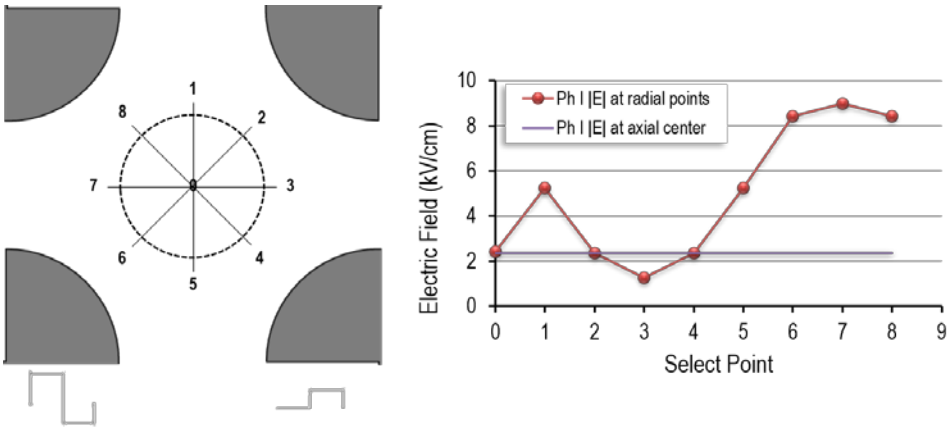

Fig. 7-6 Exploration of dynamic polarization of the CANCAN electric field around the axial center.

When the field is broken down at each point around the circle, some relevant details emerge. The nature of the non-uniform field is such that it is more or less bipolar depending on the point examined and from which perspective. Fig. 7-7 gives the breakdown of the 2-D vector field in the *x* (a) and *y* (b) directions, along with their corresponding waveforms (b, c). At the center, where electrostatic theory predicted a unipolar field upon properly synchronized anti-polar pulses, the *y* component of the field is unipolar whereas the x-component of the field has been cancelled. At opposing points 1 and 5 there is a combination of bipolar and unipolar vector field components. At points 2, 4 and 6 both *x* and *y* vector field components produced are bipolar. At points 3, 7 and 8, the x-component field is cancelled, and the *y*-component field is bipolar. The consequence and potential of these findings is that, at each point, cells or tissue will be exposed to a different field in space and respond accordingly. The simplest assumption is that electropermeabilization would correspond to the field polarity as in Table 7-3 summary. However, it must be remembered that research to date that can in part explain cell membrane responses to unipolar and bipolar fields is bi-directional. Understanding cell responses to dynamic nsPEF exposure from different directions, especially in bulk culture, has not even begun to be explored.

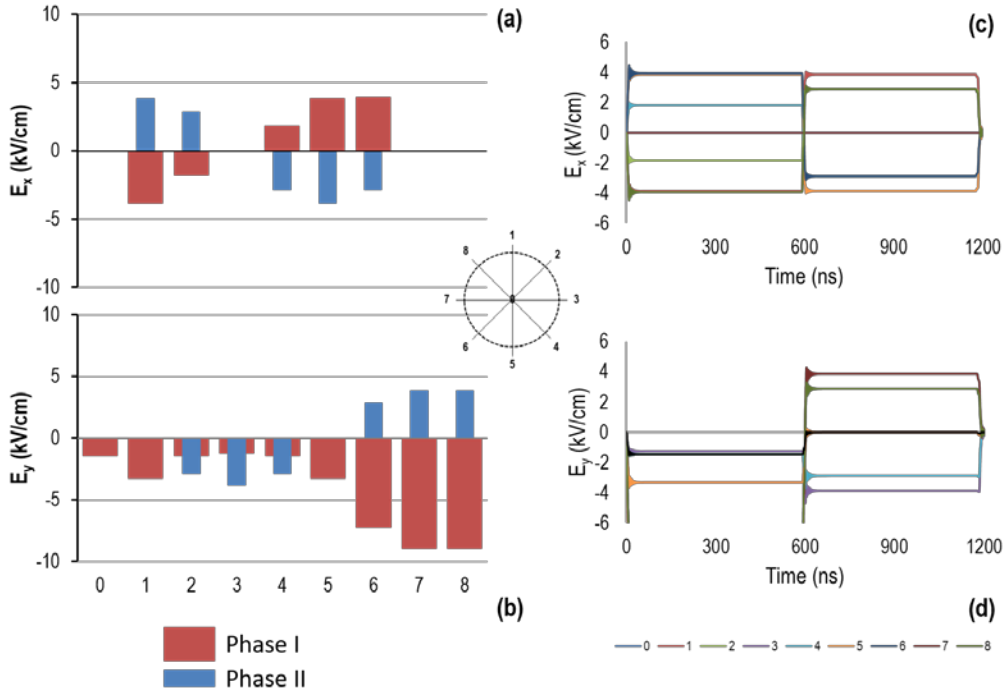

Fig. 7-7 Analysis of the CANCAN electric field at points around the axial center.

Table 7-3 Electric field polarity at points around the axial center

Field Polarity	Fraction
Unipolar	3/16
Bipolar	8/16
Additive	3/16
Cancelled	6/16

CHAPTER 8

SUMMARY

8.1 Introduction

The main research question driving this work was: how can pulse and electrode complexity be exploited to spatially modulate nsPEF electropermeabilization? Namely, what factors do pulse polarity, grounding configuration and electrode proximity play in facilitating the realization of remote nsPEF stimulation? In order to reliably determine the extent to which bipolar cancellation occurs and in what biological systems requires technologies capable of supporting multi-dimensional exploration of *in vitro* and *in vivo* responses to complex nsPEFs for various cell types. From both the biological experiments performed and numerical analysis of the 2-D electric field, this work provides evidence of how combining the right electrode configuration with independent and flexible pulsed power capabilities supports a more informative investigation of nsPEF membrane biophysics and may lead to improvement of the spatial control of nanosecond pulses to provide more effective localization of medically relevant PEFs. In silico and in vitro experimental results from this work were synthesized and are discussed in this chapter in the context of published and ongoing research to provide interpretation and assess the implications of findings against stated aims and objectives.

The principal goals of this investigation were to facilitate understanding of 2-D bipolar cancelation of nsPEF electropermeabilization in a non-uniform field, and to determine whether certain features could be exploited to control a biological response to nsPEF stimulation. A planar quadrupole electrode arrangement differentially charged by a multimodal nsPEF generator was employed to simplify comparison of unipolar and bipolar nsPEF electropermeabilization and evaluation of the feasibility of using the proposed system for remotely stimulating cells and tissues through superposition.

In this study, the need for further advancement toward the development of technologies capable of accurately targeting 3-D tissue environments (*in vitro* and *in vivo*) for nsPEF treatment was addressed. While electromagnetic field medical technology is not new, nsPEF technology has yet to be largely incorporated in current therapeutic regimens due to the uncertainty presented by so many nsPEF parameters and systems yet to be explored, as well as

the general challenge of competing with more conventional modes of treatment. This work emphasized the critical need to overcome limitations imposed by common parallel electrode-based exposure systems. Most commercially available nsPEF exposure systems cannot address the unique demands of individual research laboratories. The custom planar quadrupole electrode system demonstrated the ability to spatially modulate nsPEF electropermeabilization at the surface of a 3-D tissue model, without compromising the integrity of the surrounding tissue. Despite this achievement, certain limitations in this work, some of which are described below, prevented full realization of this novel capability at this time. New approaches to the work are therefore suggested.

8.2 Challenges, Limitations and Other Considerations

8.2.1 Apparatus

There are two principal challenges that imposed limits on this work. As both the pulse generator and an electrode interface are custom-built, their functionality has not been optimized, but much care has been taken to minimize errors and maximize accuracy during experimental design. This was largely aided by following baseline protocols that were applied for studies of the modified linear quadrupole system by Dr. Gianulis *et al.* Some voltage variance could also not be overcome between UP and BP nsEPs with the same first-phase amplitude, as well as between asymmetric amplitude BP nsEPs and those of different ground connection positioning. Due to what may be described as a combination of cross-coupling among stacks and impedance mismatching at the biological load, it was not always possible to achieve the same load voltages for all conditions being compared. Since it was impractical to continuously attempt to adjust input conditions, voltage values are only considered accurate to one decimal place.

8.2.2 Cell sample preparation and nsPEF exposure technique

Insufficient mixing or pouring can cause gel inhomogeneity and thus serve as a source of ‘noise’ in subsequent fluorescence data analyses if the cell volume isn’t fully dispersed. Another inconsistency is in making identical electrode-target contacts when manually lowering electrodes due to visual distortion between media phases in the dish. Both may be mitigated by post-processing techniques and careful selection of statistical approaches. The latter may otherwise be corrected for future work by improving the exposure set up to incorporate a physical stopper

(e.g. toothpick) when lowering the electrodes or marking the gel height segments directly on the dish prior to pulsing.

To effectively manage and ensure consistency regarding the time between exposure and image acquisition, all exposures were performed clockwise, beginning with sham. Each exposure was separated from a previous one by 1 cm to prevent mechanical disruption of the gel or exposure dose overlap. Occasionally, a few stray cells fluoresced in the sham exposure as well as in nsPEF exposure images. This was mainly attributable to YP1 uptake by cells damaged during mixing with the viscous gel. The general absence of fluorescence around the quadrupole electrodes nonetheless verified that electrode position marking did not damage cell membranes and contribute to YP1 uptake during nsPEF exposure.

8.2.3 Analysis

A prominent source of potential error that limits the precision of measured data has to do with the impact of the exposure technique used. One of the main goals of this work was to assess the possibility of using the modular pulser with planar quadrupole for non-invasive (and long-term, remote) applications. Surface-level exposure, however, was found to result in a pixel "ramp" whose intensity peaked not at the exact position associated with the electrode edge, but farther away, closer in towards the opposing adjacent electrode. One of three things likely happened: 1) the action of pressing the electrodes into a semi-soft gel culture and then lifting them to where the blunt wire ends are coplanar with the cell culture surface caused the gel culture to settle away from the ends and thus be exposed to a lower field; 2) difficulty visualizing the cell surface during exposure setup led to the electrode applicator end not aligning properly with the cell culture surface, exposing the embedded cells to a lower electric field; or 3) the cells closest to the blunt ended wires were actually exposed to weaker fringe fields rather than the maximum field normally present at electrode surfaces and upon which the theory underlying part of this work is based. As such, it must be assumed that peak electropermeabilization responses did not occur at the maximum proximal electric field. To mitigate the above, which might have occurred in combination, maximum YP1 fluorescence values proximal to electrodes were identified and typically reported as the average of bracketed pixel data in relation to a given electrode, rather than at the exact Cartesian point corresponding to the electrode-gel interface.

8.2.3.1 Detection

Membrane integrity analysis is often performed optically by measuring the uptake or release of fluorescent markers such as YOYO-1, PI, acridine orange and calcein AM. YO-PRO®-1 was used because it makes optical detection easier, but it may not be the best method for detecting electropermeabilization in this experimental system. As Napotnik *et al*. [144] point out in a detailed review article, numerous methods have been developed over decades of 'electroporation' research, each with its advantages and disadvantages, considering the available equipment and experimental conditions used. Measuring impedance is one such technique that is non-invasive and has the advantages of a fast, connected response that is often used to follow electroporation [145]. Further assessments may be valuable to ascertain which is the most suitable for this particular type of exposure study, which may be YO-PRO®-1 if the saturation and complete linear range parameters are ascertained.

8.2.3.2 Cell selection

NsPEF effects have been shown to vary for different types of cells. Of importance here is the fact that bipolar pulses do not always have the same cancelling effect in nerve cells [146]. Because CHO-K1 cells in particular lack voltage-gated channels, findings from this study cannot be generalized to all cell populations. Hence, more research is needed on other cell types.

8.2.3.3 Statistical approaches

The two-sided t-test was primarily used to determine the statistical significance between spatial electropermeabilization responses for the various pulse conditions tested. Unfortunately, time and equipment constraints meant that sample size, *n*, was too small in most cases to ensure statistical power was high enough. The likelihood of committing a Type II error (*i.e.* accepting as true the null hypothesis that there is no difference in biological response to different exposures, when in fact, there is a difference) was therefore high. This approach, however, was primarily used to identify large differences. For expanded analysis, the one-sided K-S test is useful in curve-fitting and linear regression analyses (e.g. least-squares estimation) to support predictive modeling of spatial-intensity relationships. The *Wilcoxon Rank-Sum/Mann Whitney U* approach could also be used if appropriate given: 1) the inclusion of a control group gives unpaired, two-sample (non-parametric) data; and; 2) *n* is small. To evaluate the strength of statistical claims, it

can be more insightful to use effect size – a quantitative measure of the magnitude of a phenomenon [45] – determined by means of the *Vargha and Delaney A* coefficient [147].

8.3 Future Research Recommendations

Since only a pilot study was performed as part of the work here, substantially more can be done to validate CANCAN using the planar quadrupole exposure system. First, experiments should be repeated to validate findings to date. More importantly, full validation can be accomplished by re-configuring the pulse generator to deliver the pulse amplitude ranges necessary for complete waveform cancellation and exploiting the acquired data around the full arc of the applicator electrodes. Given the challenges posed by marking electrode positioning directly in the gel, an indirect technique, such as using an electrode bumper paired with an alignment marker on the stereomicroscope, could be incorporated into the exposure system to increase accuracy and enable electropermeabilization data closer to the electrodes. Additionally, future designs should have different electrode shapes that optimize the fringing electric field in the regime where the bipolar pulse is generated. These will help minimize charge accumulation along the blunt end perimeter of the current wire electrodes.

Modeling studies show that changes in cellular dielectric parameters such as plasma membrane conductivity can significantly affect the dielectric spectrum of a cell suspension. Measuring the dielectric spectrum of CHO-K1 cells suspended in agarose gel in varying concentrations then fitting this data into proper dielectric models, such as the Maxwell-Wagner mixture model combined with a single- or double-shell cell model, could allow nsPEF-induced changes to be estimated. The temporal development of dielectric properties of CHO-K1 cells could thus be derived following exposure to quadrupole nsPEF from 50 pulses of 600 ns duration at a repetition rate of 1 Hz. Despite that there is no effective means available to image gel-embedded cells in real time, changes in plasma membrane integrity could nonetheless be assessed at various voltage amplitudes by stereomicroscopy for different times reasonably at 30 s intervals after exposure by fluorescence imaging of YP1 uptake.

Results are measured post-pulse rather than in response to what is actually a dynamic field. The temporal effects of BPC would best be understood with ultra-fast imaging, using a longer pulse width (e.g. 1600 ns) and technology like serial time-encoded amplified microscopy (STEAM), which can take an image every 163 nanoseconds. Further experiments should be run

with samples combining low- and high-conductivity media tests to determine if permeabilization is further enhanced in combination with these nsEPs in a synergistic manner.

The fidelity of the 3-D agarose gel system should be examined. According to Sigma, the manufacturers of the low-gelling temperature agarose used in this study, although anionic groups in an agarose gel are affixed to the matrix and cannot move, dissociable counter-cations can migrate toward the cathode in the matrix, giving rise to a phenomenon knowns as electroendosmosis (EEO) - a movement of liquid through the gel. Since electrophoretic movement of dye molecules like YP1 is usually toward the anode, EEO can be a confounder in the localization of membrane biomarkers due to internal convection.

Finally, these experiments, plus ones applying 100% BP nsEPs, for example, should be performed with the objective of studying cohort and abscopal effects in other areas of the cell culture gel. Due to the semi-soft nature of the gel tissue model, it is possible (especially if the gel is made at a higher percent of agarose or allowed to set longer) to cut portions of it out. DNA or RNA can then be extracted to perform polymerase chain reaction (PCR) or gene expression analysis.

8.4 Conclusions

This work demonstrated the potential for a planar quadrupole electrode system to non-invasively modulate cell membrane permeabilization in two dimensions through the selective individual or synchronized application of unipolar and bipolar nanosecond pulses. The dependency of the degree of electropermeabilization on the absolute electric field strength and vector, were quantified and analyzed, as well as the influence of electrode polarization and grounding configuration. Additionally, a pilot study was conducted to determine whether it might be possible to concentrate the biological response at the center of the quadrupole rather than proximal to the electrodes. Bipolar cancellation efficiency and CANCAN was then compared and contrasted between the planar and linear quadrupole systems. Finally, a semi-quantitative description based on spatial waveform transients of synchronized pulses was used to evaluate the potential for the planar quadrupole electrode system to remotely elicit cell responses.

Conventional methods for studying nsPEF bioeffects have relied on parallel-plate exposure of suspended cells, parallel wire exposure to single or monolayer cultured cells, or non-

specific tissue-penetrating needles. While each of these methods has its purpose and offers its own advantages, they are difficult to optimize for visualization and biophysical parameter control, such as spatial and temporal control over experimental conditions. This report provides evidence of the superiority of 2-D exposure systems over conventional methods for studying mammalian cell plasma membrane behaviors under nsPEF influence. Further, the ability to examine electropermeabilization across a field gradient suggests the quadrupole method has the advantage of providing the ability to ask previously unanswerable questions such as: What would introducing an 'excitable' cell type into an nsPEF gradient tell us about nerve cell activation given a notional tissue treatment environment?

8.4.1 Electric field versus charge magnitude

The degree of electropermeabilization from nsPEF exposure can be related to exposure parameters such as pulse amplitude, duration, number and repetition rate, a finding largely established in nsPEF studies employing unipolar pulses. The local electric field serves more as an explanatory variable because its magnitude is based on several factors that influence charge separation, distribution and migration. For these reasons, it was important to limit the parametric variables used in this study to allow for better isolation of the factors influencing spatial control of the nsPEF response. Determining the critical electric field threshold (E_c) in the quadrupole system for UP nsPEF electropermeabilization provided a crucial baseline for all subsequent analyses. Because this study relied on the measurement of changes in membrane permeabilization in a spatially non-uniform field, it was necessary to know whether electropermeabilization could be expected when bipolar or CANCAN pulses might otherwise predict lower field strengths at a given location.

For various outcomes, it has been previously established with nanosecond pulses that longer pulse durations require fewer pulses to permeabilize cell membranes *in vitro*. While other nsPEF exposure systems require multiple exposures to establish a range of electric field values through which an E_c for electropermeabilization can be derived, the lack of precision inherent in the use of discrete data points can result in overshooting the actual value of the critical field and a key parameter of permeabilization mechanisms being missed. One of the contributions of this work is that, due to the non-uniform field established with all pulse regimes and 2-D analysis,

multiple gradients are produced in a single exposure from which a more informative determination of the E_c for nsPEF electropermeabilization can be obtained.

Based on published data and results presented in Chapter 4, it was expected that UP responses would primarily depend on electric field magnitude, which would lead to the assumption that YP1 uptake would be consistent at each point of interest. It has long been held based on unipolar exposures (*i.e.* parallel electrodes where the electric field is assumed to be homogenous) and discrete measurement systems that there is a linear relationship between field magnitude and biological response. In *in vitro* samples, it is nonetheless bound by upper and lower limits based on degree of permeabilization, for example, or threshold for activation and saturation of a biomarker. Due to the field gradient produced by the planar quadrupole electrode configuration, it was necessary to examine whether the spatial response depended on the absolute value of the electric field at a given point. The small, but possibly significant differences, in spatial biological responses to unipolar pulsing may be attributed to variations in surface potential due to the differences in charge accumulation as well as the increase in charge mobility at higher applied voltages, which would exhibit a greater force on permeabilized cells and promote dye molecule localization.

8.4.2 Electrode polarization and YO-PRO®-1 uptake localization

In these studies, it was found overall that better agreement exists between the pattern of YP1 uptake and nsPEF when values are roughly between 1.5 kV/cm (E_c) and 2.2 kV/cm. Given that voltage amplitude is known to contribute to where YP1 localizes with respect to positively and negatively charged or grounded electrodes, it was necessary to determine a range of suitable charging voltages capable of inducing measurable YP1 uptake. In comparing UP nsEP responses between one pair of adjacent h.v. (‘anode’) and ground (‘cathode’) electrodes in the planar quadrupole, it was found that when the load voltage is 0.6 kV, YP1 uptake was greater at the anodal side (A−), but shifts to favor the cathodal side (C+) at 2.5 kV. For the asymmetric BP nsEPs studied, fluorescence was largely balanced between both electrodes for the 50% BP nsEP, but did appear to favor A− slightly for the 25% case and C+ for the 70% case. These results contrast somewhat with published research on polarization of nsPEF membrane responses in single cells, suggesting the possible involvement of large cell population biological double-layer formation in counter-balancing charge migration.

Valdez et al. [88] examined polarization in single cells as a function of pulse duration and waveform symmetry 350 Volts (V) that generated an electric field of 12.0 kV/cm. They noted that if hyperpolarization due to A− and depolarization by the C+ are strong enough, cell membrane potential will be driven past the threshold to allow YO-PRO®-1 to enter cells. They argued that because YP1 is a membrane-impermeable cation, its entry into the cell is driven by A− causing the local membrane to become negatively charged, allowing the dye to move down its electrochemical gradient. As a result, YP1 uptake exhibits an anodal bias given a UP nsPEF exposure. The scale of YP1 uptake is regulated by the strength of A−, which is affected in turn by the pulse parameters mentioned above, as well as whether the pulse waveform is unipolar or bipolar. This phenomenon has been observed for other cationic uptake dyes (*e.g.* Propidium iodide) [58, 59, 148, 149]. It has also been reported in single-cell systems that, in general, electropermeabilization is stronger at A– for unipolar pulses, but more symmetric between A– and C+ for bipolar pulses. Sweeney *et al.* [60] found this to be true with PI uptake in single cells during long unipolar pulsing and short bipolar pulse exposures in the microsecond range corresponding to electric field intensities of 0−1.25 kV/cm (±3.5%, depending on location of cells between two electrodes). Using a nonlinear optical probe method described by Moen et al. [150], this phenomenon was demonstrated in single Jurkat cells exposed to 300 ns UP and BP pulses at 16.5 kV/cm.

Dye uptake may be a combination of number of pulses contributing to opening of greater number of pores and longer-lived pores due to relatively longer ns duration pulses. Findings from past studies suggest that the transport of larger molecules (YP and PI) occurs largely if not exclusively post-pulse. If true, then polarization of the visualized YP1 response could be due to the relative time for the anodal electrode to discharge at lower vs. higher charging voltages, leaving more or less time for dye molecules to migrate to permeabilized cells at a given pole [151].

8.4.3 Bipolar cancellation efficiency

The results of studies in which uptake of YP1 served as an indicator of membrane electropermeabilization revealed that bipolar cancellation could be achieved by manipulating the parameters of the cathodal pulse phase in specific ways. Gianulis *et al*. [90] observed bipolar cancellation when the amplitude of the E-field of the cathodal pulse phase was reduced to 35%

of the initial anodal pulse phase. A subsequent study from the same group reported also that optimal cancellation by a single or multiple nsPEFs in different cell types could be achieved by a cathodal phase electric field amplitude ~50% lower than the anodal phase. Given the same amplitude during the first phase, it was expected that UP nsEPs would produce the greatest response compared to BP nsEPs tested over the same surface area for BP nsEP φ_2/φ_1 amplitudes at or below 0.5. Results here aligned with expectations when responses were measured directly between E1 and E2, where E1 is grounded, with the 70% BP nsEP exhibiting the highest YP1 fluorescence across all conditions compared. This is generally consistent with BPC studies on single and small-culture cells.

What is most insightful is that when examining equatorial responses beyond the flux line, the additive effect of the 70% BP nsEP observed between electrodes becomes a cancellation effect mid-way between the interior electrode edge line and the center line of the quadrupole. Essentially, the UP and BP effects are inverted. This is a critical observation, suggesting that BPC is a function of the vector field that must be taken into account when designing exposure system applicators for 2-D nsPEF exposures.

Empirical data on spatial BP nsPEF effects acquired allowed for exploration of whether an nsPEF index could be defined to predict bipolar cancelation in a quadrupole configuration. A basic linear relationship was established for points along the flux line between E1 and E2 for increasing φ_2/φ_1 amplitudes, but it was not maintained for values analyzed at the quadrupole center. Although this allowed for YP1 uptake to be predicted within an assessed range of BP nsEP phase ratios, a simple, but important, point worth noting is that models are hypotheses [152]. As such, these findings represent only a small portion of a complex biological system but are quantitatively testable. Their value thus lies in providing more rapid insights into spatial aspects of BPC than are possible with experiments alone.

The change in field magnitude across the plane of the electrodes meant that it made sense to question where the degree of bipolarity at any point in the 2-D plane and existence of a cancellation response to varied amplitude bipolar pulses affected the spatial response.

8.4.4 CANCAN in the linear versus planar quadrupole electrode configuration

Despite only having preliminary data, BP nsEPs were expected to reduce YP1 uptake at the h.v. electrode edge relative to UP nsEPs. CANCAN A and B regimes were designed to assess

biphasic-monophasic superposition and compare the effect of increasing the applied voltage, while CANCAN C was created to examine the effect of adding a third phase, specifically if it might offer the possibility of stronger cancellation. Based in part on limitations imposed by the configuration of the exposure system at the time of implementation, these were the only combinations that would allow for the possibility of effective waveform synchronization. Alternate regimes would have otherwise required certain channel resistors to be replaced in the pulse generator.

Experiments performed in triplicate for CANCAN A and synchronized phases matched to within 0.04 kV allowed for the minimum level of confidence in finding that this simple regime and low relative applied voltages does not differ from the UP response at the center-facing proximal h.v. electrode region and axial center, but does lower the response at the adjacent ground electrode (the response at the second ground was not measured). This could be due in part to the low but high-gradient field at a perimeter electrode gap distance of only 1 mm, in addition to fringe effects. The results from two CANCAN B were highly similar. Without additional numerical analysis, however, it cannot be stated with any certainty whether the higher distal response relative to the other CANCAN regime spatial responses was contributed to by the higher applied voltage producing a stronger UP type YP1 uptake, but the partial second phase cancellation would have in theory equated to delivery of an nsPEF from a 15% BP pulse. With CANCAN C, the incomplete cancellation of the second and third phases may have produced an additive effect responsible for producing the highest overall proximal h.v. electrode response. Membrane resealing at lower fields might also explain why distal effects are unseen.

The only comparison possible at this time is with CANCAN that was demonstrated in the recent paper by Gianulis *et al*. [120] between the interior (E2 and E3) electrodes of a linear quadrupole arrangement. While superposing nsEPs of various phases did produce a noticeable increase at the axial center, effects were minimal. A stronger effect is needed to be of practical use. The one-dimensional set-up makes for reliable, linearly directed nsPEFs that make exposure-response comparisons simple and direct, but its practical use is negated by a target area that is limited to a narrow band. Further, the electric field region between the high-voltage and ground electrode pairs is not unlike that of parallel wires, except that an agarose medium with high cell concentration and other dielectric components introduces capacitance and complex impedance factors. Outcomes based on the current studies using the linear system can only be

extrapolated for relevance in invasive applications. Still, lessons from the linear quadrupole study can serve to identify possible major contributing factors – such as a higher pulse number – in the stronger cancellation / CANCAN seen and help to increase CANCAN effectiveness in the planar quadrupole.

The results from unipolar and bipolar pulse *in vitro* exposure experiments suggest and inform future work on bipolar cancellation, including applications. By standardizing the delivery of synchronized pulses to various tissue types, this system may provide a potential method to reliably investigate the contextual properties of electropermeabilization *in vivo*. Understanding the impact of multi-directional field interaction with membranes of cells in a 3-D tissue environment represents a powerful, beneficial way to investigate the mechanisms that influence nsPEF electropermeabilization. Discovery of the 'cancellation effect', along with rapid advances in pulse generator technologies, presents exciting possibilities for pulsed electric field therapies that rely on stimulating the body's natural ability to heal itself, for example, rather than on potent chemicals or biopharmaceuticals, which can often be expensive, lead to addiction, or create new medical complications. Combining these and knowledge of the effects of electric field intensity range on BPC efficiency described in this dissertation may result in novel and valuable practical data to inform the parallel work of investigators on the design of antennas for possible contactless remote PEF stimulation capabilities at nanosecond and picosecond time scales.

REFERENCES

[1] P. Rat, E. Olivier, C. Tanter, A. Wakx, and M. Dutot, "A fast and reproducible cell- and 96-well plate-based method for the evaluation of P2X7 receptor activation using YO-PRO-1 fluorescent dye," *J Biol Methods,* vol. 4, 2017.

[2] H. A. Ryan, S. Hirakawa, E. Yang, C. Zhou, and S. Xiao, "High-Voltage, Polyphasic, Nanosecond Pulses to Modulate Cellular Responses," *IEEE Trans Biomed Circ Sys,* vol. 12, pp. 338-350, 2018.

[3] B. L. Ibey, C. C. Roth, A. G. Pakhomov, J. A. Bernhard, and G. J. Wilmink et al. (2011, Dose-Dependent Thresholds of 10-ns Electric Pulse Induced Plasma Membrane Disruption and Cytotoxicity in Multiple Cell Lines. *PLOS ONE 6(1),* e15642. Available: https://doi.org/10.1371/journal.pone.0015642

[4] C. Muratori, A. G. Pakhomov, L. Heller, M. Casciola, E. Gianulis, S. Grigoryev, S. Xiao, and O. N. Pakhomova, "Electrosensitization Increases Antitumor Effectiveness of Nanosecond Pulsed Electric Fields In Vivo," *Technology in cancer research & treatment,* vol. 16, 2017.

[5] C. Muratori, A. G. Pakhomov, S. Xiao, and O. N. Pakhomova, "Electrosensitization assists cell ablation by nanosecond pulsed electric field in 3D cultures," *Scientific Reports,* vol. 6, p. 23225, 2016.

[6] E. C. Gianulis, M. Casciola, C. Zhou, E. Yang, S. Xiao, and A. G. Pakhomov, "Selective distant electrostimulation by synchronized bipolar nanosecond pulses," *Scientific Reports,* vol. 9, 2019.

[7] J. Hunckler and A. de Mel, "A current affair: electrotherapy in wound healing," *Journal of multidisciplinary healthcare,* vol. 10, pp. 179-194, 2017.

[8] J. Bosavage, "How engineering is revolutionizing the healthcare industry: 3D modeling, electroceuticals, and nerve-stimulation devices are some of the technologies that are having an impact," in *The Institute,* ed: IEEE, 2017.

[9] A. Golberg, S. Khan, V. Belov, K. P. Quinn, H. Albadawi, and G. Felix Broelsch et al., "Skin rejuvenation with non-invasive pulsed electric fields," *Sci Rep,* vol. 5, 2015.

[10] A. L. Kindzelskii and H. R. Petty, "Extremely low frequency pulsed DC electric fields promote neutrophil extension, metabolic resonance and DNA damage when phase-matched with metabolic oscillators," *Biochim Biophys Acta,* vol. 1495, pp. 90-111, 2000.

[11] A. L. Kindzelskii, M. J. Zhou, R. P. Haugland, L. A. Boxer, and H. R. Petty, "Oscillatory pericellular proteolysis and oxidant deposition during neutrophil locomotion," *Biophys J,* vol. 74, pp. 90-97, 1998.

[12] D. A. Savitz, "Overview of occupational exposure to electric and magnetic fields and cancer: advancements in exposure assessment," *Environmental Health Perspectives,* vol. 103, pp. 69-74, 1995.

[13] G. M. Matanoski, "Epidemiologic studies and their role in identifying potential risks from exposure to electromagnetic fields," in *Electromagnetic Fields: Biological Interactions and Mechanisms*. vol. 250, M. Blank, Ed., ed: American Chemical Society, 1995, pp. 157–190.

[14] R. Goodman, Y. Chizmadzhev, and A. Shirley-Henderson, "Electromagnetic fields and cells," *J Cell Biochem,* vol. 51, pp. 436-441, 1993.
[15] A. W. Friend, Jr., E. D. Finch, and H. P. Schwan, "Low frequency electric field induced changes in the shape and motility of amoebas," *Science,* vol. 187, pp. 357-359, January 1975.
[16] WebMD. (2018, Pain management and bioelectric therapy. Available: https://www.webmd.com/pain-management/guide/bioelectric-therapy#1
[17] B. F. Sisken, J. Walker, and M. Orgel, "Prospects on clinical applications of electrical stimulation for nerve regeneration," *J Cell Biochem,* vol. 51, pp. 404-409, April 1993.
[18] P. T. Vernier, A. Li, L. Marcu, C. M. Craft, and M. A. Gundersen, "Ultrashort pulsed electric fields induce membrane phospholipid translocation and caspase activation: differential sensitivities of Jurkat T lymphoblasts and rat glioma C6 cells," *IEEE Trans. Dielectr. Electr. Insul.,* vol. 10, pp. 795-809, 2003.
[19] R. Nuccitelli, U. Pliquett, X. H. Chen, W. Ford, R. J. Swanson, S. J. Beebe, J. F. Kolb, and K. H. Schoenbach, "Nanosecond pulsed electric fields cause melanomas to self-destruct," *Biochemical and biophysical research communications,* vol. 343, pp. 351-360, 2006.
[20] K. H. Schoenbach, B. Hargrave, R. P. Joshi, J. F. Kolb, R. Nuccitelli, C. Osgood, A. Pakhomov, M. Stacey, R. J. Swanson, J. A. White, S. Xiao, J. Zhang, S. Beebe, P. Blackmore, and E. Buescher, "Bioelectric effects of intense nanosecond pulses," *IEEE Trans. Dielectr. Electr. Insul.,* vol. 14, pp. 1088–1109, 2007.
[21] K. H. Schoenbach, A. G. Pakhomov, I. Semenov, S. Xiao, O. N. Pakhomova, and B. L. Ibey, "Ion transport into cells exposed to monopolar and bipolar nanosecond pulses," *Bioelectrochemistry,* vol. 103, pp. 44–51, 2015.
[22] W. A. Hamilton and A. J. H. Sale, "Effects of high electric fields on microorganisms: II. Mechanism of action of the lethal effect," *Biochim. Biophys. Acta.,* vol. 148, pp. 789-800, 1967.
[23] E. Neumann, S. Kakorin, and K. Toensing, "Fundamentals of electroporative delivery of drugs and genes," *Bioelectrochem Bioenerg,* vol. 48, pp. 3-16, 1999.
[24] L. Wang, D. Liu, R. Zhou, Z. Wang, and A. Cuschieri, "Tumour cell membrane poration and ablation by pulsed low-intensity electric field with carbon nanotubes," *Int J Mol Sci,* vol. 16, pp. 6890-6901, 2015.
[25] P. Ruzgys, V. Novickij, J. Novickij, and S. Šatkauskas, "Nanosecond range electric pulse application as a non-viral gene delivery method: proof of concept," *Scientific reports,* vol. 8, 2018.
[26] S. Yin, X. Chen, C. Hu, X. Zhang, Z. Hu, J. Yu, X. Feng, K. Jiang, S. Ye, K. Shen, H. Xie, L. Zhou, R. J. Swanson, and S. Zheng, "Nanosecond pulsed electric field (nsPEF) treatment for hepatocellular carcinoma: A novel locoregional ablation decreasing lung metastasis," *Cancer Letters,* vol. 346, pp. 285-291, 2014.
[27] T. B. Napotnik, M. Reberšek, P. T. Vernier, B. Mali, and D. Miklavčič, "Effects of high voltage nanosecond electric pulses on eukaryotic cells (in vitro) A systematic review," *Bioelectrochemistry,* vol. 110, pp. 1-12, 2016.
[28] E. H. Hall, K. H. Schoenbach, and S. J. Beebe, "Nanosecond pulsed electric fields (nsPEF) induce direct electric field effects and biological effects on human colon carcinoma cells," *DNA Cell Biol,* vol. 24, pp. 283-291, 2005.

[29] P. T. Vernier, Y. Sun, L. Marcu, S. Salemi, C. M. Craft, and M. A. Gundersen, "Calcium bursts induced by nanosecond electric pulses," *Biochemical and biophysical research communications,* vol. 310, pp. 286–295, 2003.

[30] S. J. Beebe, P. M. Fox, L. J. Rec, E. L. Willis, and K. H. Schoenbach, "Nanosecond, high intensity pulsed electric fields induce apoptosis in human cells," *Federation of American Societies for Experimental Biology,* vol. 17, pp. 1493-1495, 2003.

[31] S. J. Beebe, J. White, P. F. Blackmore, Y. Deng, K. Somers, and K. H. Schoenbach, "Diverse effects of nanosecond pulsed electric fields on cells and tissues, DNA and cell biology," *DNA and cell biology,* vol. 22, pp. 785-796, 2003.

[32] A. G. Pakhomov, J. F. Kolb, J. A. White, R. P. Joshi, S. Xiao, and K. H. Schoenbach, "Longlasting plasma membrane permeabilization in mammalian cells by nanosecond pulsed electric field (nsPEF)," *Bioelectromagnetics,* vol. 28, pp. 655-663, 2007.

[33] P. T. Vernier, M. J. Ziegler, Y. Sun, W. V. Chang, M. A. Gundersen, and D. P. Tieleman, "Nanopore Formation and Phosphatidylserine Externalization in a Phospholipid Bilayer at High Transmembrane Potential," *J. Am. Chem. Soc.* , vol. 128, pp. 6288-6289, 2006.

[34] O. M. Nesin, O. N. Pakhomova, S. Xiao, and A. G. Pakhomov, "Manipulation of cell volume and membrane pore comparison following single cell permeabilization with 60- and 600-ns electric pulses," *Biochim. Biophys. Acta.,* vol. 1808 pp. 792-801, 2011.

[35] A. G. Pakhomov, E. Gianulis, P. T. Vernier, I. Semenov, S. Xiao, and O. N. Pakhomova, "Multiple nanosecond electric pulses increase the number but not the size of long-lived nanopores in the cell membrane," *Biochim. Biophys. Acta.,* vol. 1848 pp. 958-966, 2015.

[36] D. A. Stewart, I. R. Gowrishankar, and J. C. Weaver, "Transport lattice approach to describing cell electroporation: Use of a local asymptotic model," *IEEE T Plasma Sci,* vol. 32, pp. 1696-1708, 2004.

[37] T. R. Gowrishankar, A. T. Esser, Z. Vasilkoski, K. C. Smith, and J. C. Weaver, "Microdosimetry for conventional and supra-electroporation in cells with organelles," *Biochemical and biophysical research communications,* vol. 341, pp. 1266-1276, 2006

[38] T. R. Gowrishankar and J. C. Weaver, "Electrical behavior and pore accumulation in a multicellular model for conventional and supra-electroporation," *Biochemical and biophysical research communications,* vol. 349, pp. 643-653, 2006.

[39] P. T. Vernier, Y. Sun, and M. A. Gundersen, "Nanoelectropulse-driven membrane perturbation and small molecule permeabilization," *BMC Cell Biol.,* vol. 7, 2006.

[40] A. M. Bowman, O. M. Nesin, O. N. Pakhomova, and A. G. Pakhomov, "Analysis of Plasma Membrane Integrity by Fluorescent Detection of Tl+ Uptake," *J Membrane Biol,* vol. 236, pp. 15-26, 2010.

[41] A. G. Pakhomov and O. N. Pakhomova, "Nanopores: a distinct transmembrane passageway in electroporated cells," in *Advanced Electroporation Techniques in Biology in Medicine,* A. G. Pakhomov, D. Miklavcic, and M. S. Markov, Eds., ed Boca Raton: CRC Press, 2010, pp. 178-194.

[42] S. Romeo, Y. H. Wu, Z. A. Levine, M. A. Gundersen, and P. T. Vernier, "Water influx and cell swelling after nanosecond electropermeabilization," *BBA-Biomembranes,* vol. 1828, pp. 1715-1722, 2013.

[43] K. Kinosita and T. Y. Tsong, "Formation and Resealing of Pores of Controlled Sizes in Human Erythrocyte-Membrane," *Nature,* vol. 268, pp. 438-441, 1977.

[44] Y. Okada, "Ion channels and transporters involved in cell volume regulation and sensor mechanisms," *Cell Biochem Biophys,* vol. 41, pp. 233-258, 2004.

[45] K. C. Smith and J. C. Weaver, "Active mechanisms are needed to describe cell responses to submicrosecond, megavolt-per-meter pulses: Cell models for ultrashort pulses," *Biophysical journal,* vol. 95, pp. 1547-1563, 2008.

[46] Q. Hu, S. Viswanadham, R. P. Joshi, K. H. Schoenbach, S. J. Beebe, and P. F. Blackmore, "Simulations of transient membrane behavior in cells subjected to a high-intensity ultrashort electric pulse," *Phys Rev E,* vol. 71, 2005.

[47] K. C. Smith, T. R. Gowrishankar, A. T. Esser, D. A. Stewart, and J. C. Weaver, "The Spatially Distributed Dynamic Transmembrane Voltage of Cells and Organelles due to 10-ns Pulses: Meshed Transport Networks," *IEEE T Plasma Sci,* vol. 34, 2006

[48] A. T. Esser, K. C. Smith, T. R. Gowrishankar, and J. C. Weaver, "Towards Solid Tumor Treatment by Nanosecond Pulsed Electric Fields," *Technology in cancer research & treatment* vol. 8, pp. 289-306, 2009.

[49] E. B. Garon, D. Sawcer, P. T. Vernier, T. Tang, Y. H. Sun, L. Marcu, M. A. Gundersen, and H. P. Koeffler, "In vitro and in vivo evaluation and a case report of intense nanosecond pulsed electric field as a local therapy for human malignancies " *International Journal of Cancer,* vol. 121, pp. 675-682, 2007.

[50] E. B. Marsolais and R. Kobetic, "Functional walking in paralyzed patients by means of electrical stimulation," *Clinical orthopaedics and related research,* pp. 30-36, 1983.

[51] R. B. Stein, S. L. Chong, K. B. James, A. Kido, G. J. Bell, L. A. Tubman, and M. Belanger, "Electrical stimulation for therapy and mobility after spinal cord injury," *Prog Brain Res,* vol. 137, pp. 27-34, 2002.

[52] J. Zhang, P. F. Blackmore, B. Y. Hargrave, S. Xiao, S. J. Beebe, and K. H. Schoenbach, "Nanosecond pulse electric field (nanopulse): a novel non-ligand agonist for platelet activation," *Archives of biochemistry and biophysics,* vol. 471 pp. 240-248, 2008.

[53] C. M. Edelblute, S. Guo, J. Hornef, E. Yang, C. Jiang, K. Schoenbach, and R. Heller, "Moderate Heat Application Enhances the Efficacy of Nanosecond Pulse Stimulation for the Treatment of Squamous Cell Carcinoma," *Technology in cancer research & treatment,* vol. 17, 2018.

[54] U. Zimmermann, G. Pilwat, and F. Riemann, "Dielectric breakdown of cell membranes," *Biophys J.,* vol. 14, pp. 881-99, November 1974.

[55] A. Kuthi, P. Gabrielsson, M. R. Behrend, P. T. Vernier, and M. A. Gundersen, "Nanosecond pulse Generator using fast recovery diodes for cell electromanipulation," *IEEE Transactions on Plasma Science,* vol. 33, pp. 1192-1197, August 2005.

[56] S. R. Rajulapati, F. A. Husain, S. B. Ananthapadmanabha, K. H. Schoenbach, and S. Xiao, "Nanosecond biphasic pulse generators for biomedical applications," presented at the 2013 19th IEEE Pulsed Power Conference (PPC), San Francisco, CA, 2013.

[57] K. H. Schoenbach, R. P. Joshi, J. F. Kolb, N. Chen, M. Stacey, E. S. Buescher, S. J. Beebe, and P. Blackmon, "Ultrashort electrical pulses open a new gateway into biological cells," in *Conference Record of the Twenty-Sixth International Power Modulator Symposium*, San Francisco, CA, 2004, pp. 205-209.

[58] A. G. Pakhomov, I. Semenov, S. Xiao, O. N. Pakhomova, B. Gregory, and K. H. Schoenbach et al., "Cancellation of cellular responses to nanoelectroporation by reversing the stimulus polarity," *Cell Mol Life Sci,* vol. 17, pp. 4431-4441, November 2014.

[59] B. L. Ibey, J. C. Ullery, O. N. Pakhomova, C. C. Roth, I. Semenov, H. T. Beier, M. Tarango, S. Xiao, K. H. Schoenbach, and A. G. Pakhomov, "Bipolar nanosecond electric pulses are less efficient at electropermeabilization and killing cells than monopolar

pulses," *Biochemical and Biophysical Research Communications,* vol. 443, pp. 568-573, 2014.

[60] D. C. Sweeney, M. Rebersek, D. J., L. Rems, D. Miklavčič, and R. V. Davalos, "Quantification of cell membrane permeability induced by monopolar and high-frequency bipolar bursts of electrical pulses," *Biochim Biophys Acta,* vol. 1858, pp. 2689–2698, 2016.

[61] A. G. Pakhomov and e. al., "Nanoelectropulse-induced electromechanical signaling and control of biological systems," ed. Norfolk, Virginia: Air Force Office of Scientific Research, 2015.

[62] T. Heeren, J. F. Kolb, S. Xiao, K. H. Schoenbach, and H. Akiyama, "Pulsed Power Generators and Delivery Devices for Bioelectrical Applications," in *Conference Record of the 2006 Twenty-Seventh International Power Modulator Symposium*, Arlington, VA, 2006, pp. 486-489.

[63] C. Muratori, A. Pakhomov, E. Gianulis, and e. al., "The cytotoxic synergy of nanosecond electric pulses and low temperature leads to apoptosis," *Sci Rep,* vol. 6, 2016.

[64] F. Lacava, "Multipole Expansion of the Electrostatic Potential," in *Classical Electrodynamics*, ed: Springer, Cham, 2016, pp. 17-31.

[65] V. Illingworth, Ed., *The Penguin Dictionary of Physics*. London: Penguin Books, 1991, p.^pp. Pages.

[66] D. Halliday, R. Resnick, and J. Walker, Eds., *Fundamentals of Physics*. Chichester: Wiley, 2000, p.^pp. Pages.

[67] R. L. Boylestad, *Introductory circuit analysis,* Thirteenth edition. ed. Boston: Pearson, 2016.

[68] R. E. Scott, *Linear circuits. With the editorial assistance of Martin W. Essigman*. Reading, Mass.,: Addison-Wesley Pub. Co., 1960.

[69] H. Whiteside and R. W. P. King, "The loop antenna as a probe," *IEEE Trans. On Antennas and Propagation,* vol. AP12, pp. 291-297, May 1964.

[70] T. Idziorek, J. Estaquier, F. De Bels, and J. Ameisen, "YOPRO-1 permits cytofluorometric analysis of programmed cell death (apoptosis) without interfering with cell viability," *J Immunol Methods,* vol. 185, pp. 249-258, 1995.

[71] C. Virginio, A. MacKenzie, F. Rassendren, R. North, and S. A, "Pore dilation of neuronal P2X receptor channels," *Nat Neurosci,* vol. 2, pp. 315-321, 1999.

[72] F. Chekeni, M. Elliott, J. Sandilos, S. Walk, J. Kinchen, E. Lazarowski, A. Armstrong, S. Penuela, D. Laird, G. Salvesen, B. Isakson, D. Bayliss, and K. Ravichandran, "Pannexin 1 channels mediate 'find-me' signal release and membrane permeability during apoptosis," *Nature,* vol. 467, pp. 863-867, 2010.

[73] A. Michel, R. Kaur, I. Chessell, and P. Humphrey, "Antagonist effects on human P2X(7) receptor-mediated cellular accumulation of YO-PRO-1," *Br J Pharmacol,* vol. 130, pp. 513-520, 2000.

[74] Adinolfi E, Pizzirani C, Idzko M, Panther E, Norgauer J, Di Virgilio F, and F. D, "P2X(7) receptor: Death or life?," *Purinergic Signal,* vol. 1, pp. 219-27, 2005.

[75] F. Chagnon, C. Fournier, P. Charette, L. Moleski, M. Payet, L. Dobbs, and O. Lesur, "In vivo intravital endoscopic confocal fluorescence microscopy of normal and acutely injured rat lungs," *Lab Invest,* vol. 90, pp. 824-834, 2010.

[76] J. Kohler, J. Dubach, H. Naik, K. Tai, A. Blass, and D. Soybel, "Monochloramine-induced toxicity and dysregulation of intracellular Zn2+ in parietal cells of rabbit gastric glands," *Am J Physiol Gastrointest Liver Physiol,* vol. 299, pp. G170-8, 2010.

[77] F. Santos, G. MacDonald, E. Rubel, and D. Raible, "Lateral line hair cell maturation is a determinant of aminoglycoside susceptibility in zebrafish (Danio rerio)," *Hear Res,* vol. 213, pp. 25-33, 2006.

[78] D. Boffa, J. Waka, D. Thomas, S. Suh, K. Curran, V. Sharma, M. Besada, T. Muthukumar, H. Yang, M. Suthanthiran, and K. Manova, "Measurement of apoptosis of intact human islets by confocal optical sectioning and stereologic analysis of YO-PRO-1-stained islets," *Transplantation,* vol. 79, pp. 842-845, 2005.

[79] S. Fujisawa, Y. Romin, A. Barlas, L. Petrovic, M. Turkekul, N. Fan, K. Xu, A. Garcia, S. Monette, D. Klimstra, J. Erinjeri, S. Solomon, K. Manova-Todorova, and C. Sofocleous, "Evaluation of YO-PRO-1 as an early marker of apoptosis following radiofrequency ablation of colon cancer liver metastases," *Cytotechnology,* vol. 66, pp. 259-73, March 2014.

[80] S. Higashiyama, M. Noda, M. Kawase, and K. Yagi, "Mixed-ligand modification of polyamidoamine dendrimers to develop an effective scaffold for maintenance of hepatocyte spheroids," *J Biomed Mater Res A,* vol. 64, pp. 475-482, Mar 1 2003.

[81] F. Castañeda and R. Kinne, "Short exposure to millimolar concentrations of ethanol induces apoptotic cell death in multicellular HepG2 spheroids," *J Cancer Res Clin Oncol,* vol. 126, pp. 305-310, Jun 2000.

[82] E. C. Gianulis, M. Casciola, C. Zhou, E. Yang, S. Xiao, and A. G. Pakhomov, "Selective distant electrostimulation by synchronized bipolar nanosecond pulses," *Scientific Reports,* vol. 9, p. 13116, 11 September 2019.

[83] E. G. Gianulis, M. Casciola, S. Xiao, O. N. Pakhomova, and A. G. Pakhomov, "Electropermeabilization by uni- or bipolar nanosecond electric pulses: The impact of extracellular conductivity," *Bioelectrochemistry,* vol. 119, pp. 10-19, February 2018.

[84] M.M. Sadik, J. Li, J.W. Shan, D.I. Shreiber, and H. Lin, "Quantification of propidium iodide delivery using millisecond electric pulses: experiments," *Biochim. Biophys. Acta Biomembr,* vol. 1828, pp. 1322–1328, 2013.

[85] S. M. Kennedy, Z. Ji, J. C. Hedstrom, J. H. Booske, and S. C. Hagness, "Quantification of electroporative uptake kinetics and electric field heterogeneity effects in cells," *Biophys. J. ,* vol. 94, pp. 5018–5027, 2008.

[86] G. Pucihar, T. Kotnik, D. Miklavčič, and J. Teissié, "Kinetics of transmembrane transport of small molecules into electropermeabilized cells," *Biophys. J.,* vol. 95, pp. 2837–2848, 2008.

[87] A. G. Pakhomov, S. Grigoryev, I. Semenov, M. Casciola, C. Jiang, and S. Xiao, "The second phase of bipolar, nanosecond-range electric pulses determines the electroporation efficiency," *Bioelectrochemistry,* vol. 122, pp. 123-133, 2018.

[88] C. M. Valdez, R. A. Barnes, C. C. Roth, E. K. Moen, G. A. Throckmorton, and B. L. Ibey, "Asymmetrical bipolar nanosecond electric pulse widths modify bipolar cancellation," *Scientific Reports,* vol. 7, p. 16372, 2017.

[89] C. M. Valdez, R. Barnes Jr., C. C. Roth, E. Moen, and B. L. Ibey, "The Interphase Interval within a Bipolar Nanosecond Electric Pulse Modulates Bipolar Cancellation," *Bioelectromagnetics,* vol. 39, pp. 441-450, July 2018.

[90] E. C. Gianulis, J. Lee, C. Jiang, S. Xiao, B. L. Ibey, and A. G. Pakhomov, "Electroporation of mammalian cells by nanosecond electric field oscillations and its inhibition by the electric field reversal," *Sci Rep,* vol. 5, p. 13818, September 2015.

[91] G. C. Flaker, J. C. Schuder, W. C. McDaniel, H. Stoeckle, and M. Dbeis, " Superiority of biphasic shocks in the defibrillation of dogs by epicardial patches and catheter electrodes," *Am Heart J,* vol. 118, 1989.

[92] J. M. Wharton, V. J. Richard, C. E. Murry, E. G. Dixon, K. A. Reimer, J. Meador, W. M. Smith, and R. E. Ideker, "Electrophysiological effects of monophasic and biphasic stimuli in normal and infarcted dogs," *Pacing Clin Electrophysiol,* vol. 13, 1990.

[93] L. L. Y. Chiu, R. K. Iyer, J.-P. King, and M. Radisic, "Biphasic Electrical Field Stimulation Aids in Tissue Engineering of Multicell-Type Cardiac Organoids," in *TISSUE ENGINEERING: Part A*. vol. 17, ed: Mary Ann Liebert, 2011.

[94] B. L. Ibey, J. C. Ullery, O. N. Pakhomova, C. C. Roth, I. Semenov, H. T. Beier, M. Tarango, S. Xiao, K. H. Schoenbach, and A. G. Pakhomov, "Bipolar nanosecond electric pulses are less efficient at electropermeabilization and killing cells than monopolar pulses," *Biochemical and Biophysical Research Communications,* vol. 443, pp. 568-573, 2013.

[95] J. L. Jones and R. E. Jones, "Improved safety factor for triphasic defibrillator waveforms," *Circulation Research,* vol. 64, pp. 1172-1177, 1 June 1989.

[96] J. T. Rubinstein, C. A. Miller, H. Mino, and P. J. Abbas, "Analysis of monophasic and biphasic electrical stimulation of nerve," *IEEE Trans Biomed Eng,* vol. 48, pp. 1065-1070, 2001.

[97] T. R. Gowrishankar, J. V. Stern, K. C. Smith, and J. C. Weaver, "Nanopore occlusion: A biophysical mechanism for bipolar cancellation in cell membranes," *Biochemical and Biophysical Research Communications,* vol. 503, pp. 1194-1199, 2018.

[98] C. Merla, A. G. Pakhomov, I. Semenov, and P. T. Vernier, "Frequency spectrum of induced transmembrane potential and permeabilization efficacy of bipolar electric pulses," *Biophys Acta,* vol. 1859, pp. 1282-1290, July 2017.

[99] H. Helmholtz, "Ueber einige Gesetze der Vertheilung elektrischer Ströme in körperlichen Leitern mit Anwendung auf die thierisch-elektrischen Versuche," *Annalen der Physik und Chemie,* vol. 165, pp. 211–233, 1853.

[100] O. Stern, "Zur Theorie der Elektrolytischen Doppelschicht," *Zeitschrift für Elektrochemie,* vol. 30, 1924.

[101] M. Sugihara-Seki, T. Akinaga, and H. O-Tani, "Charge effects on the hindered transport of macromolecules across the endothelial surface glycocalyx layer," *Biorheology,* vol. 49, pp. 301-16, 2012.

[102] P. Mitchell, "Chemiosmotic coupling in oxidative and photosynthetic phosphorylation," *Biol. Rev. Cambridge Philos. Soc.,* vol. 41, 1966.

[103] K. Redman, *Exp. Cell Res.,* vol. 87, 1974.

[104] I. Tsoneva and T. Tomov, "Relationship between the power of energization and the electrophoretic mobility of rat liver mitochondria," *Bioelectrochem. Bioenerg.,* vol. 12, pp. 253-258, 1984.

[105] T. Aiuchi, N. Kamo, K. Kurihara, and Y. Kobatake, "Significance of surface potential in interaction of 8-anilino-1-naphthalenesulfonate with mitochondria: fluorescence intensity and zeta-potential," *Biochemistry,* vol. 16, pp. 1626-1630, 1977.

[106] A. S. Dukhin, "Biospecific mechanism of double layer formation and peculiarities of cell electrophoresis," *Colloids and Surfaces A: Physicochemical and Engineering Aspects*, vol. 73, pp. 29-48, 1993.
[107] V. Novickij, P. Ruzgys, A. Grainys, and S. Šatkauskas, "High frequency electroporation efficiency is under control of membrane capacitive charging and voltage potential relaxation," *Bioelectrochemistry*, vol. 119, pp. 92-97, Feb 2018.
[108] Y. Mi, P. Li, Q. Liu, J. Xu, Q. Yang, and J. Tang, "Multi-Parametric Study of the Viability of in Vitro Skin Cancer Cells Exposed to Nanosecond Pulsed Electric Fields Combined With Multi-Walled Carbon Nanotubes," *Technol Cancer Res Treat.*, vol. 18, Jan 1 2019
[109] K. H. Schoenbach, A. Abou-Ghazala, T. Vithoulkas, R. W. Alden, R. Turner, and S. Beebe, "The effect of pulsed electrical fields on biological cells," in *11th IEEE International Pulsed Power Conference*, Baltimore, MD, 1997, pp. 73-78.
[110] J. F. Kolb, S. Kono, and K. H. Schoenbach, "Nanosecond pulsed electric field generators for the study of subcellular effects," *Bioelectromagnetics*, vol. 27, pp. 172–187, 2006.
[111] S. Xiao, S. Guo, V. Nesin, R. Heller, and K. H. Schoenbach, "Subnanosecond Electric Pulses Cause Membrane Permeabilization and Cell Death," *IEEE Transactions on Biomedical Engineering*, vol. 58, pp. 1239-1245, May 2011.
[112] J. M. Sanders, A. Kuthi, P. T. Vernier, Y. H. Wu, C. Jiang, and M. A. Gundersen, "Scalable, compact, nanosecond pulse generator with a high repetition rate for biomedical applications requiring intense electric fields," presented at the 2009 IEEE Pulsed Power Conference, Washington, DC, 2009.
[113] R. Heller, Y. Cruz, L. C. Heller, R. A. Gilbert, and M. J. Jaroszeski, "Electrically mediated delivery of plasmid DNA to the skin, using a multielectrode array," *Human gene therapy*, vol. 21, pp. 357–362, 2010.
[114] K. H. Schoenbach, R. P. Joshi, S. J. Beebe, and C. E. Baum, "A scaling law for membrane permeabilization with nanopulses," *IEEE Transactions on Dielectrics and Electrical Insulation*, vol. 16, pp. 1224-1235, 2009.
[115] S. Čorović, J. Bester, and D. Miklavčič, "An e-learning application on electrochemotherapy," *Biomedical Engineering Online*, vol. 8, 2016.
[116] H. Hanna, A. Denzi, M. Liberti, F. M. André, and L. M. Mir, "Electropermeabilization of Inner and Outer Cell Membranes with Microsecond Pulsed Electric Fields: Quantitative Study with Calcium Ions," *Sci Rep*, vol. 7, 12 October 2017.
[117] J. C. Weaver, "Electroporation Theory," in *Plant Cell Electroporation and Electrofusion Protocols*, J. A. Nickoloff, Ed., ed Totowa, NJ: Springer New York, 1995, pp. 3-28.
[118] J. Oblak, D. Križaj, S. Amon, A. Maček-Lebar, and D. Miklavčič, "Feasibility study for cell electroporation detection and separation by means of dielectrophoresis," *Bioelectrochemistry*, vol. 71, pp. 164-171, 6 April 2007 2007.
[119] M. T. Chen, C. Jiang, P. T. Vernier, Y. H. Wu, and M. A. Gundersen, "Two-dimensional nanosecond electric field mapping based on cell electropermeabilization," *PMC Biophys*, vol. 2, 11 November 2009 2009.
[120] E. C. Gianulis, M. Casciola, C. Zhou, E. Yang, S. Xiao, and A. G. Pakhomov, "Selective distant electrostimulation by synchronized bipolar nanosecond pulses," *Scientific reports*, vol. 9, p. 13116, 2019.

[121] E. C. Gianulis, "Enhancement of membrane permeabilization by CANCAN," Frank Reidy Research Center for Bioelectrics, Old Dominion University, MURI Synergy Development Workshop, 2018.
[122] Q. F. S. team, "Quadrupole charge: 3D extrusion," quadrupole.png, Ed., ed: QuickField FEA Software. [Online].
[123] E. Pirc, M. Reberšek, and D. Miklavčič, "Dosimetry in Electroporation-Based Technologies and Treatments," in *Dosimetry in Bioelectromagnetics*, M. Markov, Ed., ed, 2017, pp. 233–268.
[124] H. Bluhm, *Pulsed power Systems: Principles and applications*. Berlin, Germany: Springer-Verlag Berlin Heidelberg, 2006.
[125] S. Xiao, "Development of A Novel Focused Pulsing System Based on the Cancellation of Cancellation Effect," in *Nanoelectropulse-induced Electromechanical Signaling and Control of Biological Systems*, AFOSR, Ed., MURI Kickoff Meeting ed. Washington, DC, 2016.
[126] D. Douglas and J. French, "Collisional focusing effects in radio frequency quadrupoles. J Am Soc Mass Spectrom 3: 398– 408," *J Am Soc Mass Spectrom,* vol. 3, pp. 398– 408, 1992.
[127] D. Douglas, "Linear quadrupoles in mass spectrometry," *Mass Spectrometry Reviews,* vol. 28, pp. 937-960, November/December 2009 2009.
[128] C. M. Noller, M. Boulina, G. McNamara, A. Szeto, P. M. McCabe, and A. J. Mendez, "A Practical Approach to Quantitative Processing and Analysis of Small Biological Structures by Fluorescent Imaging," *Journal of Biomolecular Techniques,* vol. 27, pp. 90-97, 2016.
[129] M. P. Hughes, *Nanoelectromechanics in engineering and biology*. Boca Raton, Fla.: CRC Press, 2003.
[130] K. Kantouna, L. Ekonomou, G. P. Fotis, and G. E. Chatzarakis, "Finite Element Method Analysis of an Electric Field in Wire-Cylinder Electrode Configuration during Corona Discharge," *Latest Advances in Systems Science and Computational Intelligence*.
[131] K. N. Kiousis and A. X. Moronis. Modeling and analysis of the Electric Field and potential distribution in a wire-cylinder air gap. *Recent Researches in Information Science and Applications*.
[132] E. Kuffel, W. S. Zaengl, and J. Kuffel, Eds., *High Voltage Engineering: Fundamentals*. Butterworth-Heinemann, 2000, p.^pp. Pages.
[133] Z. Li, F. Benying, L. Mian, and L. Yanchun, "A new theory and technique on measurement electric field of electric quadrupole," presented at the 8th International Conference on Electronic Measurement and Instruments, Xi'an, China, 2007.
[134] "CST EMC Studio," 2016/2017 ed: Computer Simulation Technology, 2018.
[135] R. Wildman and G. Gazonas, "A dynamic electro-thermo-mechanical model of dielectric breakdown in solids using peridynamics," *Journal of Mechanics of Materials and Structures,* vol. 10, p. 613, 2015.
[136] M. A. A. Abdelsamie, R. B. A. Rahman, S. Mustafa, and D. Hashim, "The effect of packaging shape on the distribution of electric and magnetic fields and SAR induced in 3D models of water containers," *Journal of Electromagnetic Analysis and Applications,* vol. 6, pp. 213-232, 2014.

[137] R. B. Armenta and C. D. Sarris, "Introducing nonuniform grids into the FDTD solution of the transmission-line equations by renormalizing the per-unit-length parameters " *IEEE Transactions on Electromagnetic Compatibility,* vol. 51, pp. 818-824, 2009.
[138] R. Schuhmann and T. Weiland, "A stable interpolation technique for fdtd on nonorthogonal grids," *International Journal of Numerical Modelling: Electronic Networks, Devices and Fields,* vol. 11, pp. 299-306, 1998.
[139] P. A. Garcia, R. V. Davalos, and D. Miklavcic, "A Numerical Investigation of the Electric and Thermal Cell Kill Distributions in Electroporation-Based Therapies in Tissue," *PLoS ONE,* vol. 9, p. e103083, 2014.
[140] D. Berube, F. M. Ghannouchi, and P. Savard, "A Comparative Study of Four Open-ended Coaxial Probe Models for Permittivity Measurements of Lossy Dielectric/Biological Materials at Microwave Frequencies," *IEEE Transactions on Microwave Theory and Techniques,* vol. 44, pp. 1928-1934, 1996.
[141] D. Miklavčič, N. Pavšelj, and F. X. Hart, Eds., *Electric Properties of Tissues. In Wiley Encyclopedia of Biomedical Engineering* (Wiley Encyclopedia of Biomedical Engineering. John Wiley & Sons, Inc., 2006, p.^pp. Pages.
[142] R. Pethig, "Dielectric properties of body tissues," *Clin Phys Physiol Meas,* vol. 8, pp. 5-12, 1987.
[143] E. K. Moen, B. L. Ibey, H. T. Beier, and A. M. Armani, "Quantifying pulsed electric field-induced membrane nanoporation in single cells," *Biochimica et Biophysica Acta (BBA) - Biomembranes,* vol. 1858, pp. 2795-2803, 2016.
[144] T. B. Napotnik, M. Reberšek, P. T. Vernier, B. Mali, and D. Miklavčič, "Effects of high voltage nanosecond electric pulses on eukaryotic cells (in vitro): A systematic review," *Bioelectrochemistry,* vol. 110, pp. 1–12, 2016.
[145] M. B. Fox, D. C. Esveld, A. Valero, and e. al., "Electroporation of cells in microfluidic devices: a review," *Anal Bioanal Chem,* vol. 385, 2006.
[146] M. Casciola, S. Xiao, F. Apollonio, A. Paffi, M. Liberti, C. Muratori, and A. Pakhomov, "Cancellation of nerve excitation by the reversal of nanosecond stimulus polarity and its relevance to the gating time of sodium channels," *Cell Mol Life Sci,* vol. 76, pp. 4539-4550, Nov 2019.
[147] A. Vargha and H. D. Delaney, "A critique and improvement of the CL common language effect size statistics of McGraw and Wong," *Journal of Educational and Behavioral Statistics,* vol. 25, pp. 101-132, 2000.
[148] E. B. Sözer, C. F. Pocetti, and P. T. Vernier, "Asymmetric Patterns of Small Molecule Transport After Nanosecond and Microsecond Electropermeabilization," *J. Membr. Biol.,* pp. 1-14, 2017.
[149] M. B. Sano, R. E. Fan, and L. Xing, "Asymmetric Waveforms Decrease Lethal Thresholds in High Frequency Irreversible Electroporation Therapies," *Sci. Rep.,* vol. 7, 2017.
[150] E. K. Moen, B. L. Ibey, H. T. Beier, and A. M. Armani, "Investigating membrane nanoporation induced by bipolar pulsed electric fields via second harmonic generation," *Appl. Phys. Lett.,* vol. 109, 2016.
[151] A. G. Pakhomov, E. Gianulis, P. T. Vernier, I. Semenov, S. Xiao, and O. N. Pakhomova, "Multiple nanosecond electric pulses increase the number but not the size of long-lived nanopores in the cell membrane," *Biochimica et biophysica acta,* vol. 1848, pp. 958–966, 2015.

[152] B. M. Slepchenko, J. C. Schaff, I. Macara, and L. M. Loew, "Quantitative cell biology with the Virtual Cell," *Trends Cell Biol,* vol. 13, pp. 570-576, November 2003.

VITA

Hollie A. Ryan
Department of Electrical & Computer Engineering, Old Dominion University
Norfolk, VA 23529, USA

Hollie A. Ryan received a B.Soc.Sci. degree in political science from the University of Ottawa, Ottawa, ON, Canada in 1999 and an M.A. degree in war studies from the Royal Military College of Canada, Kingston, ON in 2004. She received an M.S. degree in biotechnology from Johns Hopkins University, Baltimore, MD, USA, in 2013. Her research interests include bioelectromagnetic applications and device design, image analysis, molecular and microbial dynamics quantification and methods optimization, in addition to human cognition, neuroscience and psychology. Ms. Ryan was a three-time recipient of the Joanne Holbrook Patton Scholarship as well as a 2018 Air Force Research Laboratory Repperger Graduate Research Intern. Before starting her doctoral work, she served as an officer in the Canadian Army and held other responsible positions in government, industry, and volunteer organizations in North America and abroad. She currently works as a Project Scientist in the U.S. Army Futures Command and is the founder of Veritas Alchemy LLC, in addition to serving as a member of the Advisory Board for Envision Lead Grow.

Select Publications and Presentations

1. **H. A. Ryan**, S. Hirakawa, E. Yang, C. Zhou and S. Xiao, "High-Voltage, Multiphasic, Nanosecond Pulses to Modulate Cellular Responses," in *IEEE Transactions on Biomedical Circuits and Systems*, vol. 12, no. 2, pp. 338-350, April 2018.

2. **H. A. Ryan**, B. Ibey and C. Roth (2019, 27 June). "Low-intensity nanosecond pulsed electric field exposure modulates adenosine triphosphate in vitro." Presentation. BIOEM 2019. *The Bioelectromagnetics Society*. Montpellier, France.

3. **H. A. Ryan**, P. Graham, C. Mazur and D.H. McDaniel (2018, 13 Apr). “Optical Coherence Tomography Evaluation of Topical Oxymetazoline Hydrochloride Treatment Efficacy for Rosacea.” Presentation. 38th ASLMS Annual Conference on Energy-Based Medicine & Science. American Society for Laser Medicine & Surgery, Dallas, TX.

4. **H. A. Ryan**, J. Neuber, S. Song, S. J. Beebe and C. Jiang, "Effects of a non-thermal plasma needle device on HPV-16 positive cervical cancer cell viability in vitro," *2016 38th Annual International Conference of the IEEE Engineering in Medicine and Biology Society (EMBC)*, Orlando, FL, 2016, pp. 537-540.